Biomolecular and Biological Applications of Solid-State NMR with Dynamic Nuclear Polarization Enhancement

Wing Ying Chow, Gaël de Paëpe, Sabine Hediger

Biomolecular and Biological Applications of Solid-State NMR with Dynamic Nuclear Polarization Enhancement

Wing Ying Chow,[†,‡] Gaël De Paëpe,[*,†] and Sabine Hediger[*,†]

†*Univ. Grenoble Alpes, CEA, CNRS, Interdisciplinary Research Institute of Grenoble (IRIG), Modeling and Exploration of Materials Laboratory (MEM), 38054 Grenoble, France*

‡*Univ. Grenoble Alpes, CEA, CNRS, Inst. Biol. Struct. IBS, 38044 Grenoble, France*

E-mail: gael.depaepe@cea.fr; sabine.hediger@cea.fr

Phone: +33 (0)4 38 78 65 70 (GDP); +33 (0)4 38 78 65 79 (SH)

Abstract

Solid-state NMR spectroscopy (ssNMR) with magic-angle spinning (MAS) enables the investigation of biological systems within their native context, such as lipid membranes, viral capsid assemblies, and cells. However, such ambitious investigations often suffer from low sensitivity, due to the presence of significant amounts of other molecular species, which reduces the effective concentration of the biomolecule or interaction of interest. Certain investigations requiring the detection of very low concentration species remain unfeasible even with increasing experimental time for signal averaging. By applying dynamic nuclear polarization (DNP) to overcome the sensitivity challenge, the experimental time required can be reduced by orders of magnitude, broadening the feasible scope of applications for biological solid-state NMR. In this review, we outline strategies commonly adopted for biological applications of DNP, indicate ongoing

challenges, and present a comprehensive overview of biological investigations where MAS-DNP has led to unique insights.

Contents

1 Introduction

Nuclear magnetic resonance spectroscopy (NMR) promises to extract atomic length-scale information with minimal perturbation to the system under study, an attractive proposition for developing new understanding of biological molecules in their native state. This promise is especially emphasized in the case of solid-state NMR (ssNMR). SsNMR can solve protein structures with the advantages that, in principle, there is no limit on the size of the biological assembly (provided unlimited sensitivity), and physiologically relevant conditions such as native or native-like lipid membranes can be used.

However, it is often a *tour de force* to obtain a structural model purely by ssNMR. Systems studied so far often have fortuitous properties, such as: good overexpression in bacterial systems with isotopic enrichment ('labeling'); amenable to assemble or reconstitute into the biologically relevant form, ideally with inherent symmetry and a high packing density; stability under the mechanical shear forces within the magic angle spinning (MAS) rotor. Concurrence of many of these properties are necessary to achieve sufficient sensitivity in routine ssNMR experiments carried out on biological systems. While valuable in giving insights to systems that defy all other means of structural characterization, many of these properties severely limit the type of systems that can be fruitfully investigated with ssNMR.

With the advent of signal enhancement by dynamic nuclear polarization (DNP), a new range of applications to even more native-like systems becomes possible, and it is no longer necessary to constrain ssNMR investigations to samples demonstrating all of the fortuitous properties above. With DNP in hand, spectroscopists can be more ambitious in the biological contexts in which they operate; one can imagine tackling structural problems within the context of the cell, at physiological protein concentrations, work with unlabeled or natural isotopic abundance samples, without purification or extraction, homing into essential but sparse structural components of a larger biological assembly, and so on. Thus, DNP represents an opportunity to expand the scope of ssNMR, to redefine the types of information that we can hope to obtain, and explore the range of biological problems that we may choose

to investigate.

The biological application of MAS-DNP is a rapidly evolving area with many prior reviews,[1–13] though apart from a few,[1,4] most of them are focused on a curated subset of biological applications, or on single topics such as amyloid proteins,[9] trapping of folding intermediates,[10] trapping of photocycle intermediates of membrane proteins,[11] and plant and fungal cell walls.[12,13]

In addition, a number of reviews examined MAS-DNP in the context of ssNMR and solution-state NMR techniques that can contribute to structural investigations in a specific area of research. Recent reviews cover viral particles,[14] membrane proteins,[6,15,16] proteins in the cellular context,[17–19] and calcium phosphate biominerals.[20] In the context of achieving improved NMR sensitivity, MAS-DNP is presented as one of many optimizations in the workflow,[21] or to complement ^{1}H-detection via fast MAS.[6]

The aim of this review is twofold: firstly, to summarize the methodologies and strategies currently adopted to achieve DNP enhancement in biological applications and discuss ongoing challenges and limitations (section 2); secondly, to provide a complete overview of the current state-of-the-art of biological applications that takes advantage of DNP-enhanced ssNMR (section 3).

1.1 Scope of this review

As the focus of this review is on the biological applications of DNP-enhanced ssNMR, section 2 does not aim to provide a comprehensive coverage of DNP methodology. Rather, we focus on what might be of interest to typical biomolecular NMR spectroscopists when considering whether and how to apply MAS-DNP to their systems of interest, leaving DNP theoretical background, hardware and methodology developments to other excellent reviews on these topics in this special issue[22] and elsewhere.[4,23]

While the specific topic of oriented membrane applications are briefly covered in section 2.9, the bulk of this review is concerned with MAS-DNP. Photo-chemically induced

dynamic nuclear polarization (photo-CIDNP) technique is excluded from this review as it requires rather different mechanisms and experimental considerations. The reader is directed to other reviews for its application on proteins involved in the photosystem, for example flavoproteins.[24,25]

In contrast to previous reviews, in section 3, we aim to give a comprehensive overview of applications in all areas where MAS-DNP provided new biological insight. The years of literature covered range from work on lysozyme in 1997[26] up to the current day, with particular focus from 2017 onwards. Early MAS-DNP applications focused on methodology development for biological applications, which necessitated the use of in vitro protein preparations that were already well studied by other techniques including solid-state and solution-state NMR. As the methodology matured, DNP-enhanced ssNMR is now often used as part of a suite of techniques applied to gain insight on larger assemblies of proteins and other biomolecules. This is a highly successful approach where DNP signal enhancement plays a contributing, and sometimes major role in bringing new insight to a dazzling diversity of systems. Finally, the use of DNP enhancement can be a deliberate strategic choice in the context of the biological question being addressed, making use of advances in cell biology and biochemistry so that biological integrity can be respected in complex and challenging systems such as intact cells. All of these are valid approaches reflecting the development and maturation of the technique.

We hope our review will provide inspiration for more researchers to consider how access to MAS-DNP can be helpful to addressing ambitious biological problems creatively. We believe that MAS-DNP will play an increasing role for structural biology studies carried out within increasingly physiologically-relevant contexts.

2 Strategies and challenges

Current MAS-DNP methodology is capable of signal enhancement by at least one order of magnitude on a wide range of samples. It enables experiments to observe signals even in situations where sensitivity can be a challenge: low abundance species, such as natural abundance or sparsely labeled; very small sample masses; trapping transient intermediates or binding states. However, MAS-DNP can bring some specific challenges, especially for biological samples. Here, we highlight some common concerns and recent developments to overcome them in the context of biological applications.

2.1 DNP mechanisms and instrumentation

While a few research groups have taken on the significant challenge of designing and implementing home-built DNP instrumentation for biological investigations,[27–31] the applications mentioned in this review were predominantly enabled by the current commercial implementation of DNP-enhanced ssNMR under Magic-Angle sample Spinning (MAS), developed by Griffin and co-workers.[32–35] Often termed *high-field* and/or *high-frequency* MAS-DNP, this approach is characterized by static field strength of $\geq$ 5 T, often $\geq$ 9.4 T (400 MHz ^{1}H Larmor frequency); microwave at $\geq$ 140 GHz, using a gyrotron as the source; temperatures under 200 K; doping of the sample with a paramagnetic polarizing agent, frequently biradicals; and moderate to fast MAS of 5–40 kHz. At the conditions used by most biological MAS-DNP investigations, the cross-effect DNP mechanism dominates, requiring the use of a biradical-based polarizing agent to facilitate the two-electrons-one-nucleus three spin mechanism, though certain applications make use of the solid-effect DNP mechanism which involves only two spins (one electron and one nucleus). A number of excellent reviews already cover the theoretical framework and hardware development aspects of MAS-DNP[4,23,33,34,36,37] and thus these aspects will not be discussed further here.

2.2 Quantifying signal enhancement

The commonly used method of quantifying DNP signal enhancement is based on the signal intensity ratio $\varepsilon_{on/off}$ between a 1D spectrum acquired under microwave irradiation and a reference spectrum obtained under same conditions except for the microwave being switched off. The 1D spectra can be obtained either via $^{1}H-^{13}C$ cross polarization (CP) or from direct polarization (DP). While this method is straightforward to carry out, and these $\varepsilon_{on/off}$ values are frequently reported and compared, depolarization in nitroxide-doped samples can lead to signal loss in the reference (microwave off) spectrum,[38] leading to significant over-estimations of the real DNP enhancement over Boltzmann polarization (ε_B). Thus, for example, the depolarization effect can reach 60% for AMUPol at 10 kHz MAS.[39] While $\varepsilon_{on/off}$ can be used for optimizing DNP sample preparation on the same type of samples/biomolecules and radical, it is not always an appropriate measure when comparing between vastly different samples and radical types[40] (Figure 1). A better measure of signal enhancement is to use, where possible, a reference spectrum acquired on the same sample prepared without the polarizing agent, recorded under optimal standard NMR conditions, to obtain the absolute sensitivity ratio (ASR).[39,41,42]

Moreover, the buildup time T_B of the hyperpolarization also contributes directly to the degree to which DNP can increase sensitivity or reduce experimental time. For all DNP samples, it is advisable to carry out a T_B measurement via a saturation-recovery experiment as one of the initial investigations, especially for combinations of samples, radicals, and solvent matrices that have not been previously subjected to MAS-DNP analysis.

One more factor to consider is that addition of paramagnetic polarizing agents in the sample can reduce the relaxation time constants $T_{1\rho}$ and T_2', affecting the experimental sensitivity for NMR pulse sequences containing spin-lock or refocusing periods.[40,42] This aspect is particularly crucial for experiments with multiple transfers, such as triple-resonance experiments, or longer mixing times, such as the measurement of long-range contacts.

For heterogeneous samples, as found in complex biomolecular systems or in presence of

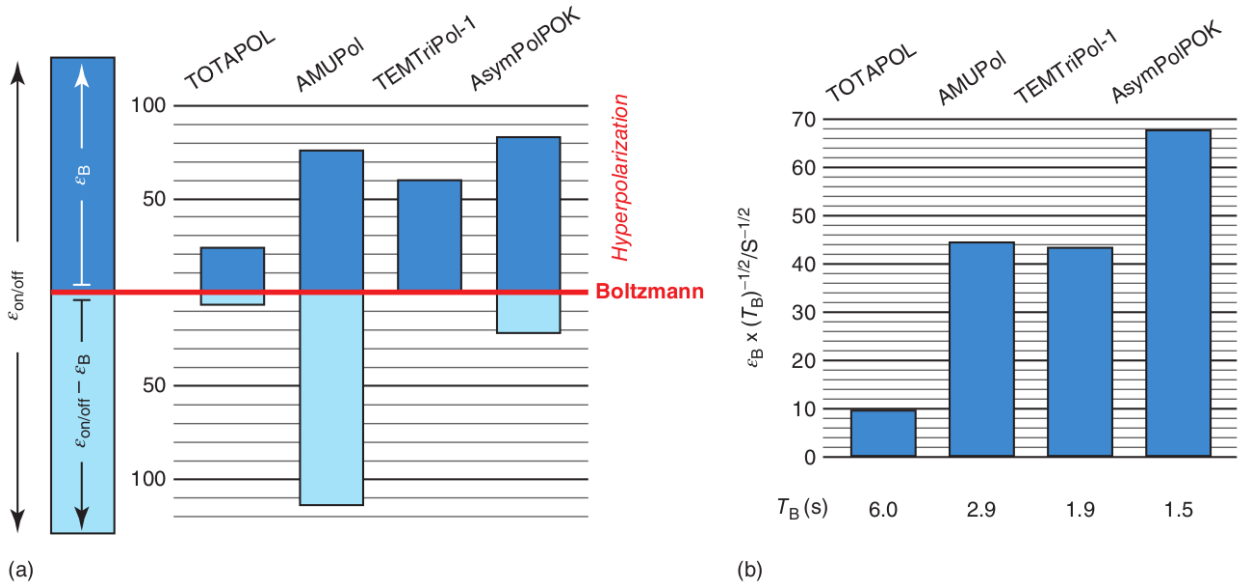

Figure 1: (a) Schematic representation of the Boltzmann hyperpolarization contribution (dark blue) to experimental $\varepsilon_{on/off}$ at 9.4 T, 10 kHz MAS frequency, and 110 K for different water-soluble biradicals: TOTAPOL, AMUPol, TEMTriPol-1, and AsymPol-POK. Note that the size of the light blue bars only represents the discrepancy between $\varepsilon_{on/off}$ and the polarization buildup ε_B. It is not proportional to the amount of depolarization, which cannot be larger than the nuclear Boltzmann polarization. (b) Schematic representation of the sensitivity, expressed as the enhancement factor ε_B divided by the square root of the hyperpolarization buildup time constant T_B , for the same biradicals as in (a). Reprinted with permission from ref. 40. Copyright 2018 John Wiley and Sons.

solid particles, the biradical molecules are often not homogeneously distributed inside the sample. The various polarization transfer pathways (section 2.7.1) may then have different efficiencies, leading to variations of $\varepsilon_{on/off}$ values across the different signals in the same sample.

For many biological applications, rather than pushing blindly for the highest $\varepsilon_{on/off}$, the key consideration should be whether the DNP experiment provides sufficient sensitivity, in terms of signal-to-noise ratio per square-root of the experimental time, to observe the signals that one seeks. Moreover, if a series of samples are to be compared, the sample preparation protocol should lead to robust and reproducible DNP enhancements. For samples that are specifically labeled and/or to be produced at significant cost in money and time, it is advisable to first test the DNP sample preparation on unlabeled samples to benchmark, optimize, and fine-tune the protocol before using labeled samples.

In this review, we may refer to certain $\varepsilon_{on/off}$ values in passing, but we do not aim to provide a comprehensive overview of $\varepsilon_{on/off}$ for different samples and preparations for the reasons above. We invite the readers to look at $\varepsilon_{on/off}$ values with a critical eye, and especially not to rule out the feasibility or utility of a particular study or methodology based on low(er) apparent $\varepsilon_{on/off}$ values alone.[40,42]

2.3 Field strength, MAS frequency, and sample temperature

The most common commercial implementation of MAS-DNP currently uses a static field strength of 9.4 T (400 MHz ^{1}H Larmor frequency), which is rather moderate by the standards of modern biomolecular NMR. DNP experiments at the commercially available higher field strengths of 14.1 or 18.8 T (600 or 800 MHz ^{1}H frequency), or even higher, can improve spectral resolution even under the low temperature conditions required for DNP. The evolution of the NMR spectral linewidth at 100 K was investigated in depth for fibrils formed from amyloid beta (Aβ), implicated in Alzheimer's disease. Lopez Del Amo et al. showed that Aβ40 fibrils at 100 K yield 2D spectra with significantly improved linewidths at 20 T

(850 MHz) compared to those at 9.4 T (400 MHz). In fact, at 20 T, the NMR linewidth of Aβ40 under cryogenic condition is fairly comparable to that obtained at room temperature at 21 T (900 MHz, see Figure 2).[43] Very recent MAS-DNP results by Bahri et al. on Aβ42 at 18.8 T confirmed this result for the core residues of the fibrils.[44] Improvement of the MAS-DNP linewidth with increasing magnetic field and MAS rate has so far been observed only for fairly rigid biomolecular systems with limited dynamics, such as amyloid fibrils as discussed above, bacterial secretion needles,[45] and viral capsids.[46] A different result may, however, be expected for a majority of biomolecules or protein regions with more local dynamics.

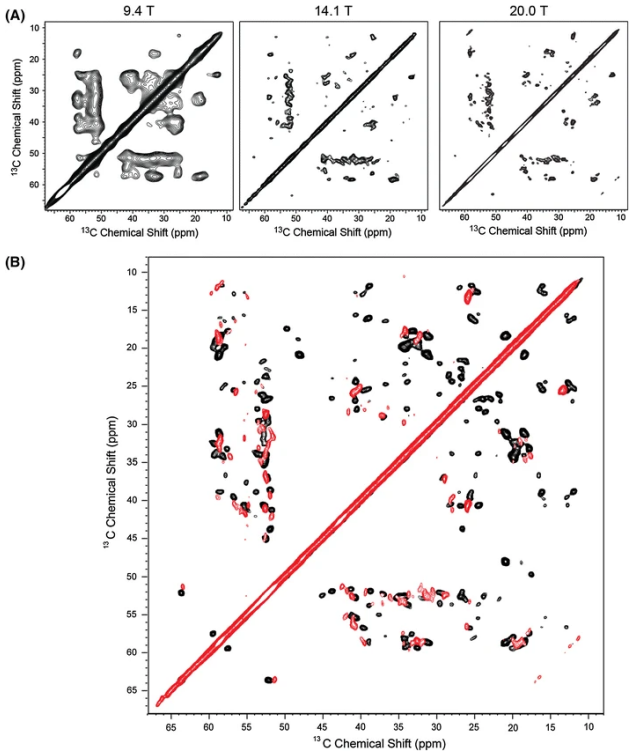

Figure 2: (a) Field dependence of 2D ^{13}C−^{13}C correlation spectra of Aβ40 fibrils at low temperatures (100 K), showing how the lines become sharper despite cryogenic conditions as used for MAS-DNP. Spectra were acquired and processed with the same parameters; the lowest contour was plotted at 20% of the maximum intensity of the isoleucine Cα–Cδ correlation signals. (b) Superposition of 2D ^{13}C−^{13}C spectra of the Aβ fibril, recorded at cryogenic (850 MHz, red) and room temperatures (900 MHz, black). At high field, the resolution does not appear to be compromised at low temperature in this favorable case where the amyloid fibril is highly rigid. Reprinted with permission from ref. 43. Copyright 2013 Springer Nature.

At the low temperatures used for MAS-DNP, typically 100 K or less, the speed of sound is significantly reduced, which imposes a limit on the maximum achievable MAS rate. Moreover, the increase in density of the nitrogen gas for bearing and drive means that higher pressures are needed to achieve the same MAS rate as compared to room temperature (RT). Thus, for a particular rotor diameter, the highest achievable MAS frequency is lower at DNP conditions compared to room temperature ssNMR. For example, at 100 K, 3.2 mm rotors enable MAS frequencies of up to 13 kHz, 1.3 mm rotors up to 40 kHz,[46,47] and 0.7 mm rotors up to 65 kHz,[48] compared to 24 kHz, 67 kHz and 111 kHz, respectively, at ambient temperatures. We envisage that broader access to faster MAS frequencies, either through using commercially available DNP probes of small rotor sizes, or through using helium gas instead of nitrogen[49] (see section 2.4), will enable more fruitful biomolecular and biological investigations using MAS-DNP.

As most of the current applications rely on the cross-effect mechanism for DNP enhancement, the achievable signal enhancement is usually significantly impacted by higher magnetic fields and faster MAS rates.[50,51] Frequently, real biological samples that show good DNP enhancement using AMUPol at 9.4 T (typical $\varepsilon_{\text{on/off}}$ of 40 or more) is likely to show a 50% or even 90% reduction in enhancement at higher fields, with the reduction scaling with the increase in field strength (Figure 3). This effect is partially mitigated by some recently introduced polarizing agents such as TEMTriPol, M-TinyPol, and AsymPol-POK (see section 2.6).

Currently, the choice of whether to carry out experiments at lower field, with higher enhancement, or vice versa, depends on the biological question being addressed, and whether the aim is to observe signals that are weak but in a non-crowded area of the spectrum, or to improve sensitivity while maintaining good resolution in a complex and highly isotopically-enriched sample. Developments in polarizing agents and understanding of alternative DNP mechanisms that can be accessed at higher fields may further alleviate this issue in the future.

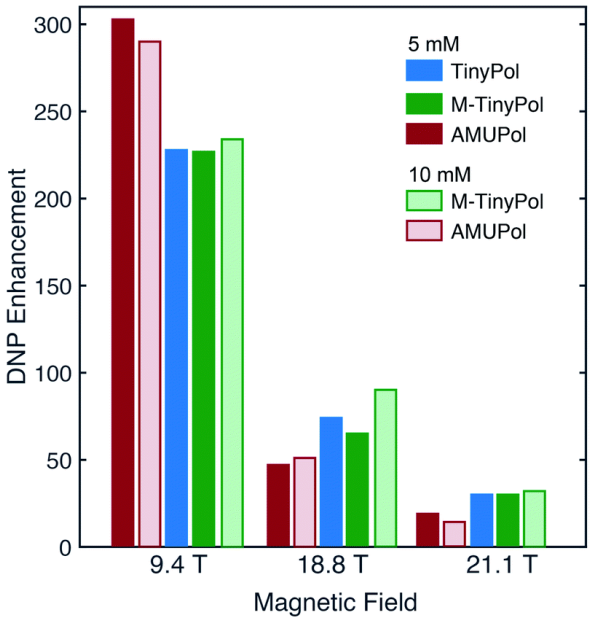

Figure 3: Proton DNP enhancement factors of 5 mM and 10 mM TinyPol, M-TinyPol and AMUPol frozen solutions in d_8-glycerol/D_2O/H_2O 60/30/10 (v/v/v) acquired at various magnetic fields. Frozen solutions are idealized standard reference samples which can deliver much higher enhancement factors than that achieved on typical biological samples, but the same trend of decreasing enhancement factor is observed in the latter. Reproduced in part from ref. 51 with permission from the Royal Society of Chemistry.

One of the key features of current MAS-DNP implementations is the use of temperatures around 100 K. Low temperature facilitates the transfer of polarization from electrons to nuclei, and plays a key role in the signal enhancement process. Currently, such temperatures are achieved by using pre-cooled nitrogen gas for sample cooling, MAS bearing, and MAS drive. The use of nitrogen gas places a lower limit on further cooling as the boiling point of nitrogen at standard pressure is 77 K, which translates to an operating temperature of around 90 K at best. Being able to access MAS temperatures at even lower temperatures, by using helium instead of nitrogen gas, enables even higher DNP enhancements. Though some prototype MAS-DNP systems were developed without helium recirculation,[28,29] the development of closed-loop MAS-DNP systems which are capable of cooling sustainably below 30 K is a long-standing effort by groups in Grenoble[49,52] and Osaka.[53–55] As mentioned above, helium-spinning technology is also capable of achieving higher MAS rates.[49]

2.4 Spectral resolution at low temperature and effect of molecular motions

The need to use low temperatures in MAS-DNP can lead to significant heterogeneous broadening[56] of the NMR resonances and complicate residue-specific signal assignment, even at 14.4 T.[57] The degree of line broadening is related to the molecular motions of the biological system, which are frozen in different conformations at the temperature used for MAS-DNP. The effects of low temperature on line broadening and spectral resolution was investigated on α-spectrin Src-homology 3 domain (SH3) microcrystalline protein[58] and amyloid fibrils formed by the fungal protein HET-s(218-289)[59] in the temperature range of 100–280 K. By decreasing the temperature, both studies showed monotonous signal broadening without sudden step changes, confirmed the inhomogeneous nature of this broadening, and highlighted that buried residues are less affected compared to exposed residues, which rapidly broaden on cooling.

Where local dynamics are present at ambient temperature, which is commonly the case

for many biological systems, MAS-DNP can present an opportunity to observe cryotrapped intermediates and conformations. For example, MAS-DNP showed low temperature structural transitions in small peptides,[60] as well as snapshots of protein conformation change, such as in fast and slow folding of the 35-residue villin headpiece (HP35) subdomain.[61] Biological applications using the low temperature aspect of MAS-DNP to trap intermediates and conformations are covered in sections 3.1.2, 3.1.3, 3.4.4.

The spectral resolution problems at 100 K prompted the investigation of higher temperature DNP. Thus, the effect on the linewidths and the achievable DNP enhancement was investigated at 178 K[62] and 200 K[63] on deuterated SH3. Some advantages were found in terms of improved resolution, as well as 5 to 8-fold shorter buildup times (enabling faster signal averaging), though at the cost of much lower DNP enhancement ($\varepsilon_{\mathrm{on/off}}$ = 10–17 on an idealized sample).

2.5 Specific and sparse labeling schemes

The heterogeneous line broadening induced by the low experimental temperature contributes to significant spectral crowding in MAS-DNP spectra of most biomolecular systems, and can greatly impede spectral assignment. For proteins and biomolecules that can be isotopically enriched, it may be possible to only label a specific molecule in its native setting, specific residues, or specific sequences that are relevant to the question at hand. Alternatively, a mixed labeling scheme can be used, where components of an assembly of biomolecules are expressed using orthogonal labeling, thus enabling intermolecular contacts to be detected (see sections 3.1.1 and 3.5.1, among others). Such specific or very sparse labeling is often insufficiently sensitive for detection via conventional ssNMR.

Sophisticated biochemical techniques are nowadays available to achieve labeling of residues in specific parts of the protein; such segmental labeling can be achieved using split intein technology. Inteins are protein sequences that are capable of removing themselves from a longer protein while splicing the two ends together. The protein sequence of interest (ex-

tein) is split into two segments as desired, which are separately overexpressed with different labeling schemes (or unlabeled), each carrying one part of the split intein sequence. When the two segments are mixed together, the split intein will come together and join the two extein parts together via a native peptide bond, in a process known as protein trans-splicing. Thus, it is possible to produce a chimeric protein that is specifically labeled in only a part of the sequence, reducing spectral complexity and crowding. This procedure, especially in the context of DNP applications, is well-described by Frederick and coworkers,[64,65] and also demonstrated by Glaubitz and coworkers on membrane proteins.[66]

In all these specific, sparse and segmental labeling approaches, signals arising from the natural abundance background becomes significant. There are spectroscopic techniques to remove this background signal, such as double quantum filtering (DQF) and difference spectroscopy, however, they impact the sensitivity. Thanks to DNP, this sensitivity issue can be overcome, and these labeling schemes are widely used in the field, especially highlighted in sections 3.5.3 and 3.6.

A novel method of overcoming spectral crowding lies in the specific incorporation of fluorinated residues in the protein, usually tryptophans, thus benefiting from the large NMR chemical shift dispersion of ^{19}F. The large CSA of ^{19}F requires, however, relatively fast MAS frequencies to achieve good resolution, ideally 40–60 kHz. Using a 1.9 mm DNP probehead and MAS frequencies up to 25 kHz , Lu et al. demonstrated good ^{19}F DNP enhancements of 77 on a HIV-1 viral assembly. While 2D ^{19}F$-^{13}$C heteronuclear correlation experiments are challenging because of the poor efficiency of this transfer, they were successfully obtained with DNP sensitivity enhancement.[67]

2.6 Design and synthesis of biocompatible polarizing agents

Under the current implementation of MAS-DNP, the cross-effect mechanism has been found to be the most robust and efficient. Since this mechanism requires the interaction of two electron spins and one nuclear spin, covalently attached nitroxides (binitroxides) have emerged

as common polarizing agents.[68] In particular for biological MAS-DNP, biradical polarizing agents that are soluble in aqueous media were developed, starting with TOTAPOL,[69] then AMUPol;[70] a summary of the biradicals compatible with biomolecular applications is shown in Figure 4. Currently, AMUPol is the most commonly used polarizing agent for biological investigations as it clearly outperforms TOTAPOL[70] and can be easily obtained commercially, even though it does exhibit strong depolarization and is not optimized for DNP at higher magnetic fields.[39]

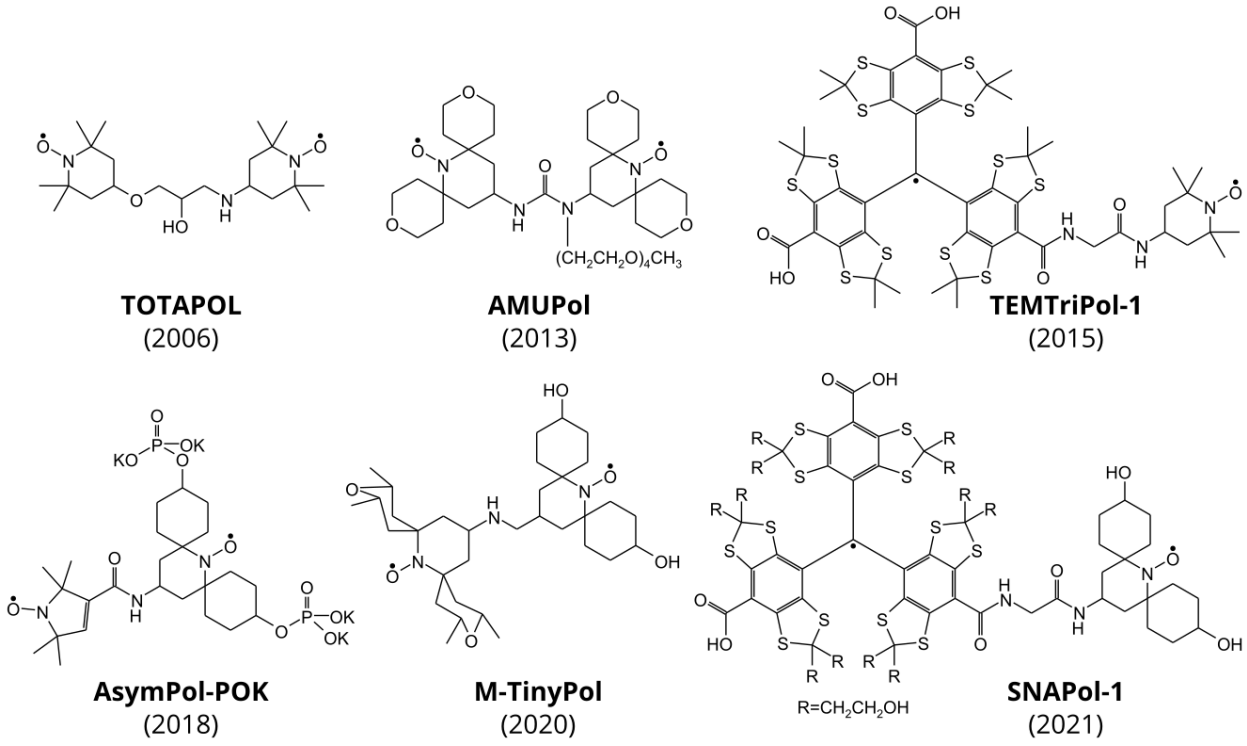

Figure 4: Organic biradical polarizing agents developed for biological applications of MAS-DNP. Apart from optimizing the DNP enhancement, these radicals are also soluble in water or aqueous buffer. The depicted biradicals include TOTAPOL,[69] AMUPol,[70] TEMTriPol-1,[71] AsymPol-POK,[72] M-TinyPol,[51] and SNAPol-1.[73] Among these, AMUPol is currently the most widely used.

The effort to design and develop better performing, biocompatible, organic radical-based polarizing agents continues in the synthetic chemistry groups of Tordo and Ouari (Aix-Marseille University, France),[51,74,75] Liu (Tianjin Medical University, China),[71,73,76] and Sigurdsson (University of Iceland),[72,77–80] frequently in collaboration with various groups spe-

cialized in MAS-DNP. Current research efforts in this area, apart from attempting to deliver ever higher DNP enhancement values, often incorporate one or several further design principles: improving aqueous solubility or hydrophilicity, ensuring stability of the polarizing agent in complex biological environments including in-cell, preventing aggregation or clustering, and maintaining DNP enhancement at higher magnetic fields and MAS frequencies. Ongoing development of radicals that are suitable for a biological context often draws inspiration from EPR-based developments for in-cell and site-directed spin labeling of biomolecules.[81–83]

AMUPol is one of the early examples of binitroxides with a bTUrea linker that was optimized for solubility, leading to significantly improved DNP enhancement performance relative to TOTAPOL.[70] Further bTUrea-style binitroxides include the bcTol[77,78] and HydrOPol family.[75] The latter have an open or closed conformation of tetrahydropyran rings surrounding the nitroxide radical, with the open conformation giving higher DNP enhancement, but the closed conformation showing better stability under reducing conditions, as found in cellular environments.

To address the issue of dropping cross-effect efficiency at higher magnetic fields, the TEMTriPol family was introduced as a first demonstration of mixed radicals, where a narrow-line trityl is tethered to a broad-line TEMPO nitroxide.[50,71] While the initial demonstrations of DNP enhancement with TEMTriPol were promising, the hydrophobicity of the trityl group led to unwanted specific interactions with hydrophobic patch on proteins such as ubiquitin. To overcome this, the NATriPols were introduced. Thanks to a linker between the trityl and TEMPO moieties that is easily tunable by thiol-click chemistry, more hydrophilic mixed radicals were obtained, where no such interactions are observed.[76] Further modifications towards even higher hydrophilicity and longer electron relaxation lead to the SNAPol family, for which good DNP enhancement (protein $\varepsilon_{on/off}$ of nearly 50 at 18.8 T) were obtained, even for in-cell DNP using human cell lines and bacterial cells.[73]

Next to the mixed radicals, binitroxide radicals for use at higher magnetic fields have been developed as well. In order to mitigate against the depolarization effect, De Paëpe's group

developed a computational approach[84] to design molecules with optimal characteristics, such as a short linker to increase intramolecular electronic dipolar coupling and J-exchange interaction, the relative orientation of the g-tensor of the two radicals, and replacing methyls by spirocyclohexanol groups to lengthen electron relaxation. The optimization process leads to a family of biradicals comprising two nitroxide rings of different size (one 5- and one 6-membered), called AsymPol.[72] Although the AsymPol family was designed with applications at 800 MHz in mind, the advantages against depolarization extend to applications at lower fields. One biradical of this family, AsymPol-POK, is specifically designed for biological applications, containing negatively charged phosphate groups that contribute to its excellent solubility and reduce clustering or aggregation of the biradicals; cAsymPol-POK, the most recent addition, is notable for achieving efficient sensitivity improvement even for proton-rich systems, including biomolecules.[85] Another approach is taken by the TinyPol family,[51] which uses two identical nitroxides joined by a short non-flexible linker to increase the intramolecular dipolar coupling.

Nitroxide-based triradicals have proven to be efficient DNP polarizing agent at very low temperatures.[86] The improved solubility in aqueous solvent mixtures of the triradical succinyl-DOTOPA is an advantage for the investigation of biomolecular systems by MAS-DNP at low temperature, achieving better sensitivity than AMUPol for temperatures below 90 K.[87] Therefore, triradicals have been used in several investigations on protein folding, including time-resolved complex formation at 25 K (see section 3.1.2).

Monoradicals may be promising polarizing agents to directly hyperpolarize heteronuclei at high magnetic fields via the solid-effect mechanism. In one investigation at 14.1 T, Wang et al. showed the feasibility to use a trityl radical OX063 to directly polarize ^{13}C and ^{15}N in a microcrystalline sample of tryptophan synthase. Moreover, for ^{15}N, the trityl-enhanced DP spectrum showed slightly better sensitivity per unit time than the AMUPol-enhanced CP spectrum.[88]

Beyond stable organic radicals, Corzilius and coworkers have a long-standing interest in

the use of paramagnetic high-spin metal ions, such as Gd^{3+} and Mn^{2+}, to achieve solid-effect DNP.[89–93] While this approach does not deliver DNP enhancements that are as high as those achieved with highly-optimized binitroxides, the relative stability of metal ion complexes (e.g. Gd-DOTA) against reduction,[81] as well as their binding capability as metal centers in proteins, make them interesting for applications where a nitroxide-based radical would be unstable. Metal ions can also be used for the investigation of binding sites with targeted approaches, where naturally-occurring diamagnetic metal ion can be replaced with a paramagnetic metal ion for DNP.[94]"

2.7 Sample preparation considerations

A step-by-step procedure for preparing a range of biological samples for DNP, including protein assemblies, membrane proteins, and precipitated proteins has been reported.[95] In a broader context, samples for DNP are commonly prepared with 10 mM of biradical-based polarizing agents in a combination of significantly deuterated solvents with a high proportion of cryoprotectants. The commonly used standard DNP matrix (so-called 'DNP juice') is a 60/30/10 volume mixture of d_8-glycerol or d_6-DMSO, D_2O, and H_2O, though many variations of this mixture, have been reported in the literature. These protocols are known to provide good DNP enhancement for frozen solutions of small molecules and molecular solids. They are relatively robust for many peptides and protein assemblies as well,[96] and can serve as a starting point for MAS-DNP investigations of novel biological systems.

2.7.1 Polarization transfers

To understand the important factors in preparing samples for DNP, it is interesting to consider the pathway taken by the polarization from the electron spins to the detected nuclear spin. Indeed, the measured hyperpolarization is the interplay of several polarization transfers. In the initial DNP step, polarization is transferred from the electron to nearby nuclear spins, usually ^1H (via the cross effect or other mechanisms). This hyperpolarization is then

relayed to greater distances through the whole sample by proton spin diffusion,[97] to be finally transferred to the heteronuclei of the system of interest; this pathway is termed *indirect DNP*. The opposing *direct DNP* pathway consists of direct polarization transfer from the electrons to the nuclear spins of the system of interest, without passing through the ^{1}H network of the matrix. The nuclear spin hyperpolarization is in this case detected after DP excitation. It allows a more targeted detection close to the polarizing agent at the cost of slow hyperpolarization buildups.[4] In addition, under DP excitation, heteronuclear cross-relaxation can occur via methyl groups in an effect named Specific Cross Relaxation Enhancement by Active Motions under DNP (SCREAM-DNP). This pathway leads to variable negative enhancements of heteronuclei that are near methyl groups, with the DNP enhancement factor influenced by the motions of these nearby methyl groups,[98,99] as well as of primary amines and ammonium groups;[100] this effect can also be driven by cyclohexane ring motion.[101] These three different transfer pathways were investigated and compared on the same protein assembly, the HIV-1 capsid protein (Figure 5), demonstrating the potential to highlight structural aspects of the system by varying the biradical concentration and/or the recycle delay or the time allotted for DNP signal buildup in order to select the desired polarization pathway.[102]

To ensure a proper DNP signal enhancement of the targeted object, for instance in a complex environment, the proximity of the polarizing agent to the biomolecule or the molecular interaction of interest has to be carefully considered. For biological systems that are tens of micrometers at the shortest dimension, such as mammalian cells, it can be advantageous to develop protocols for delivering the polarizing agent closer to the biomolecule of interest, even with the commonly used indirect DNP transfer pathway. It is necessary to optimize the method by which the polarizing agent is introduced to and mixed with each specific biological system. In section 3 of this review, we will outline the protocols that different groups have developed to achieve good DNP enhancement on a variety of biological systems.

The role that protons play in the indirect DNP polarization pathway means that non-

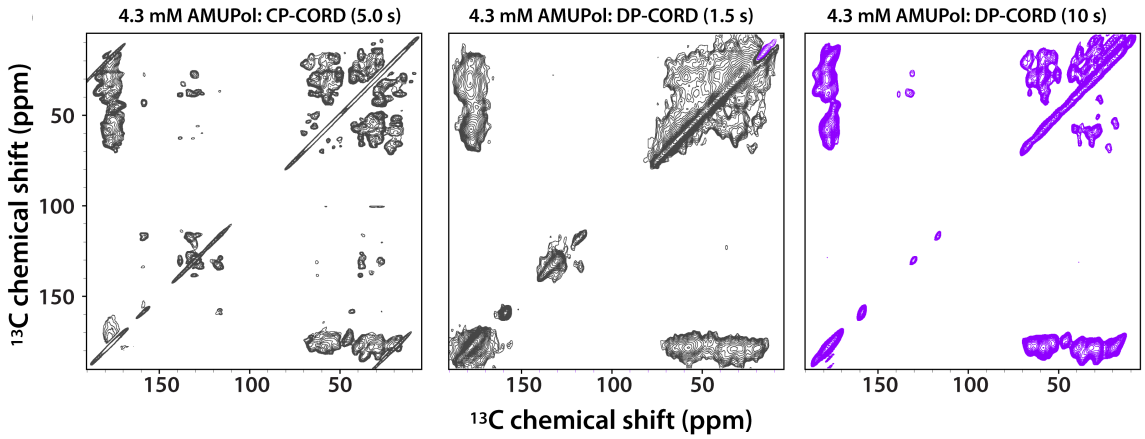

Figure 5: DNP-enhanced $^{13}C-^{13}C$ correlation spectra demonstrating indirect DNP (left), direct DNP and SCREAM-DNP (middle), and SCREAM-DNP only (right) polarization transfers on 5F-Trp, U-^{13}C, ^{15}N tubular HIV capsid assemblies, in the presence of 4.3 mM AMUPol. The spectra were obtained using the COmbined $R2^{\nu}_{n}$-Driven (CORD) pulse sequence with a mixing time of 20 ms. The modes of excitation (CP vs DP) and the recycle delays of 5 s (left), 1.5 s (middle), and 10 s (right), led to different transfer pathway(s), and demonstrated clear differences in the observed signals and spectral resolution. All spectra were acquired at 14.1 T (150.96 MHz ^{13}C Larmor frequency) at a MAS frequency of 24 kHz and 120 K. Reprinted in part from ref. 102 under a Creative Commons (CC-BY 4.0) license.

uniform DNP enhancement (measured by $\varepsilon_{on/off}$) of different components in the biological sample can sometimes be used to extract structural information. It is expected that more solvent/water-accessible components would be more likely to show higher DNP enhancement. By carefully quantifying non-uniform DNP enhancements, van der Wel et al. determined the size of crystallites formed by an amyloidogenic peptide,[103] and Ehren et al. estimated the thickness of the organic layer on biosilica.[104]

2.7.2 Cryoprotection

Ice formation is detrimental in cryogenic structural studies of many biological systems. For cellular samples, formation of intracellular ice is generally lethal.[105] Even when it is avoided, cold exposure can harm the ability of said cells to grow, divide, and retain their biological integrity after thawing.[106] The addition of cryoprotectants such as glycerol or DMSO is therefore important to ensure cellular survival of the freezing process. Such cryoprotectants

are often used at 5–15% of the volume,[107,108] but can be 30–60% for bacteria, fungal cells, and human red blood cells. The issue of cryoprotectant cytotoxicity is a complex topic. It varies, for example, with different cell types, the method of freezing, or the measure of survival after freezing (which can be based on membrane integrity, motility, adherence to substrate, and/or proliferation), meaning that it is unwise to attempt generalizations across cell types, species, or kingdoms of life. For non-cellular, purified protein assemblies, the formation of water crystals can still disrupt the ensembles and impinge on structural studies via the process of cold denaturation. In X-ray diffraction, where low temperatures are used to minimize radiation damage, it is common to add a high level of cryoprotectants (25–50% volume glycerol[109]) to prevent crack formation in protein crystals that would lead to poor quality data. SsNMR does in principle not face this kind of problems as it can be applied as well to non-crystalline and microcrystalline samples. However, for MAS-DNP, formation of ice crystals in the matrix used to disperse the polarizing agent in the system, is detrimental. It leads to phase separation of the solvent and clustering of the polarizing agent, with a direct negative effect on the DNP enhancement. Thus, samples for MAS-DNP are commonly prepared with a matrix solvent containing a high level of glycerol (or other cryoprotectants) to ensure a glassy sample state at the experimental temperature used, regardless of the cooling rate.[110] This is often a requirement for robust and reproducible DNP enhancements.

While the use of glycerol as a cryoprotectant was established early on the development of biological MAS-DNP,[26] the high cryoprotectant content of the traditional DNP solvent matrix may not be suitable for use in studies with increasingly complex and delicate combinations of biomolecules or cells. For example, mixing with a large volume of glycerol can disrupt viral assemblies,[111] interfere with membranes[11,112] and introduce a lag phase to mammalian cells.[113] Moreover, the position of glycerol signals can overlap with the ones of glycans, which may be of interest (see section 3.6). Where possible, it is advised to test the preparation of the DNP sample with a range of cryoprotectants, as well as consider impreg-

nation wetting or matrix-free sample preparation techniques, which have been successfully demonstrated now on various complex biological systems (section 2.7.4). Note that signals from the cryoprotectant used as part of the DNP matrix will appear in the spectra, and may overlap with signals of interest. This problem can be mitigated by using ^{13}C-depleted glycerol (or other cryoprotectant). Spectroscopic solutions are also possible; if the biological sample is ^{13}C and ^{15}N labeled, double-quantum or heteronuclear filtering can be used to greatly reduce the detection of non-labeled cryoprotectants relative to the signals of interest. Instead of glycerol and DMSO, glycan species can be an alternative type of cryoprotectant. For liposomes containing a lipid-anchored biradical, it was found that trehalose in an aqueous matrix can give better DNP enhancements when compared to a glycerol-containing matrix.[114] The affinity of glycans, such as trehalose, to some polarizing agents such as TOTAPOL, facilitates matrix-free sample preparation procedures which is covered further on in section 2.7.4.

Interestingly, a DNP matrix containing glass-forming solvent may not be necessary for all biological samples. Ravera et al.[115] obtained a $\varepsilon_{on/off}$ of 50 on a frozen solution of bovine serum albumin without cryoprotectants, and a slightly higher $\varepsilon_{on/off}$ of 66 for a sedimented sample. The authors proposed that the DNP improvement is due to less water crystallization in the sedimented sample. A similar result was obtained on a sedimented sample of a DNA-protein complex.[116] The omission of typical cryoprotectants (such as glycerol and DMSO) was shown not to affect DNP enhancement for membrane-associated peptides,[117,118] dried glycan-based biomaterials such as cotton,[119] collagen-based extracellular matrices[120] and biominerals.[121] Glycans species are naturally present in some of these systems, and may act as cryoprotectants to some extent.[122]

2.7.3 Deuteration

The potential role that deuteration can play in DNP improvement was noted early on,[123] where a 90% deuterated solvent matrix was shown to provide extended ^{1}H T_B buildup

times in frozen solutions. Since then, using a deuterated solvent matrix for DNP samples is currently standard practice as it often yields the highest signal enhancement values via indirect DNP polarization transfers, and is most likely to give uniform signal enhancement for different components. The extended ^{1}H T_B buildup time provides the opportunity for electron spin polarization difference to equilibriate with the dipolar-coupled ^{1}H spins, which is necessary for achieving good DNP enhancement by the cross-effect mechanism.

Following this earlier work, the commonly used DNP solvent matrices are often 90% deuterated by volume, which still contain a proton concentration of 11 M for rapid spin diffusion and CP.[123] However, the use of fully deuterated solvents to limit the polarization transfer to nuclei close to the polarizing agent is interesting to consider in so-called targeted DNP approaches[8] (section 2.8). This was demonstrated on a membrane protein tagged with a radical,[124] on samples prepared with a very low concentration of radical bound to the targeted biomolecule diluted in a complex environment,[125,126] as well as on isotopically enriched proteins placed in deuterated cellular lysates[127] or cells.[128] Still, protonated water remains a common contaminant in many preparations where complete deuteration was intended. Heiliger et al. demonstrated that the achievable deuteration level of protein samples is actually often less than 90%, even when the exchangeable sites are fully deuterated; nevertheless, distance determination seems to be possible when extensive deuteration is combined with site-specific spin-labels and direct DNP.[90]

While a fully deuterated matrix may be especially useful for limiting spin diffusion and enabling relatively targeted polarization transfers, it is worth bearing in mind that it may not be the most ideal in all applications. In certain cases, a protonated matrix may even outperform.[129] For solid-effect DNP using paramagnetic metal ions, Corzilius et al. noted that experiments with Gd-DOTA perform better for ^{1}H and ^{13}C when the matrix is fully protonated.[89] Experiments using the heteronuclear cross-relaxation/SCREAM-DNP pathway also show larger enhancement.[98]

Deuteration of the polarizing agent itself has been explored as a means to provide higher

enhancement, attempted with TOTAPOL[63,130] and other biradicals in organic solvents such as bTbK.[130,131] In both cases, it was found that while the $\varepsilon_{on/off}$ can be higher, the polarization buildup time was slower. Thus for TOTAPOL, deuteration does not seem to be a fruitful route.

Perdeuteration of the biomolecular component(s) has also been explored. Akbey et al. showed that perdeuterated microcrystalline SH3 (with 50% protonation at exchangeable sites) gave a much higher $\varepsilon_{on/off}$ value of 120 compared to 31 for protonated SH3 when the same recycle delay was used. This effect was also borne out by overall better signal-to-noise of the deuterated protein sample.[132] Specific deuteration of methyl-bearing residues in Aβ amyloid fibrils was reported to improve the DNP signal enhancement by reducing the intrinsic $^{1}H-^{1}H$ spin–lattice relaxation rates, and thus allowing more time for the hyperpolarization to buildup within the peptide self-assembly.[133] For membrane proteins, the effect of deuteration of membrane lipids on the DNP enhancement was investigated by Liao et al.; while a higher $\varepsilon_{on/off}$ value was obtained with deuteration, the absolute sensitivity was similar to that obtained on protonated lipids, likely due to a trade-off between better polarization transfer from electron to nuclear spins and poorer $^{1}H-^{13}C$ CP transfer.[134] Efficient hyperpolarization of proton-dense systems can depend strongly on the polarizing agent. Using recently developed biradicals, deuteration of the system of interest might be avoided.[85]

The improvement of DNP sensitivity by deuteration of the investigated biomolecule is also dependent on the experimental conditions. Even though current sample spinning frequencies for MAS-DNP are commonly below 13 kHz, faster MAS is becoming increasingly available, with commercial DNP probes able to deliver MAS rates of 40–65 kHz.[47,48] At this MAS regime, deuteration of biological samples was found to be beneficial for proton detection in standard ssNMR.[135–137] We expect in this context that deuteration may become helpful as well for DNP at fast MAS.

2.7.4 Impregnation and matrix-free sample preparation

Early biological investigations by MAS-DNP followed the initially developed sample preparation protocol, and were performed on frozen solutions based on the standard DNP matrix. The inclusion of solvents in the rotor, however, reduce the sensitivity of the NMR experiment by diluting the sample. Therefore, rather than the traditional frozen solution approach, various methods were developed to drastically reduce the solvent amount required for dispersing the polarization agent throughout the sample. Despite the lower solvent levels in these types of sample preparations, ^{1}H spin diffusion is still very efficient for spreading hyperpolarization across the whole sample, as the system of interest is usually protonated. These preparations can simplify sample preparation by avoiding significant protocol optimization of cryoprotectant and solvent deuteration levels, and can be relatively more economical in the use of polarizing agents.

These approaches of minimizing the solvent amount can be divided into cases where the polarizing agent is non-covalently associated or dispersed in the sample, or where the polarizing agent is covalently attached to part of the system. For cases where there is no covalent linkage between the polarizing agent and the biological sample, the main methods reported thus far are sedimentation, impregnation, and removal of excess solvent in the so-called matrix-free approach.

For sedimentation, the solution of protein or protein complex containing the polarizing agent is ultracentrifuged into the MAS rotor, where an amorphous hydrated pellet is collected for experiments. This method requires proteins or complexes that are above 30 kDa in molecular weight. It was demonstrated on the 480 kDa homo-24-mer apoferritin (ApoF) protein, with the sedimented sample showing higher DNP enhancement ($\varepsilon_{on/off}$) compared to the frozen solution,[138] as well as on the 67 kDa bovine serine albumin.[115] Thus, sedimentation can be considered as a relatively straightforward sample preparation method for amenable proteins.

For impregnation, the sample is soaked or suspended in a small amount of solvent (such

as D_2O) containing the polarizing agent. The wetted sample is then directly packed into the MAS rotor. This method has similarities to the incipient wetness impregnation technique reported on porous materials.[139,140] In cases where the final form of the sample is a protein or a proteoliposome pellet, the impregnation method is carried out with around 100 µL of stock polarizing agent solution in the standard DNP matrix, either with centrifugation for mixing,[134] or simply added on top of the pellet without stirring and left to incubate overnight.[11,111] Excess solution can be removed by pipette afterwards to ensure maximum packing density in the rotor. This method was suitable for preparation of viral assembles (section 3.3) and membrane proteins (section 3.4) for DNP experiments. In some cases, further modification to this protocol is necessary for ensuring that the protein remains functional after the sample preparation process.[141] Smaller volumes of wetting solution (5–50 µL) were recently used for preparing samples from the mammalian extracellular matrix[120] and biosilica[104] for DNP (section 3.7). In certain systems, it is possible that naturally glycosylated proteins can provide inherent affinity to the polarizing agent at well-dispersed sites on the protein, thus avoiding aggregation of the polarizing agent.

In the so-called matrix-free sample preparation approach, the suspended or soaked sample is further dried to remove the solvent almost completely.[41] This drying step has to be handled delicately as it can easily lead to aggregation of the polarizing agent. Aggregation can be avoided by using a natural affinity of the biradical to the system of interest, or using gluing agents such as glucose or trehalose to provide affinity.[142] This method has been demonstrated successfully on cellulose,[41] lysozyme,[142] and liposomes.[114]

In general, it is important to consider and assess the presence of any binding affinity between the polarizing agent and the investigated system to devise an ideal protocol. Such an affinity can indeed lead to an accumulation of biradicals in some part of the sample, and therefore to an uneven distribution of polarizing agent, as was observed in bacterial cell wall,[143] sedimented apoferritin,[138] and sedimented bovine serum albumin.[115] For example, Nagaraj et al. used isothermal titration calorimetry (ITC) to demonstrate affinity of TO-

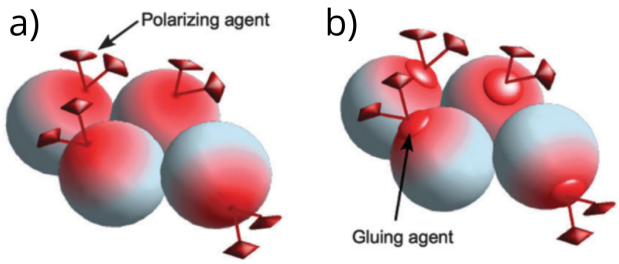

Figure 6: Schematic illustration of the two matrix-free sample preparation strategies, using either a direct (a) or an indirect (b) affinity of polarizing agents to the system of interest. Reproduced from ref. 142 with permission from the Royal Society of Chemistry.

TAPOL to CsgA and Het-S, both functional amyloids, the former bacterial, and the latter fungal. Using this property, optimal DNP enhancement could be achieved with a lower TOTAPOL concentration (0.25–1 mM) resulting in improved spectral resolution.[144]

Spin-labeling with the polarizing agents covalently linked to the biomolecules can be used as well for solvent-free DNP sample preparation. This approach ensures a homogeneous distribution of the polarizing agent around each biomolecule of interest and can maximize the rotor filling factor. To avoid excessive relaxation due to high levels of polarizing agents, the spin-label may need to be attached to only a fraction of the available sites. This method was demonstrated on a decapeptide,[145] and used in a number of studies on membrane proteins and associated peptides where the spin label was placed either on the protein[124,146,147] or on lipids[3,117,118,148,149] of the membrane (Figure 7). Some of these works are described in further detail in section 3.4. Furthermore, spin-labeled antimicrobial peptides can be a means for delivering polarizing agents to bacterial membranes and cells.[150,151]

2.8 Targeted approaches

In many biological systems there is inherent complexity in terms of types of biomolecules, interactions, and interfaces, which means that attempts to observe a specific localized part of the whole system are thwarted by low sensitivity and spectral crowding. With the advent of MAS-DNP, many groups have developed methodologies to localize hyperpolarization and restrict spin diffusion, in order to achieve targeted DNP within a complex environment.

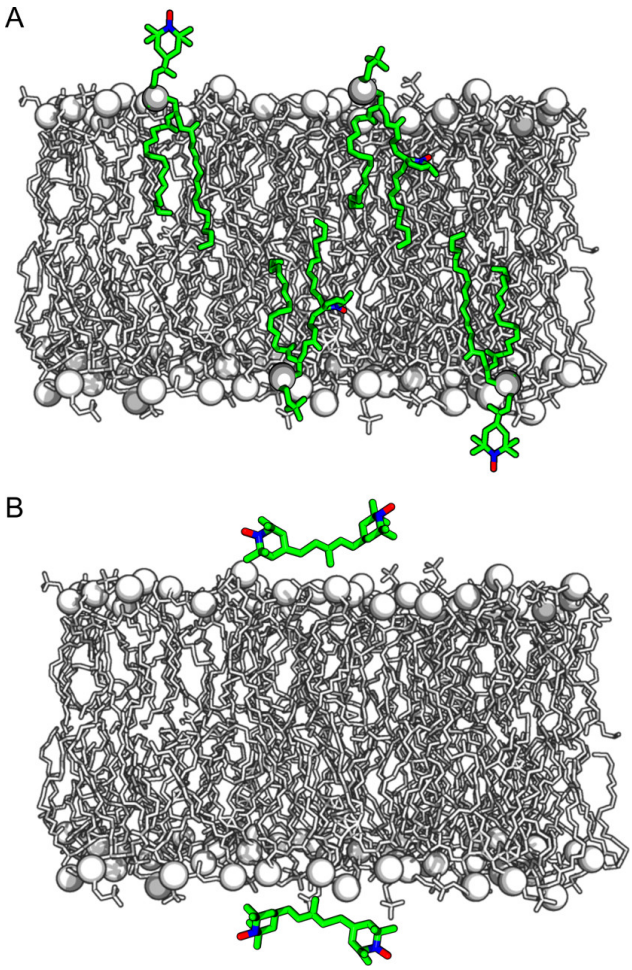

Figure 7: Schematic illustration of two sample preparation strategies for biological membranes: (A) using nitroxide labeled lipids, and (B) a conventional preparation with biradical-containing DNP matrix solution. Reprinted from ref. 3. Copyright 2016 American Chemical Society.

Rogawski et al. surveyed the use of covalent spin-tagging for DNP;[152] more recently, Gauto et al. reviewed further strategies and potential applications of targeted DNP,[8] including distance constraints, selectivity in complex environment, or investigation of protein-ligand binding sites through selective DNP.[126,153,154]

A number of methodological developments for targeted approaches envisage applications in membrane proteins, especially for observing interfaces. Wylie et al. elegantly followed the dimerization of gramicidin by using a well-positioned, covalently-attached mononitroxide spin-tag attached to the 15-residue gramicidin peptide. Dimerization in the lipid membrane led to a stable interspin distance of 7.5 Å, confirmed by EPR measurements, which enabled cross-effect DNP (with a modest enhancement of 6) across the dimer interface.[146] In a study where inter-proteomer signals were sought, specific residues of the membrane protein KcsA were tagged with monoradical or biradical via sulfhydryl chemistry. Monoradical spin-labels can still lead to DNP via the cross effect due to the tetrameric nature of KcsA channels. The enhancement factors obtained were fairly modest (14–16 at 9.4 T) and lower than that obtained with 25 mM AMUPol, but the sensitivity of the experiment was better due to shorter T_B.[147]

Using aligned lipid bilayers in both static and MAS conditions, Salnikov et al. investigated the effect of specific lipid compositions on DNP enhancement, and also studied the enhancement capabilities of a series of spin-labeled lipids, which were shown to be advantageous compared to TOTAPOL or AMUPol in matrix-free preparations.[118]

An interesting development in spin- or biradical-tagging of proteins is the use of amber suppression, which is capable of introducing unnatural amino acids into specific positions on proteins. The spin-tag can be then attached via bioorthogonal chemistry. Lim et al. demonstrated how TOTAPOL-tetrazine can be attached to ubiquitin by introduction of a norbornene-lysine residue, while maintaining ^{13}C, ^{15}N labeling of the rest of the protein.[155]

Recently, a spin-labeling strategy has been developed for any protein that contains a disulfide bond. This technique inserts a TEMPO-derived monoradical spin label inbetween

the sulfur atoms. EPR spectroscopy and HPLC showed that the spin label is intact and covalently inserted as expected into eptifibatide, a glycoprotein drug. DNP enhancement was demonstrated on the glycerol signals of the DNP matrix. Since eptifibatide was at natural abundance, and potentially subject to bleaching from the radical, it was not observed in the conditions of the experiment.[156]

As the indirect polarization pathway relies on spin diffusion, the degree of selectivity that targeted DNP can achieve is limited. In addition, the signal intensity of nuclear spins in the closest vicinity to the radical tag are strongly affected by bleaching effect due to paramagnetic relaxation enhancement (PRE), and may not be detectable in targeted approaches. Nevertheless, highly resolved spectra of localized regions of the biomolecule can be recovered using targeted DNP combined with difference spectroscopy, as demonstrated in the selective DNP (*Sel*DNP) approach[154] (Figure 8).

By carrying out direct ^{13}C DNP with paramagnetic metal ions[89] and accessing alternative polarization transfer pathways such as SCREAM-DNP, the group of Corzilius and coworkers have demonstrated the potential to achieve more targeted polarization transfers on model proteins such as ubiquitin.[90,98,129] The approach combining the heteronuclear cross-relaxation effect of SCREAM-DNP in ^{13}C-labeled system with more restricted ^{13}C$-^{13}$C spin diffusion has been termed Selective Detection of Internuclear Contacts by Methyl PoLarization Enhancement (SIMPLE). It enables highly selective local transfers as demonstrated on a membrane protein (green proteorhodopsin) with a bound retinal chromophore.[157]

2.9 Oriented membranes

The ability of biological lipid bilayer membranes to form uniaxially oriented samples can enable the characterization of additional structural (and sometimes dynamic) features by limiting the conformational space that can be adopted by the embedded proteins. The orientation can occur naturally by placing the membranes in a magnetic field, or by preparing the sample on a solid physical support, such as a flat film that can be rolled up and placed

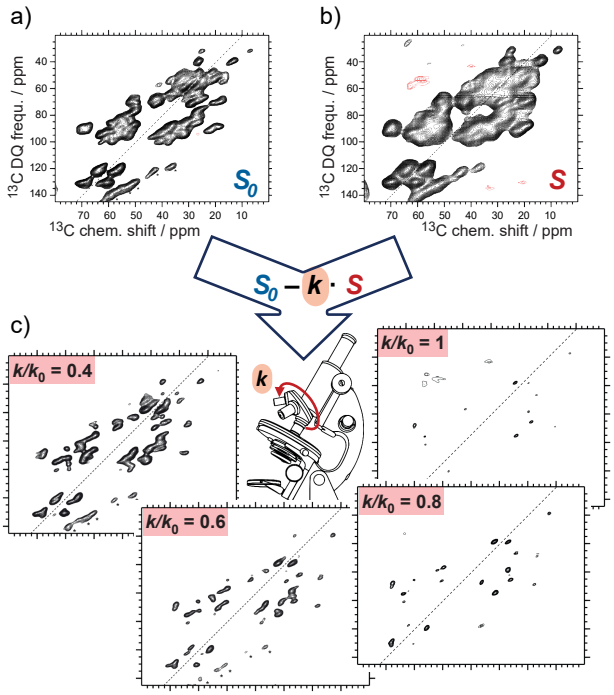

Figure 8: Schematic principle of the *Sel*DNP approach. (a) Reference dataset S_0 recorded on the sample prepared with the protein and its native ligand together with a non-specific polarizing agent (PA). (b) Targeted DNP dataset S recorded on the sample prepared with the protein and the ligand functionalized with the PA (acting as paramagnetic tag). The difference of the two datasets using a variable relative scaling factor k (selectivity factor) produces a set of *Sel*DNP spectra given in (c) for $k = 1$, 0.8, 0.6, and 0.4, with increasing number of peaks for lower values of k. These peaks correspond to residues at increasing distances from the paramagnetic tag. Spectra (a) and (b) are 2D 13C–13C double-quantum single-quantum correlation spectra. Figure prepared with spectra from the protein LecA as described in ref. 154. Reproduced from ref. 8 with permission from the Royal Society of Chemistry.

into an MAS rotor. A number of DNP investigations of oriented membrane samples have been carried out,[158,159] either with MAS,[118,160,161] or under static conditions using custom-built hardware, such as a stripline RF probe[30] (using Overhauser DNP), or a flat-coil ssNMR probe[31,162] (using cross-effect DNP). While DNP enhancements obtained on static samples are relatively low, often under 20, it is nonetheless an interesting direction of further development, especially as the DNP enhancement can be achieved at ambient temperature.[30] For oriented samples investigated under MAS, the DNP enhancement can be improved (^{1}H $\varepsilon_{on/off}$ of up to 71) by optimizing the geometry of the membrane sample so that it is evenly distributed (equilibrated) on the walls of the rotor. The improvement in DNP enhancement was suggested to come from presumably more rapid and more homogeneous freezing of the membrane sample when it is well-equilibrated.[161]

3 Biomolecular applications

Prior to embarking on our overview of MAS-DNP applications, we feel it is important to recall what is biological structure and why it is of interest, in order to better contextualize how the technique can make contributions. For small organic molecules in solution, structure refer predominantly to the arrangement of atoms and covalent bonds; once these are determined, the distribution of conformations is relatively limited and can be accurately and quickly determined by computational techniques; though one must bear in mind that in the solid-state, the structure of crystalline packing of small molecules is frequently more challenging to determine.

Due to the large size of biological molecules, knowledge of the covalent linkages is insufficient for a full structural characterization in either solution- or solid-state. Proteins, nucleic acids, and glycans, are found as long chains which can potentially adopt a wide range of conformations, but often show strong preference towards a limited set. The determination of biomolecular structure requires knowledge of both the covalent linkages and

three-dimensional conformational arrangements. The conformations give an overall shape to the biomolecule, and also reveal specific exposed surfaces and interfaces, which are key to the function of the biomolecule. Classically, structural biologists aim to characterize the three-dimensional shape of biomolecules in order to gain insight into their function, which can inspire development of therapies and diagnostics.

For proteins, structure is understood hierarchically: the *primary structure* is the sequence of covalently bound amino acids; *secondary structures* are local conformations driven by hydrogen bonds, building typical structural elements like α-helices and β-sheets; the *tertiary structure* is the conformational arrangement of the linear polypeptide chain and all its local structural elements into a three-dimensional 'fold'; and finally, the *quaternary structure* is the arrangement of multiple folded polypeptide chains, generally with specific interfaces, as many proteins only function as multimeric assemblies. The RCSB Protein Data Bank (PDB) rcsb.org[163] contains essentially all known protein (as well as DNA and RNA) structures that were experimentally determined, mostly by X-ray diffraction, but also by NMR (both solution- and solid-state), and recently by 3D electron microscopy (most often cryo-EM). As for computational prediction of protein structure from the sequence alone, it is only very recently that robust success has been demonstrated by machine learning approaches.[164] Prior to this, the tertiary structures could only be determined experimentally. Even now, structure prediction at the quaternary level remain difficult, which is essential for multimeric proteins, protein complexes and assemblies, filamentous or fibrous proteins.

Given the astronomical possible degrees of freedom, it is impressive that many proteins will spontaneously adopt the precise conformation(s) that leads to biological function. Francis Crick famously hypothesized that 'folding is simply a function of the order of amino acids',[165] only guided by the physical forces that act upon the protein chain. This idea is subsequently followed by Anfinsen's thermodynamic hypothesis, that 'the three-dimensional structure of a native protein in its normal physiological milieu is the one in which the Gibbs free energy of the whole system is lowest; that is, that the native conformation is deter-

mined by the totality of interatomic interactions and hence by the amino acid sequence'.[166] The hypotheses above were then frequently simplified into 'one sequence, one structure' and accepted as dogma.

Since then, many exceptions have been found to contradict this simplified 'one sequence, one structure' concept. While some proteins do fold smoothly to a single well-defined structure, this folding behavior is not universal to all proteins. Local flexibility and dynamics of the native structure, including various conformations of the constituent domains, can be essential to protein function and are not always predicted by current computational methods or detected in experimental structural studies. Under certain physiological and in vitro conditions, instead of the native fold, many proteins have been shown to misfold. Such misfolded proteins can become kinetically trapped in a non-functional but stable and ordered form, the most well-characterized of which is the amyloid fold (see section 3.1.1). Especially in cases of proteins which can be found in various biological contexts or 'physiological milieus', it is not too surprising that the same protein sequence can adopt different structures, which are all functional; these are known as metamorphic or fold-switching proteins.[167,168] Finally, some proteins (or some regions of proteins) may be simply disordered at physiological conditions, and their energy landscape does not contain any clear set of thermodynamic minima; these are known as intrinsically disordered proteins or regions.[169]

Modern MAS-DNP was developed with the aim of eventually applying this technique on challenging protein systems, at the time where the first protein structures solved solely by solid-state NMR spectroscopy were published.[170,171] As the sequence-specific assignment of the protein requires numerous time-consuming multidimensional experiments, and long-range contacts often have to be extracted from especially weak cross peaks, the initial hope was that MAS-DNP could contribute to structural biology by enabling more rapid solving of protein structures.

The group of Griffin and coworkers has been key in driving the use of MAS-DNP in biological applications. A first proof-of-concept study demonstrated the potential of MAS-

DNP for biomolecular applications with the successful signal enhancement of a frozen solution of lysozyme at a static magnetic field strength of 5 T (140 GHz for the electron and 211 MHz for ^{1}H Larmor frequency), using helium gas for MAS to achieve a sample temperature as low as 25 K at a MAS frequency of up to 5 kHz[26] (Figure 9a). DNP enhancements were obtained thereafter on more complex biological assemblies, including fd bacteriophage, a type of filamentous viral particle, and bacteriorhodpsin (bR) in purple membrane, a dense assembly of proteins embedded in lipid membranes (75 weight % bR). This early work exemplified the capacity of MAS-DNP to improve sensitivity in a range of biological samples, though under static (non-MAS) conditions.[97] The first 2D MAS-DNP spectrum was obtained on an aqueous solution of proline, now using nitrogen gas to achieve MAS at 80–100 K. This work established a benchmark for the development of water-soluble radicals that would enable further biological applications of DNP[172] (Figure 9b). Subsequently, MAS-DNP was demonstrated on two U-^{13}C, ^{15}N cryoprotected proteins: a membrane protein (bR), and a soluble enzyme (α-lytic protease, α-LP). ^{15}N 1D spectra were obtained with good signal-to-noise ratio and clearly showed, in the former case, the lysine Schiff base in the 26 kDa bR, and in the latter case, the single histidine sidechain in the 18 kDa α-LP, thus demonstrating the power of MAS-DNP to probe functionally important residues present at low levels within moderate-sized proteins.[173]

As MAS-DNP became commercially available, signal enhancement was demonstrated on an increasing range of biomolecular systems under in vitro conditions, showing the broad applicability of this technique. In the process, it became clear that while MAS-DNP can deliver signal enhancement relatively robustly, the loss of resolution due to line broadening at low temperatures will prevent the technique from being a general structural biology technique in terms of solving protein structures on its own. However, it is unfair to assess the value of MAS-DNP solely on its (in)ability to independently solve protein structures thus far; the strength of MAS-DNP lies in delivering unique insights that cannot be feasibly observed in reasonable signal averaging time by conventional ssNMR, or other structural techniques.

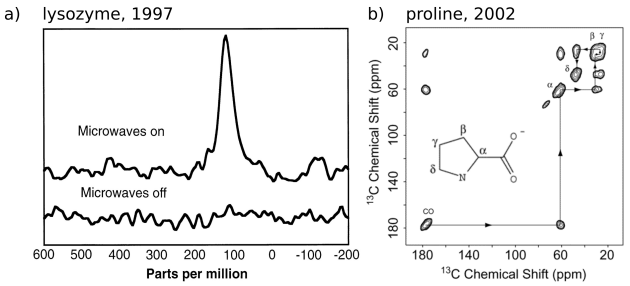

Figure 9: First applications of MAS-DNP on biomolecules. (a) DNP-enhanced ^{15}N CP-MAS spectra of ^{15}N-Ala–labeled T4 lysozyme (25 mg/ml) in glycerol/buffer (60/40, v/v) doped with 40 mM 4-amino-TEMPO, at a temperature of 40 K and a MAS frequency of 3.2 kHz. Top: microwave irradiation (139.60 GHz) was performed for 20 s with 1 W at the sample, 64 acquisitions were averaged with a 15-s recycle delay. Bottom: recorded under identical conditions with no microwave power. The magnetic field was set to maximize the positive enhancement, which is approximately 50. (b) 2D ^{13}C$-^{13}$C proton-driven spin-diffusion (PDSD) spectrum obtained on U-^{13}C, ^{15}N proline (120 mg/mL) in glycerol/water (60/40, v/v) doped with 40 mM 4-amino-TEMPO, at a temperature of 90.0 $\pm$ 0.5 K, the spinning frequency at 4.55 kHz $\pm$ 20 Hz, and the microwave power at 0.5 $\pm$ 0.05 W. All three variables remained stable over the course of this short 2D experiment (about 22 minutes), a first carried out under DNP conditions. For (a), from ref. 26. Reprinted with permission from AAAS. For (b), reprinted from ref. 172. Copyright 2002 American Chemical Society.

Within the rich landscape of biological structural diversity, MAS-DNP can indeed play an important role. Currently, the frozen conditions of MAS-DNP preclude determination of physiological dynamics, but can enable freeze trapping of transient or low-level conformations of importance. Moreover, MAS-DNP can potentially give a more accurate picture of the distribution of conformations present, illuminating the degree of polymorphism and the number of minor species present.

In addition, biological function is not only carried out by proteins, but involves a whole repertoire of molecules including nucleic acids, glycans, lipids, with covalent bonds and/or non-covalent interactions between all of these. Recognizing the myriad of biological contexts in which ssNMR is sensitivity-limited, and devising ways to overcome them by MAS-DNP, opens up multiple fruitful avenues of research. Especially successful investigations combine expertise in MAS-DNP with a deep knowledge of the biological system, in order to carry out the study in a manner that respects biological integrity and capture highly relevant insights on biological functions and mechanisms.

There is therefore great value in using MAS-DNP as part of integrative approaches where multiple techniques contribute complementary information on highly challenging systems. Thus, although many in vitro biomolecular systems have already been subjected to extended investigation by conventional solid-state NMR spectroscopy, the sensitivity gain enabled by MAS-DNP can bring further insights. In recent years, the field of structural biology has progressed from solving structures under in vitro conditions to investigating structures 'in situ', in the context of the cell or of extended complex biological environments, with many potential sensitivity-limited applications where MAS-DNP could play a role. Thus, MAS-DNP sits at a unique position to contribute highly specific insights on binding sites, interfaces, and for understanding structural diversity and disorder, all of which are current ongoing areas of research interest in broader structural biology.

For the following overview of MAS-DNP applications, we made the choice to present the various investigations in an approximately but not strictly chronological manner, grouping topics on the same biological context or theme together. Obviously, the first DNP applications were based on a more traditional approach, with studies carried out using biomolecular systems on which the investigator had a high degree of control. Frequently, these are relatively small proteins, possibly as well-defined multimeric assemblies. Later on, as the MAS-DNP technique became more established and accessible, investigations in ever more complex contexts, such as in cellular membranes, whole cells, cell walls, and human tissues, were performed. In these studies, there is less focus on structural details of a single biomolecule, but more emphasis on biomolecular interactions, cell physiology, or impact of metabolism.

3.1 Protein folding, misfolding and disorder

3.1.1 Amyloid fibrils

Depending on the conditions of folding, such as concentration, pH, temperature, and agitation, many proteins with different primary sequences were found to adopt a common

fold known as amyloid, where many protein units self-assemble into a stable fibril with a high degree of order and a distinct cross-β diffraction pattern, indicating the arrangement of β-sheet secondary structure elements perpendicular to the fibril axis. First identified in the pathological context of human neurological diseases, where normally functional proteins misfold to form amyloid assemblies,[174] amyloid folds have since then been observed to play functional roles in multiple other contexts, not only in bacteria and fungi but also in humans,[175,176] where they are part of normal physiology.[177] Interestingly, amyloids which are non-pathological and functional are becoming to be seen as the norm rather than the exception. It is envisaged that studies on non-pathological amyloids will illuminate broader pathways in biology, linking structure and assembly of these proteins to essential functions including pigment production and necrosis regulation in humans.[178,179]

Many of the neurological diseases associated with amyloid fibrils, such as Alzheimer's, Parkinson's, and various prion diseases, currently have no treatment; the hope is that by studying the structure of amyloid fibrils, and the mechanism by which they assemble, new routes for treating these degenerative and highly debilitating diseases can be found. SsNMR is a key tool in the structural characterization of amyloid fibrils; it is capable of obtaining atomic resolution information on these fibrillar assemblies and has successfully determined structures in a number of cases, though generally, isotopic labeling and in vitro fibril formation was required.[180] Since 2017, cryo-electron microscopy has been used to determine an increasing number of amyloid fibril atomic structures, especially with ex vivo samples isolated from patients suffering from these diseases.[181]

Despite the high degree of order and overall similarities, there is a propensity for disease-associated amyloids to form several polymorphic fibrils, even for proteins of the same primary sequence, and both in the case of in vitro assembled as well as ex vivo samples. Tycko has specifically reviewed amyloid polymorphism in many ssNMR structures;[182] more recently, Willbold et al. provided an in-depth review of the formation process of amyloid protein fibrils, illustrating some of the important structural variations,[183] while König et al. has specifically

reviewed the use of DNP-enhanced ssNMR to study amyloid fibrils.[9] Due to the relatively ordered nature of amyloid fibrils, ssNMR studies without DNP can often give spectra with very reasonable sensitivity and excellent resolution, especially for fibrils formed from smaller proteins/peptides. Early studies of amyloid fibrils using MAS-DNP frequently used rather short peptides or small amyloidogenic proteins to optimize methodological aspects, such as the functional yeast amyloid Sup35,[103,184] the bacterial amyloid CsgA,[144] a model amyloid PI3-SH3,[185] as well the pathogenic human amyloids transthyretin,[186] and Aβ40.[43] While some of the work was already covered in section 2, further context and biological significance of some of this early work is discussed below.

One of the earliest amyloid fibrils investigated by MAS-DNP is the yeast Sup35, which is not associated with human disease, but affects the inheritance of the color phenotype of yeast in a prion-like, non-Mendelian fashion due to the role it plays in translation termination.[187] From the prion domain of Sup35, the 7-residue core segment (GNNQQNY) is capable of forming amyloid fibrils and also nanocrystals, but with different dimensions. Therefore, it was used in the early investigations of MAS-DNP to establish how far hyperpolarization can be spread by spin diffusion.[103] Higher DNP enhancement were found on the fibrillar assemblies compared to the nanocrystalline preparation, as a result of the narrow width of the fibrils. Using different labeling schemes of the core peptide, assignment was obtained by DNP-enhanced 2D spectra. DNP enhancement was likely required to enable observation of interatomic correlations of up to 4Å, which were expected to have very low TEDOR transfer efficiency.[184] In order to better understand the structure of Sup35 prions, consisting of the N-terminal domain and the "M" middle domain (Sup35NM), Frederick et al. designed an elegant study using segmental isotopic labeling, where only the first 14 amino acids out of the 253-residue-long protein are enriched in NMR-active nuclei. This approach greatly reduced NMR spectral crowding, and enabled the authors to observe that different chemical shifts are obtained for the GNNQQNY (residues 7–13) core within the context of full-length NM fibrils, compared to the microcrystalline form of the protein, or to fibrils formed from the 7-residue

peptide alone. MAS-DNP was essential in this study to overcome the sensitivity challenge of a relatively small amount of labeled sample within its unlabeled context, as well as to obtain long-range TEDOR correlations.[65] Sup35NM was also investigated by MAS-DNP at endogenous concentration in cell lysates (see section 3.5).

Another early MAS-DNP study was performed on the well-characterized amyloid fibril composed of the SH3 domain of one of the subunits of bovine phosphatidylinositol 3-kinase (PI3-SH3). PI3-SH3 normally adopts the SH3 β-barrel fold (usually 60–85 residues) and is not associated with any amyloid diseases. It has, however, been used as an amyloid model system as it forms fibrils under specific in vitro conditions, and contributed to the insight that such fibrils can form regardless of the original sequence or structure.[188] Long-range heteronuclear experiments using DNP enhancement provided 52 assigned cross-peaks in 32 hours, compared to about 23 obtained under routine ssNMR conditions after 16 days of signal averaging.[185] Similarly, on amyloid fibrils formed with a 11-residue segment from transthyretin (TTR), a 55 kDa transport protein normally circulating in plasma and cerebrospinal fluid which can form amyloid fibrils leading to nerve degeneration and cardiac dysfunction,[189] the sensitivity enhancement brought by DNP shortened a DQF-DRAWS buildup experiment from 3.5 days to 1.5 hours. Interpretation of the DNP data confirmed the parallel in-register intra-sheet arrangement.[186]

Weirich et al. investigated amylin, also known as islet amyloid polypeptide (IAPP), a 37-residue protein hormone secreted by the pancreas and prone to amyloid formation especially in type 2 diabetes mellitus patients. In this protein, the eight-residue N-terminal loop was considered to be well-ordered with particularly narrow lines in conventional ssNMR spectra. However, spectra acquired with MAS-DNP showed very broad lines, indicating in fact a drastic loss of dynamics.[190]

Interestingly, many intrinsically disordered proteins (IDPs) appear to be associated with amyloid diseases. The most famous of which is α-synuclein (αS), a 140-residue IDP that is important for function and integrity of nerve synapses, has a chameleon-like conformational

plasticity, but is also found in amyloid fibrils in Parkinson's disease, dementia with Lewy bodies, and multiple system atrophy. αS is known to adopt a α-helical conformation in the presence of membranes, and a β-sheet conformation (as is common) when in an amyloid fibril. By [2-^{13}C] glucose supplementation, Uluca et al. obtained αS that was specifically labeled at valine Cα and Cβ which acted as reporters on local secondary structure. MAS-DNP was used to investigate the distribution of trapped conformations of αS in frozen solutions of monomers, of monomers bound to lipid nanodiscs, and in amyloid fibrils. The distribution of α-helical and β-strand αS was found to vary across the three cases as expected. Surprisingly however, a subpopulation of valines in an α-helical conformation was present even for αS amyloid fibrils, which may report on disordered regions of the amyloid fibril assembly (Figure 10).[191]

In a further study by the same group, the interaction of αS monomers with phospholipid bilayer nanodiscs was investigated in detail. The nanodisc environment was explored by varying the composition, size, fluidity, and charge. The authors also investigated the influence of post-translational modifications of αS such as N-terminal acetylation, which can affect membrane association. While most of this study was carried out with solution-state NMR, MAS-DNP was specifically used to detect the nanodisc-bound state of non-acetylated αS, which confirmed that about 92% of valines are in an α-helical conformation and likely interact with the membrane. This observation provided a direct confirmation of the expected proportion (94.7%) of membrane-bound valines obtained from the solution-state NMR attenuation profile.[192]

Another IDP that can form amyloid fibrils and is implicated in Alzheimer's and other neurodegenerative diseases is tau. Normally associated with microtubules of the cytoskeleton, tau is a multidomain protein with six isoforms, ranging from 352 to 441 residues. In order to form amyloid fibrils of recombinant tau in vitro for structural studies, negatively charged co-factors such as heparin are generally required. These co-factors can however predispose formation of artificial polymorphs that are not found in patient-derived samples.[193]

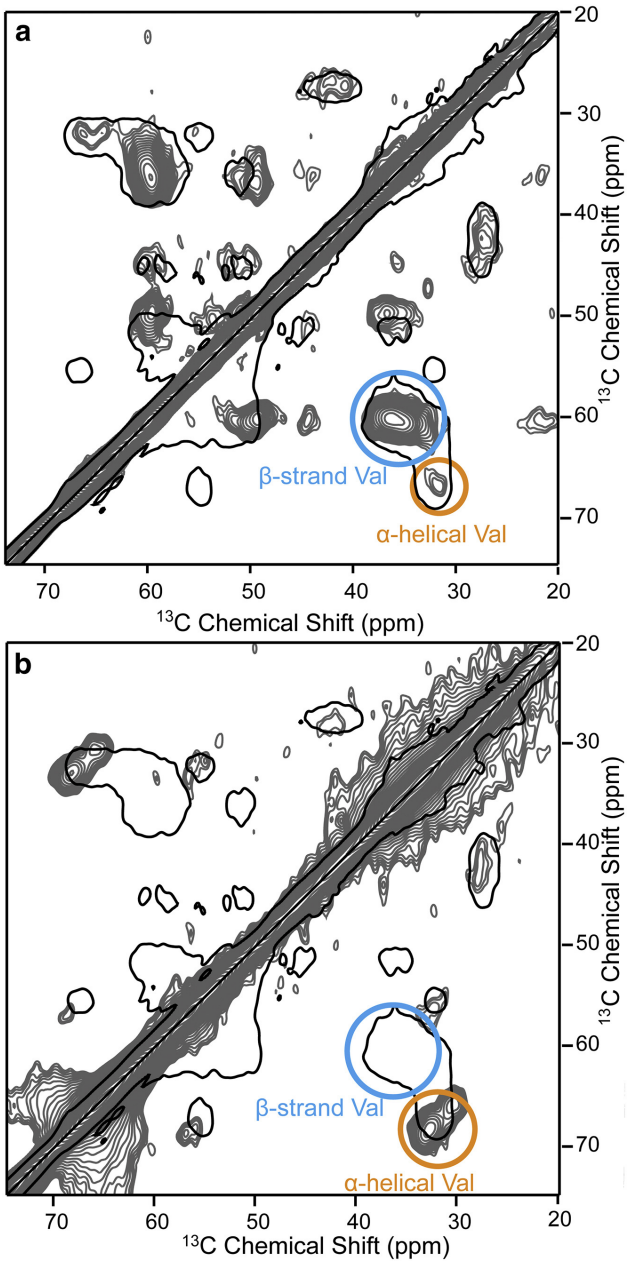

Figure 10: DNP-enhanced 2D ^{13}C−^{13}C PDSD spectra of specifically ^{13}C-labeled α-synuclein (a) fibrils and (b) monomers bound to lipid nanodiscs. Circles indicate areas of valine chemical shift corresponding to α-helical (orange) and β-strand (blue) secondary structures. The black outline is the lowest contour level of the spectrum of monomeric α-synuclein, provided for comparison. Reprinted with permission from ref. 191. Copyright 2018 Elsevier.

Chakraborty et al. developed a method to produce co-factor free amyloid fibrils using the longest isoform of tau. Due to the size of this protein and the presence of repeating domains, it is highly challenging to obtain specific assignments and structural features by NMR. While much of this study was carried out with conventional solution and solid-state NMR, highly specific labeling of valine $^{13}C_{\gamma}$, phenylalanine ^{13}C-ring, and histidine ^{15}N was used to seek out correlations in the assembled fibrils using MAS-DNP. These correlations are in agreement with the cryo-EM structure of patient-derived ex vivo tau fibrils, but differ from the structure of heparin-induced tau fibrils that were commonly investigated. Despite the sensitivity challenge, the importance of investigating co-factor free tau fibril is illustrated by its different surface charge distribution, which give rise to strong RNA interactions possibly implicated in disease progression.[194]

Thus far, most MAS-DNP investigations of human-disease associated amyloids have been performed on recombinantly expressed U-^{13}C, ^{15}N proteins, instead of patient-derived or ex vivo fibrils. The development of MAS-DNP methodology to provide sufficient sensitivity on natural abundance samples, especially those with a certain degree of polymorphism and heterogeneity, is essential for future investigations in this area. A step in that direction has been done by De Paëpe's group with a study on amyloid fibrils based on mutant Huntingtin fragments at their natural isotopic abundance. Huntingtin is a protein with intrinsically disordered regions, which plays a role in cellular homeostasis, especially in the brain. Mutations can lead to an expanded polyglutamine (polyQ) domain prone to form amyloid fibrils, resulting in the severely debilitating Huntington's disease. Thanks to the sensitivity enhancement of MAS-DNP, Smith et al. demonstrated 2D $^{13}C-^{13}C$ and $^{15}N-^{13}C$ correlations experiments using natural abundance samples of in vitro-assembled protein (111 residues) or peptide (19 residues) fibrils. An advantage of working at natural abundance is that the $^{13}C\alpha-^{13}C\alpha$ DQ buildup curves were not affected by dipolar truncation,[195] enabling the extraction of long-range inter-strand distance contributions which are in agreement with the antiparallel arrangement of the β-strands (Figure 11). The analysis was completed without

supplementary conventional ssNMR experiments and suggest a possible route for analysis of ex vivo patient-derived amyloid samples.[196]

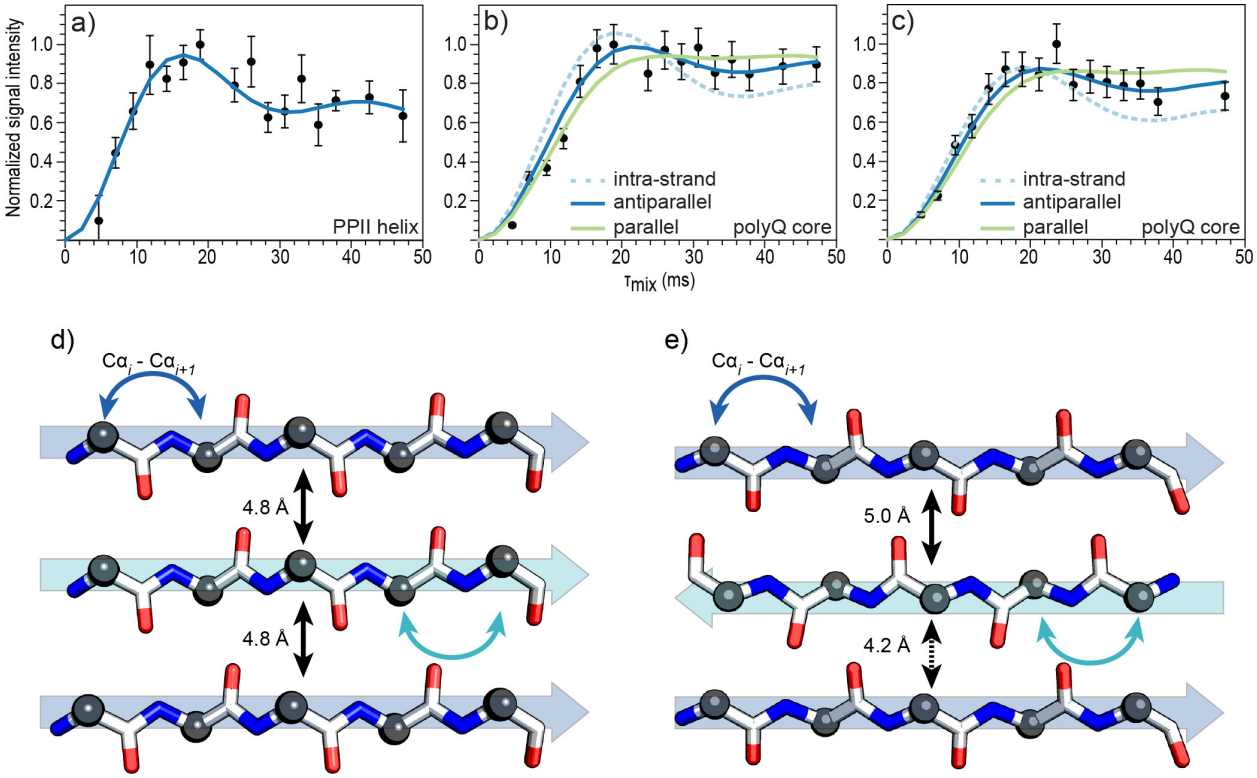

Figure 11: $^{13}C\alpha-^{13}C\alpha$ buildup curves for (a) the polyproline helix segment of Q44-HttEx1, a mutant huntingtin serving as model for the disease protein, (b) the polyQ core of Q44-HttEx1, (c) the polyQ core of the peptide model $D_2Q_{15}K_2$. Experimental data (black circles) were obtained by monitoring the buildup of signal intensity of C$\alpha-$Cα correlations as a function of DQ mixing time. Simulations for intrastrand distances (dashed line), parallel β-strand arrangement (green line), and antiparallel β-stand arrangement (blue line) are shown in panels (b) and (c), while a 3.6 Å distance is used in panel (a). Canonical backbone conformations of (d) parallel and (e) antiparallel β-strands are illustrated. The antiparallel arrangement of the β-strands was found to provide a best fit to the data. The absence of dipolar truncation in natural abundance samples resulted in sensitivity of the buildup curves to distances up to 5+ Å in this case. Reprinted from ref. 196. Copyright 2018 American Chemical Society.

3.1.2 Folding pathways

The timescale of the protein folding process varies widely, with smaller proteins (shorter polypeptide chains) generally folding faster, up to the order of milliseconds. Not all regions of the protein fold at the same rate—frequently, secondary structures such as α-helices are

formed first, in the same time range as certain domains functioning as a structural unit, followed by more global folding of the whole protein chain with secondary structure elements and domains coming together in space. At the low temperature conditions of MAS-DNP, it is possible to trap transient states and conformations which would not persist over the measurement time of conventional NMR. Tycko has reviewed ongoing development on this topic using solid-state NMR and DNP at nitrogen and helium cooling temperatures.[10]

In an extensive study of the successive stages of Aβ40 self-assembly into amyloid fibrils, Potapov et al. produced four different samples in specific experimental conditions to obtain either monomers (high pH), oligomers (neutral pH), protofibrils (incubation for 4 h at neutral pH), or fibrils (after cycles of sonication and incubation). These different states of Aβ40 were then characterized by various biophysical methods, with MAS-DNP as the main structural characterization tool to improve the sensitivity of ssNMR experiments. Indeed, the use of frozen solutions instead of lyophilized powders allow retention of transient species, but reduces sensitivity. In order to overcome line broadening and spectral overlap, several highly specific labeling patterns were used, with no more than 4 sites of the 40 residue Aβ40 peptide labeled in any sample; this approach led to straightforward spectral assignment. 2D $^{13}C-^{13}C$ correlation spectra acquired with MAS-DNP provided side-chain contacts which indicated that a U-shaped conformation was present in all stages of fibril formation and not only in mature fibrils. This structural property could potentially be used to disrupt fibril formation.[133] This work was carried out on a home-built MAS-DNP probehead that can operate at 25 K via helium cooling[197] and uses a triradical polarizing agent.[86]

Based on insights from this previous work, Tycko and coworkers developed instrumentation for rapid mixing and freeze-trapping of solubilized proteins on a precooled rotating copper plate (Figure 12a). Using this setup, they investigated the dynamics of the folding and aggregation process of melittin, a 26-residue peptide found in bee venom. This peptide undergoes rapid conformation change from unstructured to helical when the pH is increased. This folding process is accompanied or followed by further self-assembly into dimers and

tetramers. Using a series of 2D DNP-enhanced $^{13}C-^{13}C$ correlation spectra, the structural evolution of melittin labeled only at three residues was followed after a sudden increase in pH. Within the first 10 ms after the pH jump, a significant decrease in linewidth of the NMR signals from 5 to 2 ppm was observed (Figure 12c), indicating a transition from the unstructured to the helical structure.[198] In this study, only 20% of glycerol was used, high enough to maintain formation of a glassy frozen matrix, but low enough to avoid an increase of the solution viscosity, which could have interfered with the mixing process prior to freezing and affect the time scale of the folding process.

The folding of a protein complex including calmodulin (CaM) was studied using the same rotating copper plate setup as above. CaM, a 149-residue protein, is involved in calcium binding. Once charged with two Ca^{2+} in each of the two domains, CaM can bind to M13, a 26-residue peptide which is part of skeletal muscle myosin light chain kinase. In this study, CaM was either unlabeled or specifically labeled at the methionine methyl carbon, while M13 was labeled at three to four specific residues. The small number of labeled residues made it easier to assign and observe intermolecular correlations broadened by the frozen state. MAS-DNP at 25 K, with a triradical polarizing agent[87] was required to overcome the strongly limited sensitivity of the diluted protein frozen solution. Using rapid mixing and freezing, the formation of the protein complex can be observed at the millisecond timescale, with strong spectral changes observed even in the first 1.5 ms.[199] In a follow-up study, the MAS-DNP data obtained on the CaM–M13 complex was quantitatively analyzed and combined with EPR-based double electron-electron resonance data for a global fit that can link known structures of known states in this highly dynamic complex.[200] These studies provide a unique view into CaM conformational change during complex formation and is of interest to understand the biological role and function of this very highly conserved protein.

Protein folding can begin while the protein chain is still being produced on the ribosome during the process of translation ('co-translational folding'). This type of folding can proceed via different intermediate states compared to the folding of the whole protein in dilute

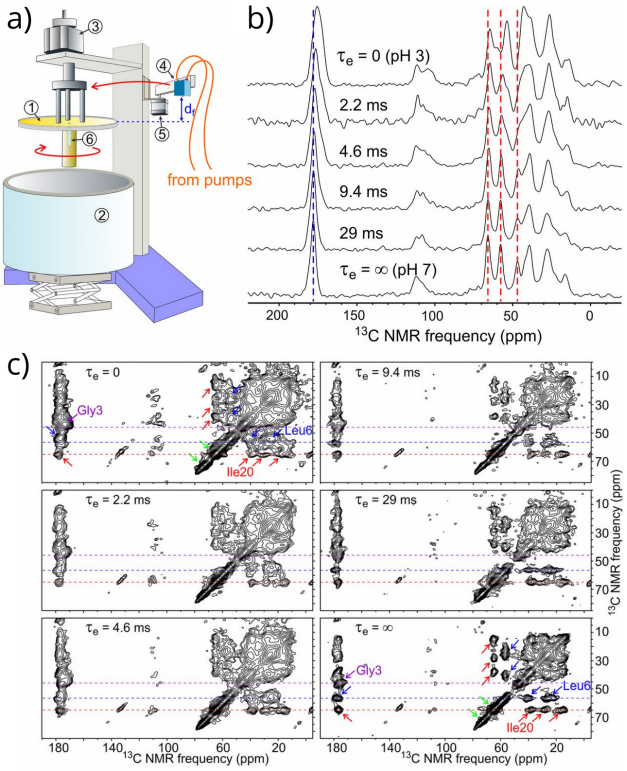

Figure 12: a) Schematic of the apparatus for rapid mixing and freeze-trapping of solubilized proteins. A copper plate (1) is precooled by immersion in a liquid-nitrogen bucket (2), and then rotated continuously by a motor (3). Two solutions are pumped through a mixer (4) that sweeps across the rotating plate under the control of a stepper motor (5). A jet of mixed solution freezes on the rotating plate after traveling a variable distance d_f that determines the structural evolution time τ_e. After rotation stops, the plate is immersed in liquid nitrogen. The frozen solution is scraped from the plate and packed into a MAS rotor (6) for low-temperature ssNMR measurements. b) DNP-enhanced DQ-filtered ^{13}C spectra of frozen melittin at increasing structural evolution time. c) DNP-enhanced ^{13}C$-^{13}$C spectra of melittin solutions at increasing structural evolution time, with spectral change indicating structural rearrangements through the folding process. The dashed lines indicate the $^{13}C_\alpha$ chemical shifts for Gly3, Leu6, and Ile20 in the fully folded tetrameric state at pH 7.0 (i.e., $\tau_e = \infty$). Adapted from ref. 198, 2019 National Academy of Sciences.

solutions, due to the balance between the rates of protein folding and of translation. Folding can also be influenced by interactions of the nascent chain with the ribosome surface.[201] The processes involved in initiation of translation and the subsequent folding are highly dynamic and structurally interesting. However, observing a relatively small translation initiation factor or nascent chain (around 10 kDa) that is bound within the far larger ribosomal complex (2–4 MDa) is very challenging in terms of sensitivity and inherent instability of the complex. A few studies have made use of both the sensitivity enhancement and the additional stability provided by the experimental low temperature conditions of MAS-DNP to enable observation of nascent peptide chains as well as their conformation and interactions with the ribosome.

Gelis et al. tested a number of sample preparation protocols to optimize the enhancement factor $\varepsilon_{on/off}$ to 25 for sedimented ribosome samples. An important methodological point investigated in this work was the usage of viscous glycerol- or sucrose-containing buffers acting as a 'cushion' during ultracentrifugation, to selectively sediment the bound complex and not its constituent parts into the rotor. The complex investigated was the prokaryotic translation initiation factor (IF1), a protein of about 70 residues in length, bound to the small ribosome subunit of *E. coli* (E30S). To alleviate spectral crowding, selective labeling was used for histidine and tyrosine residues of IF1. Even when complexed to unlabeled E30S, IF1 yielded 2D DNP-enhanced spectra with a good ^{13}C resolution of 1 ppm at 9.4 T.[202]

The nascent protein chain, which is the segment that is initially formed during translation, contains a so-called signal peptide that indicates the fate of the protein in the cell via interactions with specific cellular biomolecules. In this context, conformation of the signal peptide within the ribosome may be of importance. Lange et al. investigated the conformational state of a construct consisting of the 20-residue signal peptide of disulfide oxidoreductase A fused to a 17-residue stalling sequence (SecM). The role of the stalling sequence was to arrest translation at a consistent point, ensuring the formation of a stable ribosome–nascent chain complex (RNC). DNP-enhanced DQ-SQ ^{13}C$-^{13}$C correlation spec-

tra were used to filter out background signal from the unlabeled ribosome. The measured chemical shifts of some resolved residues of the labeled peptide were used together with the known dimensions of the ribosomal exit channel to model the likely secondary structure of the peptide within the ribosome. Interestingly, the authors found that the peptide adopted a mostly extended conformation, instead of the expected helical conformation present in solution.[203]

On the same topic, a multidisciplinary, highly collaborative study by Schulte, Mao, Reitz et al. provided a detailed view of the eye-lens protein γB-crystallin (GBC) in the ribosomal exit tunnel. In this work, RNCs were also used to produce a translation-arrested state using SecM. Multiple ribosome complexes with nascent chains of varying lengths were expressed, with specific labeling at cysteine residues to follow disulfide bond formation. For the ssNMR part of the study, DNP enhancement was required as the large size of the RNCs allowed only for a small number of complexes (2–3.4 nmol) to be packed into the rotor. After significant optimizations a good $\varepsilon_{on/off}$ of 150 was achieved, enabling tracking of the proportion of oxidized and reduced cysteine residues in the Cα–Cβ region of the DQ-SQ $^{13}C-^{13}C$ correlation spectra. The large number of signals detected indicated that the nascent chain adopts multiple conformations within the exit channel, including non-native compact conformations.[204]

3.1.3 Conformation distributions in other applications

Besides understanding folding pathways, characterizing structural disorder and conformational distribution is of high relevance to understand biomolecular function. The low temperature used in MAS-DNP leads to the freezing-out of conformations, potentially giving access to this information. Thus, the conformational sampling of the isoleucine sidechains in small peptides and proteins was investigated using MAS-DNP, which can enable low-populated states to be observed.[205] In a recent multidisciplinary investigation, Holmes et al. reports on an intermediate of the enzyme tryptophan synthase. Using conventional ssNMR at room temperature, it was determined that this intermediate is in equilibrium between the

phenolic (89%) and the protonated (11%) Schiff base tautomers. At 95 K, the tautomeric equilibrium is expected to shift predominantly to the phenolic form (more than 90%), which was confirmed experimentally using MAS-DNP.[206]

MAS-DNP has been applied as well to the topical issue of vaccine development. Vaccine formulation requires relatively small amounts of the active biomolecule, which is diluted with other components to maintain the stability and delivery efficacy. Koers et al. investigated a 15-residue peptide vaccine formulated in liposomes, that was designed to target Alzheimer's disease. Considering the low peptide to lipid ratio (1:200), DNP was essential to overcome the strong sensitivity limitation. The conformations of the liposome surface-bound peptide were analyzed, leading to the finding that a proportion of the peptide is undergoing spontaneous aggregation into β-sheet-like units.[207] Another study on vaccine formulation was carried out in collaboration with Sanofi Pasteur, where several aluminum-containing gels used as vaccine adjuvants were compared by MAS-DNP. The antigens to be delivered in these vaccines are typically at 10–100 µg of protein per mg of Al, therefore requiring DNP signal enhancement for their NMR investigation. The system was composed of hepatitis B surface antigen particles tightly associated to phospholipids and the aluminum-based adjuvant. These components were respectively tracked using ^{31}P and ^{27}Al NMR, and the associations therein investigated with INEPT and REAPDOR experiments, with DNP enhancement factors of 92–128. Thus, the type and strength of binding of three different aluminum-containing gels to the antigen were characterized, which may contribute to the optimization of vaccine formulations.[208]

In a further study by the same group, the structure of antigens chemically coupled to the surface of large virus-like particles was investigated by sensitive NMR techniques, including MAS-DNP and ^{1}H-NMR detection under fast MAS. The antigen under study was the influenza virus hemagglutinin stalk long α-helix (LAH), which is highly conserved and could potentially serve as a universal influenza vaccine component, though it suffers from low efficacy; thus, the authors coupled LAH to the surface of virus-like particles (VLPs), which

are used in the pharmaceutical industry to heighten the immune response. To ensure that the coupling process did not perturb the structure of LAH, MAS-DNP and ssNMR proton detection at fast MAS were used to characterize VLP-coupled LAH structure and compare it to the structure of microcrystalline LAH determined via ^{1}H-detected ssNMR. DNP spectra indicated that the antigen core remained intact upon coupling to VLP (Figure 13).[209]

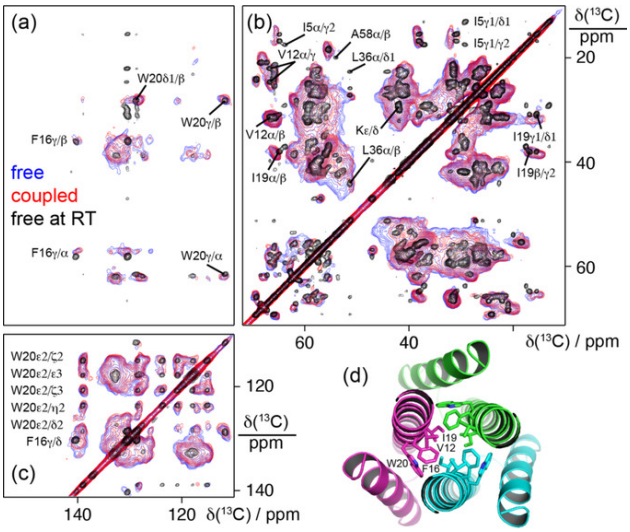

Figure 13: Comparison of free and VLP-coupled LAH antigen. a—c) Overlays of DNP-enhanced 2D CORD spectra of U-^{13}C,^{15}N-labeled free (blue) and VLP-coupled (red) LAH antigen at 800 MHz and 115 K with 40 kHz MAS with the room temperature 2D DARR spectrum of free LAH antigen (black) at 800 MHz with 20 kHz MAS. d) Crystal structure of LAH antigen showing the side chains of V12, F16, I19, and W20 that make up the hydrophobic core of the trimer. The similarities between the MAS-DNP spectra (blue, red) and the room temperature spectrum (black) indicate the same structural features are likely to be found in both free and VLP-coupled LAH antigens. Reprinted in part with permission from ref. 209. Copyright 2021 John Wiley and Sons.

3.2 Nucleic acids and their complexes

Nucleic acids are essential for carrying genetic information and transferring it into the biosynthesis, structure, and interactions of other biomolecules. Of the nucleic acids, ribonucleic acids (RNA) are especially versatile, performing a range of key enzymatic functions that transfer genetic information into proteins. From the perspective of structural characterization, RNA molecules and complexes can be difficult to crystallize for diffraction stud-

ies; NMR characterization of RNA is generally more challenging than that of proteins due to spectral crowding, conformational flexibility, and difficulty of establishing sequential assignment. Still, many small RNA complexes and their dynamics have been investigated by solution-state NMR. Solid-state NMR can be attractive for characterizing larger RNA complexes, though it often suffers from broad linewidths and poor sensitivity. From the perspective of MAS-DNP, nucleic acids have the fortuitous property of having fewer methyl groups than other biomolecules, which can potentially lead to more efficient DNP enhancements. The group of Corzilius has been very active in developing DNP methods to investigate RNA-based systems, e.g. using paramagnetic metal ions instead of biradicals as polarizing agents. This choice leads to the use of the solid-effect rather than the cross-effect mechanism for generating nuclear polarization. In a methodologically-motivated study, methyl groups were re-introduced to a 57-mer RNA aptamer via tight-binding to tetracycline to enable SCREAM-DNP investigations.[210]

As a proof-of-principle, Wenk et al. investigated the well-studied hammerhead ribozyme (HHRz) by MAS-DNP, which contains a divalent metal ion co-factor required for the RNA cleavage function of this enzyme. While minimal HHRz constructs have been studied by solution-state NMR, this is the first NMR study on the full-length variant. The 18 kDa, 59-mer full-length inactivated HHRz was expressed with uniform ^{13}C, ^{15}N labeling and bound to Mn^{2+} or Mg^{2+} metal ion co-factors. The endogenously bound paramagnetic manganese(II) ion in the former was used for DNP enhancement via the solid effect, giving a moderate $\varepsilon_{on/off}$ of 8, while DNP via the cross effect with the more conventional biradical AMUPol was also carried out for comparison and achieved an $\varepsilon_{on/off}$ of 240. Despite the lower enhancement, this work illustrates the possibility of achieving noticeable signal enhancement using paramagnetic metal ions, with capacity for further optimization.[211]

A subsequent study on a 67-mer HHRz formed from the spontaneous hybridization of two differently isotope-labeled strands was carried out by Daube et al., enabling the investigation of inter-strand/stem contacts. With 5 mM AMUPol in the standard glycerol/water

mixture, an $\varepsilon_{on/off}$ of 160–200 was obtained on frozen solutions containing 500–840 µM HHRz. In fact, this enhancement enabled the acquisition of 1D spectra of good signal-to-noise in only 4 scans, while no signal at all could be observed after one hour (512 scans) of signal averaging without DNP. Using DNP-enhanced TEDOR and PDSD experiments, subtle differences of canonical and non-canonical base-pairing in HHRz with and without Mg^{2+} could be observed (Figure 14). The use of direct DNP with solid effect via Mn^{2+} was again demonstrated, though only qualitative structural information could be obtained in terms of residue proximity in the differently labeled strands.[94]

Wiegand et al. carried out a MAS-DNP investigation of DnaB helicase, a large DNA-protein complex from *Helicobacter pylori*. The large multimeric protein (12×59 kDa) of this complex unwinds DNA during replication. The authors investigated the binding of DnaB to an ATP-analogue (AMP-PNP) and to single-stranded DNA. For this, a sample directly sedimented in the rotor without glycerol was found to be the most sensitive (likely due to better filling of the rotor), despite a lower $\varepsilon_{on/off}$ enhancement of about 20 compared to 30 for the glycerol-containing sample. The polarization transfer from the ^{31}P of the nucleotide to the ^{13}C spins of the uniformly labeled protein was carried out via a single $^{31}P-^{13}C$ CP step. This direct polarization transfer (without proceeding via ^{1}H) is of rather low efficiency and can be difficult to achieve without MAS-DNP. Results of this study allowed the authors to propose residues potentially involved in ADP- and DNA-binding.[116]

3.3 Viral particles

A virus is an infectious agent that is only capable of replicating inside a living host cell. Each type of virus can infect specific host cells, with the specificity applying to a type of cell in multicellular organisms, a species, or even a kingdom of life. Viral particles are usually much smaller than cells. They consist of a core of genetic material in the form of nucleic acids surrounded and protected by a protein-based shell known as the capsid, which can adopt various morphologies. Sometimes, the capsid is further enveloped by a

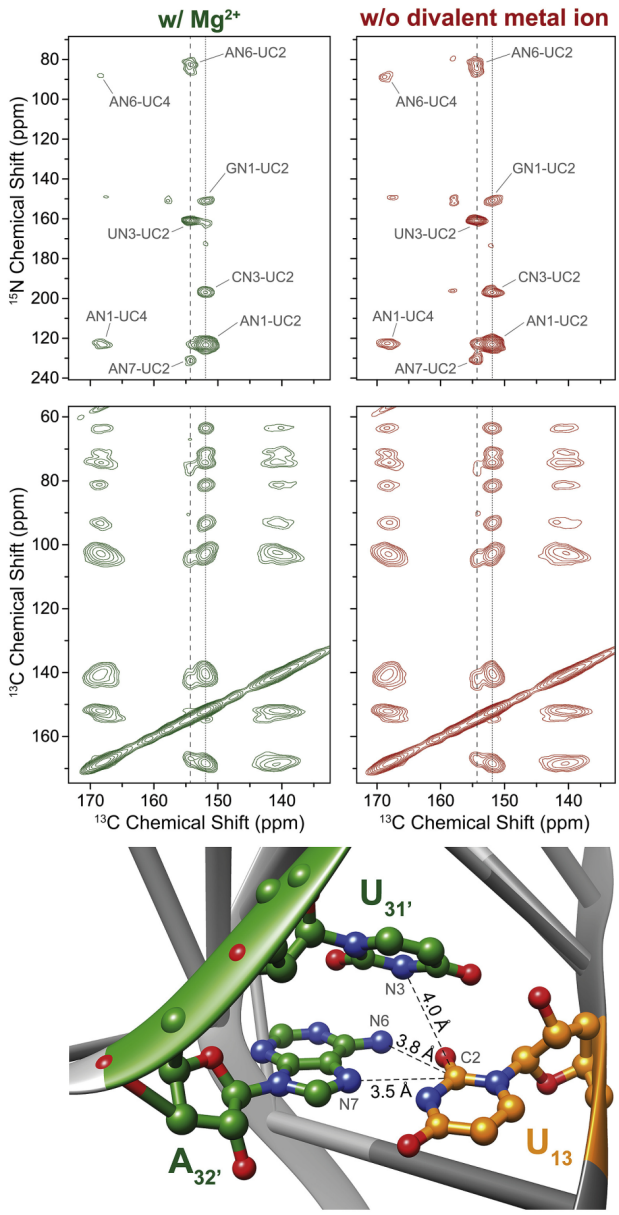

Figure 14: DNP-enhanced 2D spectra obtained on hybridized HHRz with Mg^{2+} (left panels) and without divalent metal ion (right panels). $^{15}N-^{13}C$ TEDOR (top spectra) and $^{13}C-^{13}C$ PDSD (bottom spectra) indicate presence of canonical base pairing (solid line, ^{13}C 152 ppm) and non-canonical base pairing (dashed line, 154 ppm). A structural model indicating the observed non-canonical, reverse Hoogsteen-type base pairing is shown on the crystal structure (PDB 2OEU). Adapted with permission from ref. 94. Copyright 2019 Elsevier.

lipid bilayer membrane. Viral capsids are often composed of multiple components, have a high degree of symmetry, and frequently have some degree of structural heterogeneity and/or conformational flexibility. Understanding the structure of viral particles, in particular insights on their assembly, can lead to development of new interventions for viral human diseases. The challenges of the relatively large size (often in the megadalton range) of the viral assemblies and the potential structural heterogeneity can be overcome by using ssNMR. A recent review provides an overview of the use of ssNMR, including MAS-DNP, for structural studies on virus and viral assemblies.[14] In this section, we focus on insight specifically enabled or delivered by MAS-DNP on these systems.

Human Immunodeficiency Virus Type 1 (HIV-1) is the causative agent of acquired immunodeficiency syndrome (AIDS). HIV-1 is a spherical viral particle which contains a conical capsid assembly when the virus has undergone maturation, that means after the virus has been released from the previous host cell but before it is capable of infecting a new host cell. The maturation process involves a poorly-understood cascade of proteolytic events of the Gag protein. The Gag protein contains several domains, of which the capsid (CA) and spacer peptide 1 (SP1). Both domains form an assembly that reflects an intermediate of the maturation process. Cleavage of the SP1 peptide leads to the final mature assembly. Using MAS-DNP at 109–180 K, various structural aspects of this maturation intermediate state were revealed, which were not previously observed by conventional ssNMR. This includes the presence of multiple conformers at cryogenic temperatures, the random coil conformation of SP1, and the dynamics and intermolecular contacts of aromatic residues in the hinge region of the capsid protein.[111]

The degree of disorder was further investigated in two viral assemblies, the HIV-1 CA and bacteriophage AP205 virus-like particles (VLPs). For the former, 2D and 3D heteronuclear NCACX correlation spectra were recorded in only 0.6 and 1.7 h with DNP enhancement. With the help of previous assignments obtained at ambient temperature using conventional ssNMR and solution-state NMR, analysis of the DNP-enhanced 3D spectra led to the assign-

ment of some residues which had poor or undetectable sensitivity with conventional ssNMR, such as aromatic side-chains and residues involved in a flexible loop of CA that interacts with cyclophilin A (CypA). The conformational plasticity of CA and its interaction with host factors such as CypA are critical for capsid assembly and maturation. For both viral assemblies, a good agreement was found between the experimental chemical shift distributions observed under the cryogenic conditions of MAS-DNP and molecular dynamics simulations performed to probe the conformational distribution, suggesting that this combined approach may give insight in the degree of order and disorder at a residue level in viral assemblies.[212]

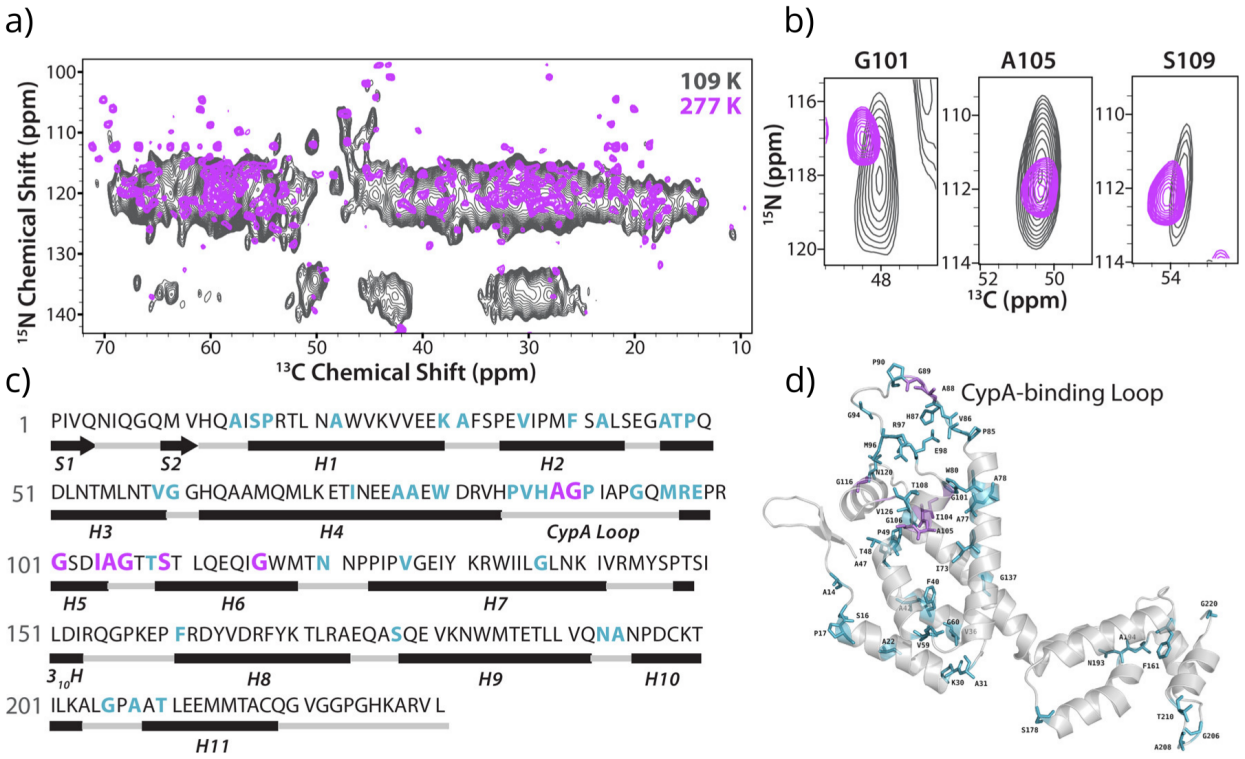

Figure 15: Comparison of MAS-DNP and ssNMR spectra of U-^{13}C,^{15}N CA tubular assemblies. (a) Overlay of 2D NCACX spectra acquired with MAS-DNP (14.1 T, 109 K, gray) and at ambient conditions without DNP (21.1 T, magenta) with (b) three relatively well-resolved signals. (c) Primary amino acid sequence of CA annotated with the secondary structures for α-helices (H) and β-sheets (S). (d) Structure of CA (PDB: 3NTE) on which the DNP-assigned residues are labeled in cyan. In (c,d), the residues for which the chemical shift distribution under DNP conditions were analyzed are colored magenta. Reprinted in part from ref. 212. Copyright 2019 American Chemical Society.

Filamentous bacteriophages are viruses with a long, rod-like morphology, consisting of

a helical protein capsid that contains genetic material in the form of a single molecule of circular single-stranded DNA. Due to their ease of culture and dense protein content, as well as their ability to orient in a magnetic field, filamentous bacteriophages have been investigated by ssNMR and also used in early proof-of-concept MAS-DNP studies.[97] The unusual conformation of the single-stranded DNA in Pf1 bacteriophage was investigated by Sergeyev et al. MAS-DNP enabled the most complete ^{13}C and ^{15}N assignment to nucleotide type in this work, though some assignments were carried out without DNP at 213–243 K for resolving crowded regions. The assigned chemical shifts were compared to previously reported values in the Biological Magnetic Resonance Bank (BMRB),[213] and were found to often be shifted above or below known chemical shift ranges. These observed chemical shifts are likely due to the unusual conformation of DNA in these viruses that is not base-paired in the filamentous virion.[214]

In a further study by the same group, a sequential side-chain–side-chain (S^3) pulse sequence was introduced, based on two directional SPECIFIC-CP steps, which is suitable for carrying out residue-specific assignment of proteins using side-chain resonances to overcome the issue of spectral crowding. Using MAS-DNP, 3D S^3 spectra were obtained in one day. On the base of a suite of 3D experiments, the authors were able to assign de novo 100% of the ^{13}C and 94% of the ^{15}N resonances of the Pf1 major coat protein (46 residues). The linewidths of the DNP spectra were further improved with sparse labeling and faster MAS of up to 25 kHz using 1.9 mm rotors. In this case, the S^3 sequence was shown to be superior to more conventional NCACX/NCOCA experiments by providing direct Cα–Cα correlations. Chemical shift perturbations (CSPs) were observed in specific regions of the protein, in correlation with larger linewidths under DNP conditions, suggesting that both are sensitive to hydration.[215]

In the context of the study of bacteriophage ϕ6, an interesting labeling method was developed by Alphonse et al. The inner icosahedral capsid of bacteriophage ϕ6 was reported to assemble in vitro by mixing four purified protein components (P1, P2, P4, P7), but only

with an efficiency of 25%.[216] For more efficient assembly and enabling the investigation of the P4 component in the capsid, a sequential expression method was designed in *E. coli*. It made use of two plasmids with orthogonal induction mechanisms, such that P4 component is isotopically labeled while the other components remain unlabeled. After expression, the proteins undergo intracellular assembly into procapsids (inner capsids without the genomic content), which were then extracted and isolated for further ssNMR study. As the labeled protein P4 (33 kDa as isolated protein, 2 MDa in procapsids) is a minor component of the procapsid (over 13 MDa), enhancement by MAS-DNP was crucial. The procapsid samples provided a DNP enhancement $\varepsilon_{on/off}$ of up to 41, enabling e.g. 2D $^{15}N-^{13}C$ correlation experiments with ^{13}C at natural abundance (procapsids with ^{15}N-labeled P4).[216]

3.4 Proteins in synthetic lipid membranes

All biological cells are surrounded by a membrane consisting of amphiphatic lipid molecules that spontaneously self-organize into an enclosed bilayer in aqueous environments. The membrane provides a barrier to limit or prevent the diffusion of certain species, such as large molecules and charged ions. Apart from providing a selective barrier to contain and compartmentalize the cell, many important biological functions are carried out by proteins that are embedded or associated with the membrane. Such proteins can be enzymes, channels or pores, transporters or pumps, receptors; the range of possible function is accompanied by variation in structural features. Membrane proteins are notoriously difficult to crystallize for diffraction studies, where the detergent-based extraction of the protein from the membrane can disrupt the native structure and interfere with function. For solution-state NMR characterization, the lipid membrane frequently reduces molecular tumbling frequencies, making it challenging to obtain well-resolved signals (or even any signal at all), and often requires the protein to be embedded in smaller membrane-mimicking complexes such as micelles, bicelles, or nanodiscs. SsNMR has the advantage that it can, in principle, characterize membrane proteins directly in lipid membranes, in order to carry out functional and structural studies

in the same conditions that bear more relevance to the physiological state.

While there is a diverse range of lipids in typical cell membranes, the complexity and heterogeneity of cell-derived membranes can be detrimental to the sensitivity of the protein under study. It is common, therefore, to study proteins in lipid membranes derived from one or several type of synthetic lipid molecules, which enable membranes with a defined charge and morphology to be robustly reconstituted in a reproducible manner. This approach forms the basis of work reviewed in this section. MAS-DNP can overcome sensitivity challenges introduced by the lower filling factor for many membrane proteins, as part of the rotor is occupied by the lipid environment required for the correct folding of these proteins. For MAS-DNP work carried out in native cellular membranes, see section 3.5.1.

MAS-DNP investigations of membrane proteins have formed significant parts of biological DNP reviews.[5,7,217] Additionally, several insightful reviews focus on membrane proteins as a whole, including work from other biophysical techniques such as conventional ssNMR, which is often a prerequisite for MAS-DNP investigations.[6,15,16] Several reviews that include a section on MAS-DNP focus on specific classes of membrane proteins such as enzymes[218] and G-protein-coupled receptors (GPCRs).[219]

One of the significant challenges of working with membrane proteins is that there are many possible parameters that can be varied, with implications for protein stability but also potentially for DNP enhancement. One can customize the membrane composition, its charge, the level of hydration, the reconstitution process, as well as the method by which the polarizing agent is introduced. Therefore, various procedures and workflows have been published on how to prepare DNP samples specifically for membrane proteins (see also sections 2.7.4 and 2.9). Lee et al. carried out a detailed analysis of different cryoprotectants using a 24-residue α-helical influenza M2 transmembrane (M2TM) peptide selectively labeled at 5 residues, and an 18-residue β-hairpin antimicrobial peptide protegrin-1 (PG-1) selectively labeled at 3 residues. These two model peptides were investigated in a range of synthetic lipids with different cryoprotectants, tracking changes in linewidth from am-

bient temperature down to 203 K.[220] To investigate sample preparation protocols ideal for membrane proteins, Liao et al. used the same M2TM peptide as above, and ROCKER, a designed Zn^{2+} transmembrane transporter. In this extensive work, the effects of lipid composition, lipid deuteration, the method of radical-mixing, and the type of cryoprotectant, were some of the factors investigated. Very similar absolute sensitivity were found for protonated and deuterated lipids, even though larger apparent $\varepsilon_{on/off}$ were obtained with deuterated lipids (69–100, against 56–78 for protonated lipids). The radical distribution in lipid membranes was investigated quantitatively via the paramagnetic relaxation effect (PRE), demonstrating that glycerol can facilitate radical mixing with the membrane even at ambient temperature via partitioning to the membrane-water interface, and also suggesting that radical distribution is bimodal, with different surface- versus lipid core-associated proportions for TOTAPOL and AMUPol.[134] Long and coworkers carried out MAS-DNP methodological developments on KL_4, a 21-residue synthetic peptide that mimics lung surfactant protein in its ratio of positively charged and hydrophobic residues, and is currently used in clinical trials for treating respiratory distress. Due to its amphipathic properties, KL_4 partitions to the the hydrophobic interior of membranes and adopts a helical conformation. Using KL_4 embedded in membranes, the authors demonstrated that spin-labeled lipids deliver higher and more consistent DNP enhancements compared to TOTAPOL.[117,148] Recently, the same group carried out further optimization of sample preparation using KL_4 in multilamellar lipid vesicles, using AMUPol, 10% DMSO, and freeze/thaw equilibration to achieve improved enhancements.[112] Section 2.7.4 also provides an overview of matrix-free sample preparation approaches using covalent spin-labeling of membrane proteins or lipids.

The following sections focus on MAS-DNP applications on membrane proteins grouped by functional similarities, such as receptors for specific molecules, enzymatic activity, and channels or transporters across the membrane. Due to a large number of studies on light-sensitive proteins, work on these are categorized together in a separated subsection even though the proteins involved may also have transporter or receptor functions.

3.4.1 Membrane enzymes

In a study using conventional ssNMR as well as MAS-DNP, Möbius et al. investigated an *E. coli* inner membrane protein, diacylglycerol kinase (DGK). DGK is an α-helical homotrimeric integral membrane protein that catalyzes the ATP-dependent phosphorylation of diacylglycerol to phosphatidic acid, an important step in the biosynthesis of membrane-derived oligosaccharides, which is part of the bacterial stress response. In this study, MAS-DNP was used to enable TEDOR experiments and probe specific salt-bridges at the interface between the protomers of the trimeric protein. Conventional ssNMR was not able to detect such cross-protomer contacts, possibly because of the sparseness of these contacts and their relatively long range, which weakens the dipolar interaction. Using MAS-DNP on a mixed labeled sample consisting of U-^{13}C-DGK and ^{15}N(Arg,Lys)-DGK, the occurrence of one or more salt bridges involving Arg residues could be observed (Figure 16). Using mutagenesis, R9, R81, and R91 were identified to contribute to these interactions out of the 6 possible Arg residues in DGK.[221]

The ability of MAS-DNP to contribute to the study of membrane-bound enzymes was reported by Yamamoto et al., who investigated a complex of two full-length mammalian cytochrome proteins (total 72 kDa), which are important for carrying out redox reactions in the liver and can play a role in drug metabolism. At full length, these membrane proteins are bitopic, consisting of a transmembrane α-helix linked to a hydrophilic heme-containing N-terminal domain with cytosolic catalytic activity. Frequently, the transmembrane helices are truncated in structural studies of cytochrome proteins to overcome difficulties in sample preparation for crystallography, but their presence is important for full enzymatic function of the catalytic domains. To mimic physiological conditions, a relatively large amount of lipids (1:250 protein:lipid molar ratio) was used, exacerbating the sensitivity challenge of detecting the full-length cytochrome P450–cytochrome b_5 complex in the membrane. Using MAS-DNP 2D ^{13}C$-^{13}$C correlation spectra of the complex could be obtained, while spectral crowding issues were addressed by highly selective isotope labeling. Protein-lipid interac-

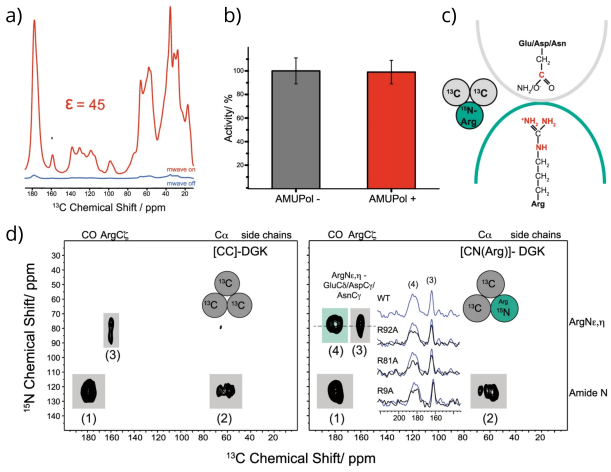

Figure 16: MAS-DNP spectra of DGK, showing (a) $\varepsilon_{on/off}$ of 45 using ^{13}C-CP and 20 mM AMUPol. (b) Activity of DGK with (+) and without (-) AMUPol, demonstrating that the presence of the biradical has no influence on the activity. (d) DNP-enhanced ^{15}N$-^{13}$C TEDOR spectra (6.25 ms mixing time) of a U-^{13}C-labeled control sample of ([CC]-DGK) (left), and mixed-labeled [CN(Arg)]-DGK trimers (right). Both spectra show natural abundance crosspeaks (grey box): intra-protomer N-C' (peak 1), intra-protomer N-Cα (peak 2), intra-residue Arg-Nε,η-Arg-Cζ (peak 3). An additional crosspeak (green box) is observed in [CN(Arg)]-DGK (peak 4). It can be assigned to an interprotomer contact, representing a through-space correlation between Arg and Asn/Asp/Glu. (c) This cross-peak demonstrates that salt bridges or H-bonds between Asp/Glu/Asn and Arg must exist at the protomer interfaces. Mutations R9A, R81A and R92A cause a reduction in intensity of peak (4) demonstrating their involvement in these cross-protomer contacts. Reprinted in part from ref. 221 under a Creative Commons (CC-BY 4.0) license.

tions could be identified between specific residues in cytochrome b_5 and the DMPC lipids, providing structural restraints to extract a 15° tilt of the transmembrane alpha-helix relative to the bilayer normal, in agreement with previous experiments carried out in oriented bicelles with conventional ssNMR.[222] The interaction between transmembrane helices of the protein complex was investigated with an ambitious 2D $^{13}C-^{13}C$ REDOR-filtered correlation experiment, with magnetisation passing via ^{15}N-enriched cytochrome P450 to natural abundance ^{13}C in the same protein, followed by spin diffusion to ^{13}C-enriched cytochrome b_5. Although cross-peaks were detected with sufficient sensitivity, their interpretation remained difficult due to signal overlap in this crowded region of the spectrum.[223]

3.4.2 Channels and transporters

EmrE exporter The efflux-multidrug resistance E (EmrE) is a 12 kDa *E. coli* inner membrane protein that is capable of exporting a variety of toxic polyaromatic cationic species while importing protons. It consists of four transmembrane helices and functions as a homodimer. The highly conserved glutamic acid E14 of helix 1 is essential for the transport function of EmrE, but direct evidence of an interaction between E14 and the substrate had not been obtained thus far. Using MAS-DNP, Ong, Lakatos et al. were able to detect an interaction between the sidechain carboxylate Cδ of E14 and the C_{meta} of tetraphenylphosphonium (TPP+) in a 2D $^{13}C-^{13}C$ correlation experiment. For that, they used sparsely ^{13}C-labeled EmrE obtained with 2-^{13}C-glycerol as the sole carbon source and TPP+ ^{13}C-labeled at one phenyl ring. An additional advantage of MAS-DNP in this application was the reduction of the phenyl ring-flip motion, which interfered with the detection of this key interaction at ambient conditions.[224]

KcsA potassium channel The K^+ channel of streptomyces A (KcsA) is an extensively-characterized membrane protein that is frequently used as a model system in NMR studies, which consists of a tetrameric arrangement with two transmembrane α-helices per protomer.

An early MAS-DNP study at 18.8 T (800 MHz ^{1}H/527 GHz electron spin frequency) investigated U-^{13}C,^{15}N-KcsA prepared in liposomes. Besides some methodological investigation about polarizing agents, deuteration of the sample, paramagnetic relaxation and intrinsic linewidth effects, and despite low enhancements (8.3 and 13.2 for protonated, respectively deuterated KcsA, both with AMUPol), the authors were able to probe specific residues in the closed-conductive and open-inactivated states of KcsA. DNP data of the latter conformation showed peak doubling that was not observed at ambient temperature, suggesting the presence of two conformations with different degrees of channel opening.[225] A further study of KcsA in native bacterial membranes[226] is covered in section 3.5.1.

M2 proton channel The M2 protein of the influenza A virus forms a homotetrameric proton channel, which plays essential roles in the infection process; during initial steps of infection, the acidification of the virion leads to release of the viral genome in the host cell; during replication, M2 generates membrane curvature, which leads to budding and release of the mature virus. The full-length protein is 97 amino acids, but various shorter constructs retain the ability to form the membrane channel for proton conductivity, the shortest being the M2 transmembrane (M2TM) peptide consisting only of the residues 22–46 which was used for methodological developments (see section 2.7.3).[134]

The binding of the adamantane-based antivral drug rimatadine (Rmt) to $M2_{18–60}$ has been investigated in an early MAS-DNP study. Using ^{13}C-labeled M2 proteins and ^{15}N-labeled Rmt, conventional ssNMR gave only two correlations after 23 days of signal acquisition, while DNP-enhanced TEDOR gave additional crosspeaks after only 2 days of experimental time. One of the key signals obtained in both conventional and DNP-enhanced ssNMR is the correlation to glycine G34Cα, providing the first direct structural evidence of a drug interaction observed at the protein pore within a construct of this size.[227]

The budding and membrane scission role of M2 requires the presence of cholesterol, which is found in eukaryotic but not in prokaryotic membranes. However, the known structures of

M2 were solved without using cholesterol as a membrane component, thus the binding site of M2 to cholesterol is still unknown. Using a combination of conventional ssNMR and MAS-DNP, the cholesterol-M2 interaction was probed. To enable distance measurements, Elkins et al. used a ^{13}C-labeled construct of $M2_{22–61}$ and cholesterol ^{13}C-labeled at the isopropyl chain end (C25, C26, C27). In a 2D $^{13}C-^{13}C$ correlation experiment acquired with a long mixing time of 1.0 s and a DNP enhancement of 38-fold, the authors were able to observe correlations between I39 of M2 to cholesterol, corresponding to a 9.0 Å distance. This result was consistent with $^{13}C\{^{19}F\}$ REDOR-based distance measurements carried out under conventional ssNMR with cholesterol fluorinated at the isopropyl chain end.[228]

A further, more detailed study of the cholesterol-binding interface of M2 was reported by the same authors in the following year. To overcome spectral crowding issues, cholesterol was produced from 1-^{13}C glucose by a genetically engineered strain of yeast, leading to cholesterol that is skip-labeled at alternate carbons with only few adjacent ^{13}C-^{13}C pairs. The construct used was $M2_{22–61}$ with specific ^{13}C labeling on only two residues, G34 and I39. Even with these highly selective labeling schemes, spectral congestion in DNP-enhanced 2D $^{13}C-^{13}C$ correlation experiments was such that the authors had to implement a DQ filter to further simplify them, thus removing 75% of cholesterol intramolecular crosspeaks. The resulting DQ-filtered 2D correlation spectra enabled detailed intermolecular assignments in synthetic (POPC/POPG) and virus-mimetic membranes, and provided distance restraints for molecular docking to create a model of the cholesterol-binding interface (Figure 17).[229]

The bound water at a key histidine (H37) of $M2_{18–60}$ was very recently investigated using ^{1}H-detection under fast MAS, MAS-DNP, and DFT calculations. In this study, MAS-DNP was carried out with TEMTriPol-1 in standard DNP matrix at 600 MHz (14.1 T) using a 2.5 mm Phoenix HFXY probe. DNP-enhanced ^{1}H-detected spectra were acquired at 24 kHz MAS. While the bound water signal was already detectable in ssNMR experiments at ambient conditions, DNP-enhanced $^{15}N-^{1}H$ correlation spectra at cryogenic temperatures (90–100 K) helped to confirm that the observed water signal is not involved in chemical

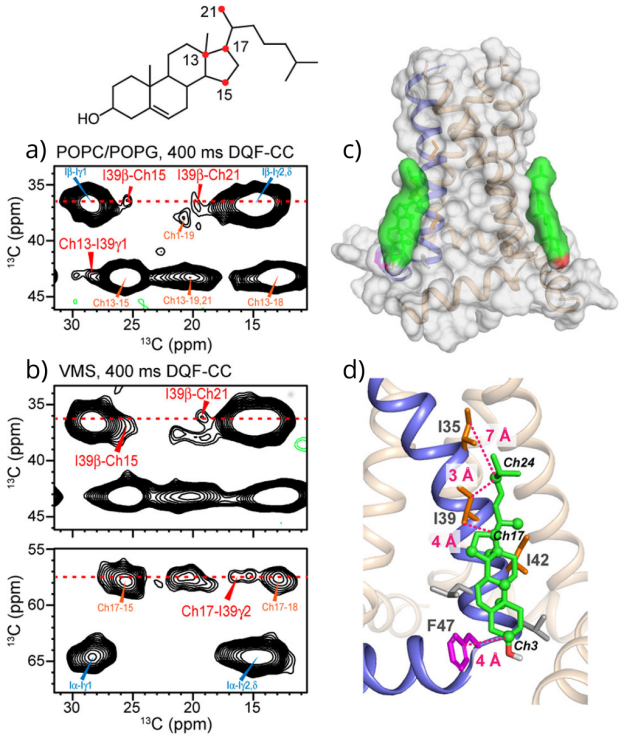

Figure 17: M2 protein–cholesterol correlations (red labels) obtained from DNP-enhanced 2D DQ-filtered-^{13}C$-^{13}$C spectra, with two types of lipid membranes: (a) synthetic POPC/POPG, and (b) virus-mimetic membranes. (c) Cholesterol molecules (green) docking onto M2 (PDB 2L0J) using HADDOCK, with distance restraints obtained from DNP-enhanced 2D ^{13}C$-^{13}$C spectra. (d) Close-up view of the cholesterol binding interface, showing key Ile and Phe residues. The cholesterol carbons that show crosspeaks with M2 protein are shown as spheres. Adapted from ref. 229. Copyright 2018 American Chemical Society.

exchange, thus really corresponding to a bound species.[230]

ABC transporter ATP-binding cassette (ABC) transporters are a family of membrane proteins that are capable of transporting many types of substrates across membranes, using ATP to power the translocation against the concentration gradient. The structure of ABC transporters generally consists of two nucleotide binding domains (NBDs) and two transmembrane domains (TMDs); the former are highly conserved and bind ATP to drive the transport, while the latter are responsible for substrate specificity and show more sequence and structural diversity. The multiple structural states involved in the complex, multi-step, and highly dynamic transport mechanism often defy structural characterization by conventional NMR and crystallography approaches.

The transporter associated with antigen processing (TAP) is a 150-kDa human ABC exporter involved in the adaptive immune response against virally- or malignantly-transformed cells. It has a high affinity for the 9-residue antigentic peptide RRYQKSTEL, derived from human histone H3.3. Using MAS-DNP as well as carefully-designed biochemical assays, Lehnert, Mao et al. characterized the substrate-bound state of human TAP, which had not been successfully elucidated by crystallography so far. To ease assignment, the peptide sequence was modified to KRYQNSTVY for better signal dispersion under DNP conditions, while keeping an identical affinity to TAP as the native peptide. Achieving a high concentration of peptide–TAP complex in the limited rotor volume was challenging because TAP tended to aggregate and lose activity at higher protein-to-lipid ratios. Thus, the authors developed a specific DNP sample preparation method: isolated peptide–TAP complexes were prepared in a detergent solution containing 1% initial glycerol; after flash freezing, the excess water was gradually removed by freeze-drying. Careful controls were carried out to ensure that the complex was intact within the optimized condensed glycerol matrix. Using DNP-enhanced 2D DQ–SQ $^{13}C-^{13}C$ and TEDOR correlation experiments, chemical shift perturbation was observed for peptide resonances upon binding to TAP. This information

allowed the backbone conformation of the peptide to be determined in the bound state.[141]

The ABC exporter MsbA is a homodimeric (2 × 65 kDa) ABC exporter from *E. coli* that translocates lipopolysaccharides (LPS) to the outer membrane of gram-negative bacteria. The nucleotide binding modes of MsbA were investigated using a combination of conventional ssNMR, MAS-DNP, pulsed EPR, and MD simulations. Apart from the two canonical nucleotide binding sites, it was known that MsbA has an additional ATP-binding site (AK-site), which shows reverse adenylate kinase activity.[231] Four of the five states that are involved in the coupled ATPase–rAK catalytic cycle were trapped, and the binding of AMP/ADP in the AK-site was investigated with DNP-enhanced TEDOR experiments. The investigation was carried out with U-^{13}C-MsbA and ^{15}N-AMP/ADP. The interaction observed was assigned to the Q-loop, a conserved structural motif featured in other NBD of ABC transporters.[232] A separate study on MsbA, also by the Glaubitz group, focused on the use of ssNMR and MAS-DNP to investigate the TMD. The authors designed a pair-labeling approach to probe specific sites of the transmembrane helices 4 and 6 in the apo- and vanadate-trapped states, as well as observe conformational changes in the presence of substrates.[233]

Bam complex The β-barrel assembly machinery (Bam) is a large pentameric protein complex that is associated to the outer membrane of gram negative bacteria such as *E. coli*. It is essential for catalyzing the formation and insertion of β-barrel proteins into the outer membrane. Of this large complex, the key protein BamA consists of a transmembrane β-barrel domain and a long periplasmic domain. BamA has a 'lateral gate' or a weak point between the first and last strands of the β-barrel, which is important for allowing protein substrates to insert, fold, and be released into the bilayer. Pinto et al. investigated the structure of the lateral gate and its relationship to other parts of BamA, such as two globular subdomains of the periplasmic domain (P4P5) and an extracellular loop (EL6). This work was carried out within the context of DLPC liposomes, using high sensitivity ssNMR techniques including

MAS-DNP and highly specific labeling of ^{13}C-Ile, ^{13}C-Phe and ^{15}N-Gly residues. The large protein construct size (130 kDa) and the use of ^{15}N-filtered ^{13}C$-^{13}$C experiments lead to sensitivity challenges that were overcome with DNP enhancement ($\varepsilon_{on/off}$ of 110 at 9.4 T), with key differences observed in spectra where the lateral gate was open versus closed.[234]

3.4.3 Receptors

In humans, G-protein-coupled receptors (GPCRs) are a family of over 800 cell surface membrane proteins. GPCRs are activated by the presence of a wide range of stimuli outside the cell (hormones, neurotransmitters, ions, odorants, photons of light); in response they initiate a range of intracellular signaling cascades, and thus mediate signal transmission across the cell membrane. GPCRs share a common architecture consisting of a bundle of seven transmembrane α-helices, joined by three extracellular and three intracellular loops. GPCRs are important pharmacological targets, but frequently exhibit a high degree of conformation flexibility, making investigations of various functional conformational states for structure-based drug design challenging.

The human bradykinin receptors are GPCRs which are activated by peptide hormones derived from blood proteins. They lead to vasodilation and play a role in blood pressure regulation and inflammation responses. Of the two subtypes of bradykinin receptors, B_1R and B_2R, the binding mode of the B_2R peptide ligand was elucidated previously by solid-state NMR.[235] On the other hand, B_1R suffer from low expression levels and poor stability, making a similar study quite challenging. The NMR sensitivity limitation resulting from the very small amount of protein to which the ^{13}C-labeled peptide ligand can bind, was overcome by the use of MAS-DNP, with the associated cryogenic temperature helping to extend the sample lifetime for structural characterization. Due to issues with sample stability, B_1R was characterized in mixed detergent micelles, in which the peptide binding affinity was close to that found in native membranes, yielding an unusually high MAS-DNP $\varepsilon_{on/off}$ of 169. To reduce signal overlap, six different ^{13}C,^{15}N labeling scheme of the peptide were utilized.

By comparing chemical shifts of B_1R-bound and free peptides, the residues involved in the protein–ligand interaction could be identified. Structural data obtained from MAS-DNP was then used in docking to provide a model of the interaction of the peptide ligand with B_1R.[236]

The neuropeptide Y2 receptor (Y2R) is a 44 kDa GPCR that is considered as an important drug target to fight against obesity and anxiety, but structural data for drug development is still lacking. A site-specific structural analysis of Y2R in various functional states in bilayer membranes has been conducted by following the chemical shift modifications of the six native Trp residues present in Y2R. In order to assign the six Trp residues, mutagenesis was first attempted but failed due to unpredictable changes in chemical shift. Instead, each separate ^{13}C-Trp was combined with ^{15}N labeling of the following residue, leading fortuitously to unambiguous labeled pairs of residues for the 6 Trp in the Y2R sequence. MAS-DNP was used to improve the sensitivity of the 1D NCOCX spectra acquired for each of the six samples, using the glycerol signals as internal reference. Somewhat unusually, the assignments obtained under MAS-DNP were then transferred back to ssNMR spectra recorded at 243 K (-30°C) to investigate the conformational changes upon neuropeptide- and arrestin-3 binding.[237]

3.4.4 Light-sensitive proteins

An important area of application for MAS-DNP is the investigation of light-sensitive proteins. Light-sensitive proteins play diverse and important biological roles such as energy conversion, intra- or intercellular signaling in bacteria, and they are key for enabling vision in animals. A deeper structural understanding of such proteins can enable bioengineering applications such as optogenetics.

MAS-DNP investigations have focused predominately on retinal-containing rhodopsins, which are embedded in membranes, whereas other light-sensitive proteins such as phytochromes may not be embedded in or associated to membranes. In rhodopsins and phytochromes, a small chromophore molecule undergoes conformational change while absorbing

light energy via a process known as photoisomerization. The conformational change of the chromophore is transmitted to the covalently-linked protein, leading to signal transduction to other cellular processes. After light-activation, the protein-chromophore complex need to return to its ground state before another photon of light can be detected.

Rhodopsins, the main topic of this section, share a common architecture of seven transmembrane helices, one of which contains a key lysine residue that binds the retinal chromophore via a Schiff base. There are several key differences between microbial and animal rhodopsins: the arrangement of the transmembrane helices, different retinal bonds involved in the photoisomerization step, the way that retinal returns to its initial ground state via a photocycle involving K-, L-, M-, N-, O-states, and the immediate protein function(s) triggered by photoactivation.[238] The cryogenic conditions required for MAS-DNP are very convenient to stabilize and trap intermediates involved in the photocycle, the structures of which are important for understanding the function of rhodopsins. The use of very specific labeling (e.g. specific types of amino acid) can be implemented to overcome spectral crowding issues encountered with MAS-DNP. Another important methodological aspect is the reconstitution of the rhodopsin protein with retinal ^{13}C-labeled at specific sites.[239] In 2018, Becker-Baldus et al. have reviewed MAS-DNP methodology and applications on retinal proteins with a specific focus on microbial rhodopsins.[11]

bR Bacteriorhodopsin (bR) is a light-driven proton pump that occurs at very high density in the native purple membrane of the archaeon *Halobacterium salinarum*, and thus was extensively studied and serve as a paradigm for other light-driven retinal-binding ion pumps. Early on, the Griffin group used bR as a model system to demonstrate the feasibility of DNP-enhanced ssNMR for biomolecular applications, specifically for membrane proteins.[97,173,240] Subsequently, investigations with a focus on biological functionality were also carried out as detailed below.

On light illumination, the retinal of bR undergoes conformational change and is then

regenerated in-place through a multi-step cyclic reaction scheme known as the photocycle, involving changes in hydrogen bonding, protonation, and double bond rotation. Using a custom-built DNP probehead equipped with an optical fiber, a number of early intermediate states of the bR photocycle were generated by light illumination at specific wavelengths and cryo-trapped for observation. Some of the generated states had never been detected by NMR, though were known via other techniques. Using [ζ-^{15}N]lysine-labeled bR and MAS-DNP, different intermediates could be characterized thanks to the distinctive and highly-dispersed ^{15}N chemical shift of the Schiff base (165-318 ppm).[241] In a subsequent study, the same group further characterized photocycle intermediates using U-^{13}C, ^{15}N bR, based on the observation of correlations between the lysine-bound Schiff base and C15 of retinal in DNP-enhanced 2D ^{15}N$-^{13}$C correlation spectra. In this way, all photocycle states of bR, including some with unexpected heterogeneity, were detected and assigned.[242]

To understand the proton pumping mechanism of bR, an extensive investigation was enabled by MAS-DNP with an enhancement factor $\varepsilon_{on/off}$ of 75. By cryo-trapping key intermediates of the photocycle, the authors were able to confirm one proton pathway out of three possible routes that were proposed by QM/MM calculations. More specifically, the Schiff base (SB) N–H bond distance was measured in various intermediates. The elongated bond found in the protonated L-state indicates that the SB is poised to deprotonate at this step. The ^{1}H chemical shift obtained from the subsequent deprotonated M_o-state points towards Thr89 being the stabilizing counterion. 2D ^{13}C$-^{13}$C correlation spectra revealed the proximity to Thr89 of the Asp85 residue located on the extracellular side of bR. Taken together, these different findings provided clear evidence of the primary proton transfer pathway, which is a key irreversible step in the bR photocycle.[243]

GPR Green proteorhodopsin (GPR) is the first retinal-based photoreceptor discovered in bacteria. It is a light-driven proton pump initially identified in γ-proteobacteria, a type of marine bacteria. Though proteorhodopsin-like sequences were subsequently found to be

widespread, GPR is the prototype that has been most often investigated. Compared to bR, proteorhodopsins (pRs) can be optimized for absorbing different wavelengths of light, a behavior termed spectral tuning, which is advantageous for engineering optogenetic applications. While GPR shares the heptahelical architecture of other rhodopsins, it is also known to oligomerize in lipid bilayer membranes, forming donut-like complexes of hexamers and pentamers. GPR has been extensively studied by Glaubitz and coworkers using MAS-DNP as well as conventional ssNMR.[244]

The optimum light absorbance of pRs can be modulated through the L105 and A178 residues.[245] The former is close to the chromophore, but the latter occurs further away from the chromophore, on the cytoplasmic EF loop. It was therefore surprising that the mutation A178R induces a large redshift of 20 nm. To understand this aspect, retinal specifically labeled at C14 and C15 was incorporated into WT GPR and the A178R mutant. MAS-DNP was required to enable detection of the specifically labeled chromophore. In particular, clear chemical shift changes of C14 could be observed in DQ-filtered experiments, which were found to result from mutation-induced changes in the photo-intermediate states.[245] The L105Q mutation, which tunes the sensitivity of pR from green light to blue light, was investigated as well by MAS-DNP. Again, 14,15-$^{13}C_2$-all-*trans*-retinal bound to WT and L105Q GPR were compared. Here, the larger chemical shift change was found on C15 of the mutant, and more detailed conformation of retinal at C14–C15 was probed via DQ spectroscopy.[246] In a more methodological aspect, retinal detection by MAS-DNP showed that GPR produced via split intein *trans*-splicing yielded the same retinal chemical shifts as classically-expressed WT GPR, demonstrating the potential of protein *trans*-splicing technology to produce segmentally-labeled membrane proteins in a robust manner.[66]

The conformational changes of retinal and the surrounding residues in the binding pocket were investigated in further detail with 10,11,12,13,14,15-$^{13}C_6$-retinal incorporated into ^{15}N-Lys-labeled GPR. In situ sample illumination in the DNP probe in conjunction with cryo-trapping enabled detection of signals arising from the K- and M-state photointermediates.

The very low population of the deprotonated M-state in the WT protein was enhanced by an E108Q mutation, which slows down reprotonation; the mutation was shown to not have any detectable effect to the rest of the chromophore and protein structure. Two different M-states were observed and large chemical shift changes in the K- to M-state transition indicated correspondingly large structural distortions of the chromophore in this step of the photocycle.[247]

The oligomeric states of GPR affect the dynamics of the photocycle. The protomer interfaces were investigated through 2D ^{15}N$-^{13}$C TEDOR experiments using mixed ^{13}C, ^{15}N labeling. Since the number of interfaces with the correct labeling is only of the order of 1.25 per pentamer, MAS-DNP was necessary to achieve sufficient sensitivity. To prepare the sample, a careful choice of detergents was required to disrupt the initial complexes formed with only one type of labeling and achieve well-mixed oligomeric states with a statistical distribution. Key residues for salt bridge formation at the interfaces were identified to modulate the oligomerization, leading to monomers or hexamers instead of pentamers that are typically assembled by the WT protein in proteoliposomes and micelles. Despite ^{13}C-depletion, natural abundance correlations were still observed in the DNP-enhanced TEDOR data (50% reduced); careful control experiments were required to differentiate from bona fide cross-protomer correlations.[248]

In another MAS-DNP study on the protomer interface of GPR using amino acid-specific ^{13}C or ^{15}N labeling, the conserved H75 residue was shown to form a cross-protomer hydrogen bonding network in a triad involving W34 and D97. Using AMUPol, an $\varepsilon_{on/off}$ of 40–60 was obtained on all samples. This sensitivity enhancement made possible the acquisition of insensitive 2D ^{15}N$-^{15}$N PDSD experiments on GPR that was specifically ^{13}C,^{15}N-labeled at the single H75 histidine residue (Figure 18). These experiments unambiguously demonstrated the tautomerization and ring reorientation of H75 from the dark- to the M-state.[249] Sensitivity enhancement delivered by MAS-DNP in conjunction with cryo-trapping of specific states in the photocycle were essential for the above studies.

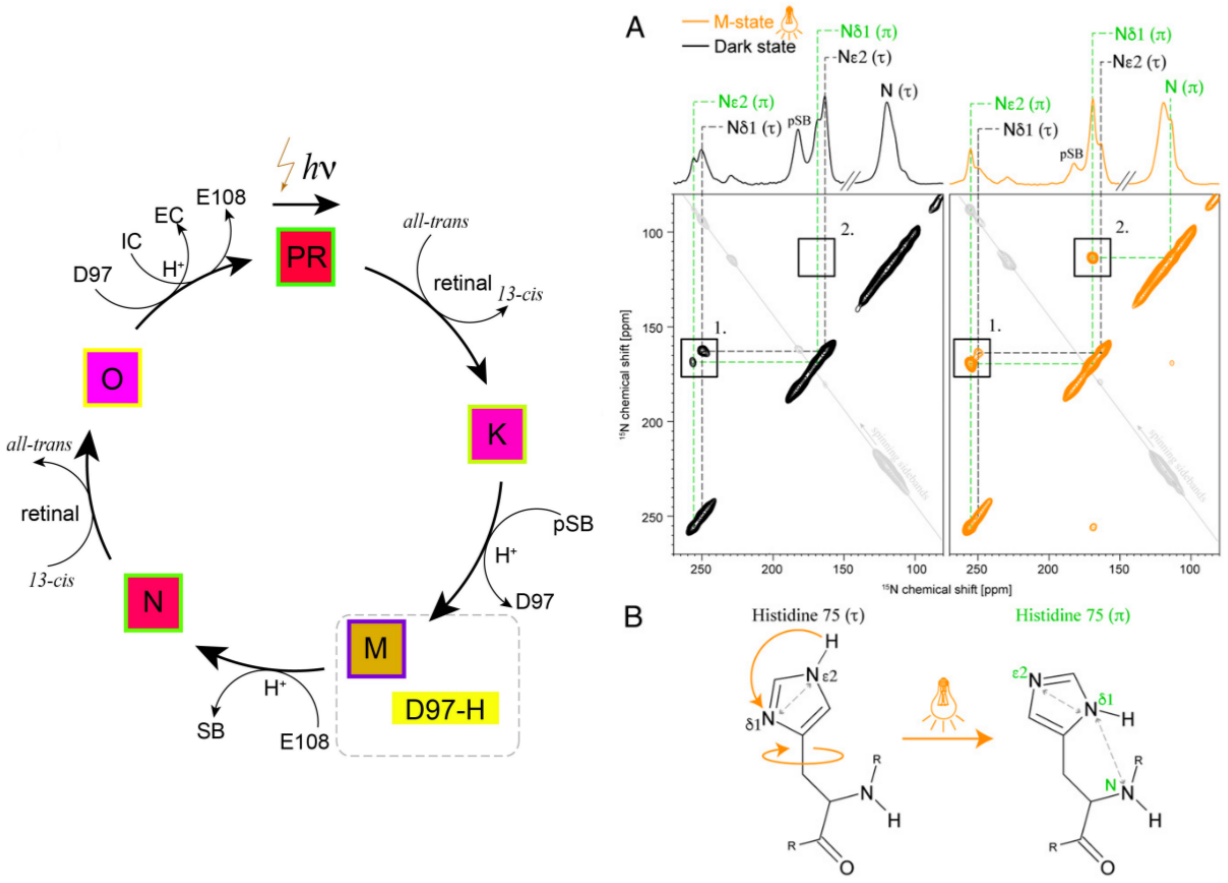

Figure 18: Left: photocycle of GPR. Right: (A) DNP-enhanced $^{15}N-^{15}N$ PDSD spectra of ($^{13}C_6$-$^{15}N_3$-His, $^{15}N\varepsilon$-Lys)-GPR_{E108Q} in the dark state (left, black) and the illuminated M-state (right, orange) showing the change in H75 tautomer and ring conformation (B). Spectra were recorded with a mixing time of 1 s. Adapted from ref. 249, 2019 National Academy of Sciences.

ChR2 Channelrhodopsins (ChRs) are ion channels from the single-cell green algae *Chlamydomonas reinhardtii* which conduct (but do not pump) cations in a light-dependent manner. Of the two forms of the protein, ChR1 and ChR2, the former has a faster photocycle and reduced inactivation, but the latter shows higher cation selectivity and different dark-adapted states; the former is the dominant photoreceptor in the algae, but the latter is more frequently studied due to higher expression levels and potential for optogenetic applications.[250]

The C1C2 chimera of ChR is about half the length of full-length WT ChR2 (342 instead of 737 amino acids) and was used for solving the first crystal structure of a ChR-like protein.[251] Bruun, Stoeppler et al. combined solution-state NMR, solid-state NMR, and optical spectroscopy to investigate C1C2, and showed the presence of two photocycles corresponding to different ion conducting states with different selectivity. MAS-DNP was mainly used in this study to confirm the all-*trans* chromophore conformation in fully dark-adapted (ground state) ChR, as derived from the detection of crosspeaks between C12, C15 and C20 of retinal, which was selectively labeled at these three positions[252]

In another report on ChR in the same year, Becker-Baldus et al. used a truncated ChR2 construct (residues 1–315) which contained all the transmembrane domains of ChR2 and demonstrated its ability to conduct ions upon light illumination. Again, the presence of two coupled photocycles was proposed, each with its own opened and closed state of the channel. The authors deduced the all-*trans* conformation of retinal in the ChR2 ground state on the basis of its characteristic C14 chemical shift. Furthermore, cryo-trapping by illumination of the sample within the DNP probe at various temperatures led to the observation of retinal conformations corresponding to three different states of the photocycle, including accumulation of the long-lived desensitized P_4^{480} state (a closed state that results in reduce photocurrents).[253]

In a further study, Becker-Baldus et al. followed up on the desensitized P_4^{480} state of ChR2, a state formed during continuous light illumination (either at ambient temperature or 245 K). In the desensitized state, the channel is closed and in contrast to the ground

state, does not reopen on light illumination. The position of the desensitized state in the photocycle was so far unclear. Again, by using the light-illuminating DNP probehead, the conformation of the chromophore was followed via [12,15-$^{13}C_2$]-retinal by determining the distance between C12 and C15 through DQ buildup curves. The retinal was determined to be in the 13-*cis* conformation for the P_4^{480} state. The cryo-trapping procedure involves cycling the temperature for the system to undergo some thermal relaxation before lowering the temperature again to trap a new desired state. By modifying the cryo-trapping procedure, it was possible to determine that the P_4^{480} state occurs at a late stage of the photocycle and to propose an overall photocycle for ChR2[254] (Figure 19).

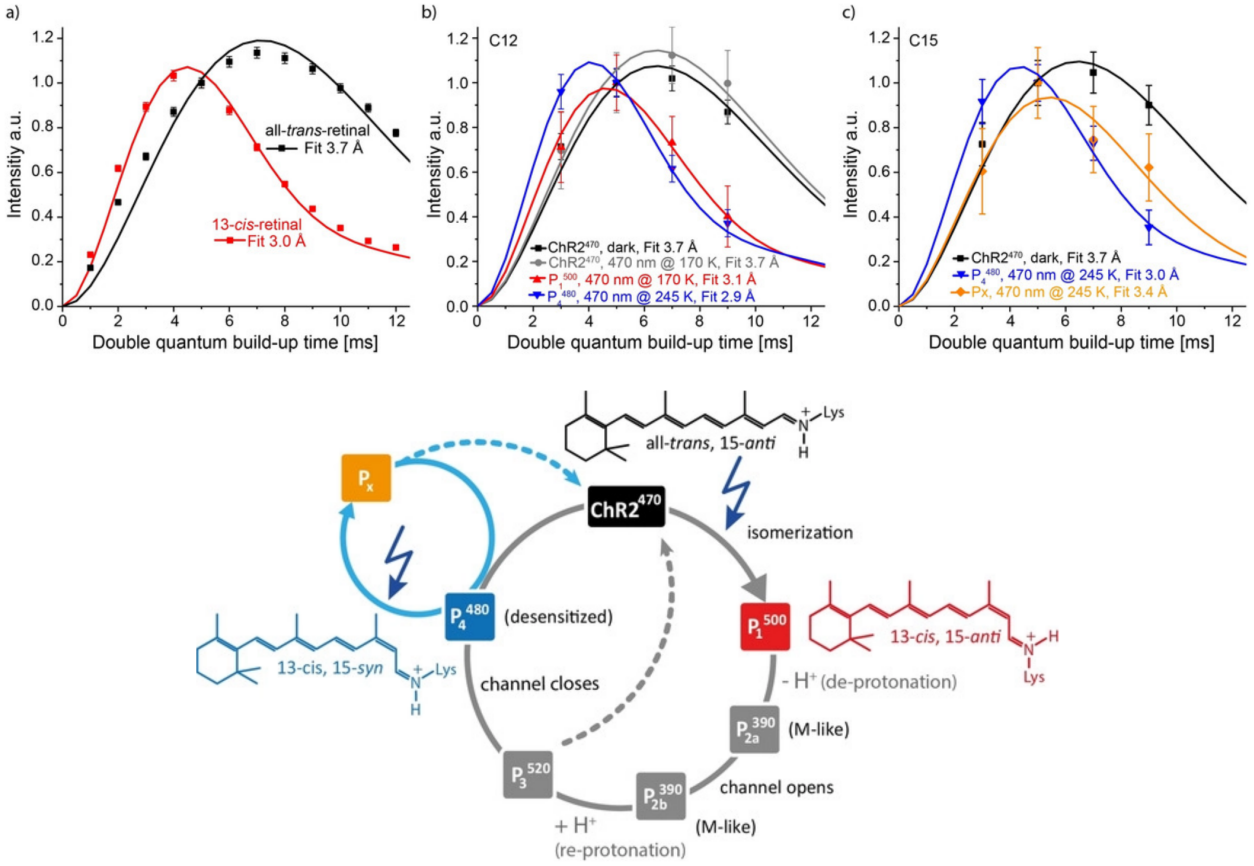

Figure 19: Top: DQ buildup curves obtained with DNP enhancement, showing the clear difference between *cis* and *trans* conformations. Bottom: the photocycles of ChR2, showing branching at a late stage of the photocycle. Adapted from ref. 254 under a Creative Commons (CC-BY 4.0) license.

Mammalian rhodopsin While only microbial rhodopsins were covered thus far in this section, an elegant study has been carried out on a mammalian rhodopsin by Kubatova, Mao et al. using a combination of liquid-state NMR, DNP-enhanced ssNMR, and time-resolved optical spectroscopy. The bovine G90D mutant of rhodopsin is associated with an impaired visual cycle and leads to congenital stationary night blindness. A crystal structure is only available for one of the multiple states of this mutant. After carefully establishing the relevance of disulfide bond-stabilized constructs of rhodopsin, investigation of the protein-bound retinal conformation was carried out by MAS-DNP using ^{15}N-Lys labeled rhodopsin and specifically ^{13}C-labeled retinal. The characteristic ^{15}N signal of bound retinal confirmed the protonated Schiff base form in the G90D mutant in three states: the dark state, the cryo-trapped early photointermediate bathorhodopsin state, and the light-activated Meta II state (Figure 20). This finding was in contrast with WT rhodopsin where the Meta II state involves deprotonation of the Schiff base. The impact of the G90D mutation on the protonation of the Schiff base is likely due to changes in the stabilization and counter ion effect, suggesting a mechanism of how this mutation leads to night blindness disease.[255]

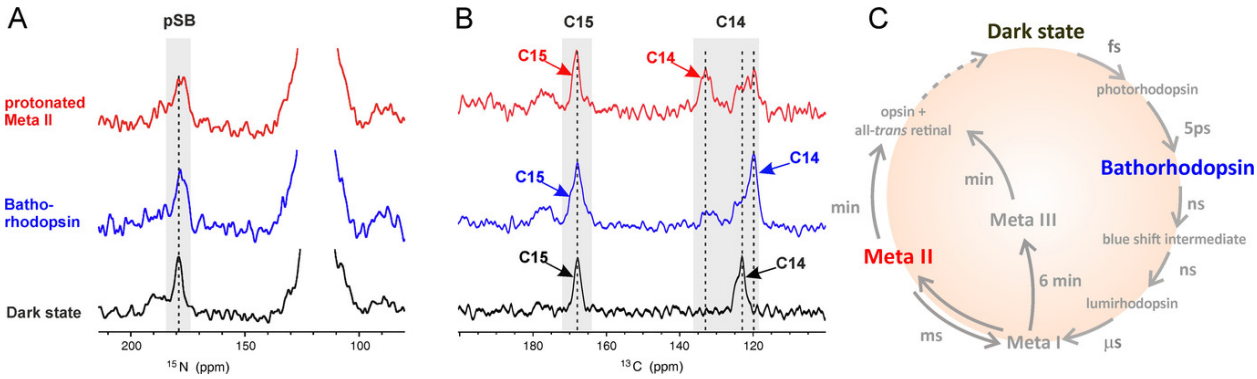

Figure 20: DNP-enhanced MAS-NMR spectra of the G90D$_{S\text{-}S}$ mutant under three states: : the dark state (black), bathorhodopsin state (blue), and protonated Meta II state (red). (A) ^{15}N-Lys labeling of the protein showed the characteristic chemical shift for the retinal-bound protonated Schiff base (pSB) in all states, with the two intermediates having a broader linewidth than the dark state, suggesting conformational heterogeneity. (B) DNP-enhanced DQ-filtered spectra, showing multiple C14 signals in the ^{13}C-labeled retinal of the Meta II state, indicating conformational heterogeneity that corresponds to a mix of the other states. (C) Photocycle of rhodopsin. Reprinted from ref. 255 under a Creative Commons (CC-BY 4.0) license.

Non-membrane associated light-sensitive proteins While many light-sensitive proteins are membrane-bound or associated, there are exceptions such as phytochromes, which are light-sensitive proteins of plants cells. Phytochromes are localized in the cytoplasm before activation, or in the nucleus after activation, and play an important role in gene regulation. The phytochrome chromophore is not retinal, but phycocyanobilin (PCB), a molecule consisting of an open chain of four pyrrole rings. MAS-DNP has been used to investigate U-^{13}C, ^{15}N-PCB in natural abundance Cph1Δ2, the sensory module of a cyanobacterial phytochrome. 2D ^{15}N$-^{13}$C spectra contained all expected crosspeaks of PCB (Figure 21) and the assigned chemical shifts suggested partial localization of a positive charge on ring B. The functionally-relevant water molecules associated with PCB were investigated as well.[256]

3.5 Biomolecules in the cellular context

The native environment of many biomolecules is the cell, which can impact on many structural, dynamical and functional features of the system of interest, but is very challenging to incorporate into NMR structural studies. Cells contain many types of molecules and present an environment with strong molecular crowding, which leads to many potential interactions on different time scales; such interactions may be key for correct folding and functioning of certain proteins. However, it adds to the heterogeneity of the overall sample and reduces sensitivity for NMR experiments. The molecular complexity of native cellular membranes can influence the conformation and clustering of embedded proteins. Moreover, the low endogenous level of many biomolecules can add to the sensitivity challenges. MAS-DNP offers the opportunity to overcome some of these challenges for investigation of biomolecules in an environment that is as relevant as possible to their native state.

In the applications reviewed in this section, the main focus is often on observing and interpreting signals arising from proteins within their cellular context. For clarity, this section is further subdivided into three areas: proteins embedded or strongly associated to cell membranes, biomolecules investigated in cell lysates, and studies of intracellular

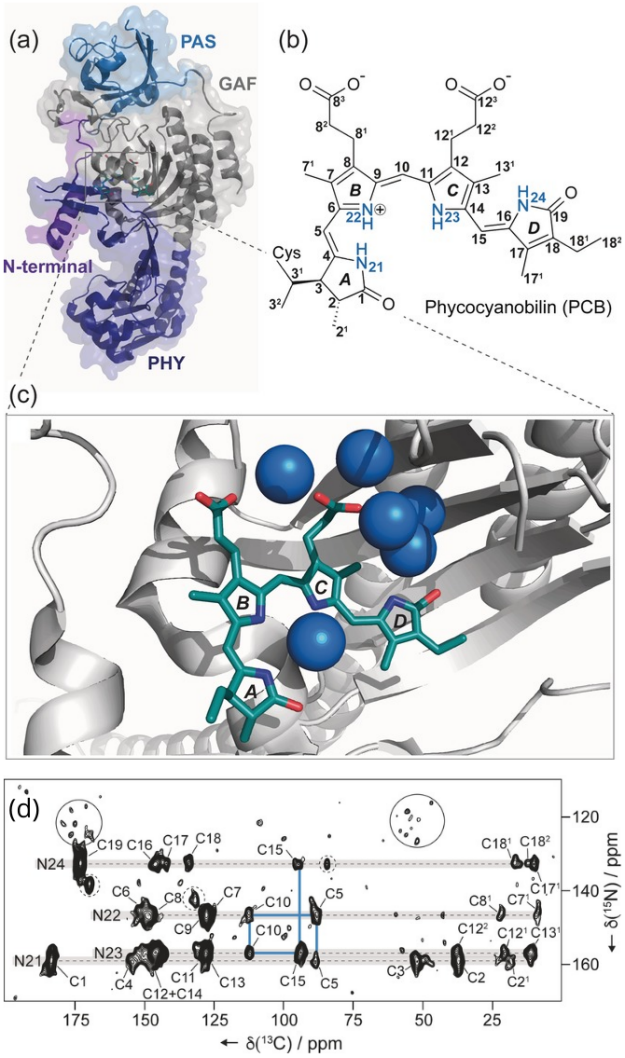

Figure 21: a) Structure of Cph1Δ2 (PDB 2VEA). b) The bilin chromophore, which is covalently bound via a thioether link to Cys 259. c) The chromophore is coordinated with six H_2O molecules (blue spheres) in the binding pocket. Nitrogen atoms are depicted in blue, carbon in cyan, and oxygen in red. (d) 2D DNP-enhanced $^{15}N-^{13}C-^{13}C$ spectrum of U-[^{13}C, ^{15}N]-PCB in Cph1Δ2 in the red light-absorbing Pr state. The blue lines indicate the sequential connection of the ^{15}N resonances via methine carbon atoms C5, C10, and C15. The cross peaks in solid circles correspond to natural abundance signals of the protein background. Adapted with permission from ref. 256. Copyright 2016 John Wiley and Sons.

biomolecules in bacterial cells and human cell lines. Further on in this review (sections 3.6 and 3.7), we cover applications where samples containing other types of whole cells can be found, but the work in those sections are more often focusing on a non-protein or extracellular aspect.

In-cell NMR is a topic of great interest since many years. Efforts in methodological developments were first reported for solution-state NMR, and later for solid-state NMR including DNP.[17–19] MAS-DNP studies were also part of several broader in-cell NMR reviews that cover techniques in both solution- and solid-state NMR.[257–259]

3.5.1 Proteins in native cell membranes

While lipid bilayers can be formed from a single type of lipids due to entropic-driven hydrophobic interactions, the typical membranes found in cells (for both prokaryotes and eukaryotes) are far more complex. Within native cellular membranes, multiple types of lipids and proteins are found together with cholesterol and polysaccharides, often with covalent modifications that lead to species such as lipoproteins and glycolipids. Many cellular membranes are asymmetrical, with different components on each side. The molecular composition is specific to the organism and the cellular compartment, and can be highly heterogeneous, with microdomains that vary spatially across the membrane surface. Membrane proteins placed within the context of a cellular membrane may show affinity to certain components, have different clustering patterns, and adopt different conformations compared to when reconstituted in a simplified model membrane. From the perspective of NMR, proteins are found typically at lower concentrations in cellular membranes compared to model membranes, which reduces sensitivity; MAS-DNP can be a strategy in these cases to overcome the sensitivity challenge. In principle, as the protein of interest is localized at the membrane, the membrane fraction extracted from cells is sufficient to provide a native environment, without the need to use intact cells. Many biological applications in this area rely on bacterial membranes due to the relative ease of culturing, though a few studies were performed on

membranes extracted from higher organisms such as fish[260] and human cell lines.[261] Weingarth, Baldus, and coworkers have published detailed experimental protocols for preparing membrane protein samples in native bacterial membranes for MAS-DNP studies.[262,263]

One of the earliest MAS-DNP work on proteins embedded in cellular membrane was carried out by Linden et al. They investigated a snake neurotoxin protein which targets the nicotinic acetylcholine receptor. This ligand-gated ion channel is found at neuromuscular junctions and in the central nervous system. As this receptor occurs at a high concentration in the electric organ of the pacific electric ray, it was used to extract receptor-rich 'membrane patches', which were incubated with labeled neurotoxin proteins and subsequently investigated by MAS-DNP. While the initial DNP enhancement was 26, the resolution in 2D $^{13}C-^{13}C$ spectra was very poor. After storing the sample for 4 weeks in a -20°C freezer, the spectra showed a decreased DNP enhancement to 12, but an improved resolution. This effect was attributed to the partial quenching of TOTAPOL radicals associated to membranes components.[260] This first preliminary study highlights the potential of the technique for the investigation of complex cellular systems, but at the same time, the difficulties associated with such complex samples.

In a study on the Sec translocon (SecYEG), a protein which can transport other proteins across biological membranes, Reggie, Lopez et al. used MAS-DNP to overcome the significant sensitivity challenge of observing the 25-residue LamB signal peptide in *E. coli* SecYEG (over 600 residues). Only four residues of the signal peptide were ^{13}C-labeled to provide sufficient resolution at DNP experimental conditions. With an $\varepsilon_{on/off}$ of 32, 2D $^{13}C-^{13}C$ correlation spectra were obtained on the bound signal peptide in 20 hours, instead of weeks or even months which would have been necessary for a similar experiment by conventional ssNMR. The observed chemical shifts suggested an α-helical conformation of the signal peptide.[264]

In a preliminary study, Yamamoto et al. explored the capacity of MAS-DNP for the study of cytochrome b_5, a single-pass membrane protein consisting of a transmembrane α-helix with an extended cytosolic catalytic domain. The protein was overexpressed in *E. coli* and the

whole cell pellet (with membrane embedded cytochrome b) was directly used for MAS-DNP measurements. Selective labeling enabled a relatively resolved 2D $^{13}C-^{13}C$ spectrum to be obtained with a DNP enhancement of 16.[265]

Jacso et al. investigated Mistic, a bacterial protein that can autonomously fold into the cell membrane without involving other intracellular transport proteins. In this study, *E. coli* cells expressing Mistic were lysed, and the lipid membrane fraction separated by many low-speed centrifugation steps to yield a 25 mg wet cell membrane pellet that contained approximately 0.28 mg of Mistic. The authors demonstrated that 2D and 3D correlation experiments involving ^{13}C and ^{15}N dimensions (NCACX and NCOCX) can be obtained successfully on labeled Mistic protein in native cellular membrane. Analysis of the data confirmed the α-helical secondary structure at specifically labeled residues.[266]

While Mistic is a relatively small (13 kDa) model protein, the same approach is also successful in much larger membrane complexes. Kaplan et al. reported on the study of the bacterial type IV secretion system core complex (1 MDa) in extracted *E. coli* cell envelope fractions. Using protein prepared either uniformly ^{13}C, ^{15}N or very selectively labeled in specific amino acids to obtain maximal spectral dispersion, the authors were able to obtain expected sequential correlations using 3D NMR data obtained at 9.4 T (DNP $\varepsilon_{on/off} \approx 60$). The data validated the structural model previously generated via in vitro crystals in a more native-like context.[267]

The epidermal growth factor receptor (EGFR) is a transmembrane protein associated with cell division and survival, and thus is one of the most commonly targeted protein in anti-cancer therapy. In a multidisciplinary and comprehensive study, Kaplan et al. cultured human epidermoid carcinoma cell line (A431) that is known to have a high EGFR expression level, from which vesicles/liposomes with a large amount of EGFR proteins in native cell membrane (5.5 fold enrichment relative to whole cells) were derived. MAS-DNP was combined with very specific labeling of ^{13}C-Met and -Phe, as well as ^{15}N-Thr and -Leu residues, a strategy that allowed the authors to provide tentative assignments to sequential residue pairs

of EGFR. The MAS-DNP data suggested a ligand-induced protein stabilization revealed by reduced linewidths upon EGF binding.[261]

Following a fist MAS-DNP study of the bacterial K^+ channel KcsA in liposomes, Visscher et al. reconstituted KcsA in *E. coli* polar lipids using a low protein/lipid molar ratio of 1/400 for MAS-DNP, while 1/100 is usually the minimum required to obtain enough sensitivity by conventional ssNMR. A low protein/lipid ratio was required here to avoid spurious contacts between channels and be able to study the relationship between the channel-gating and -clustering behavior without biasing the results by random contacts. By mixing channels labeled in either only ^{13}C or ^{15}N, heteronuclear intermolecular correlations could be observed in NHHC experiments. Variation of the pH to alter the state of the channel between opened and closed revealed the reversible and dynamic nature of KcsA clustering, as well as potential concerted channel opening in clusters.[226]

Nisin is a 34-residue antimicrobial peptide able to target bacterial membranes by forming pores and at the same time interacting with lipid II, a precursor used in cell wall synthesis (see section 3.6.1 for further background). Medeiros-Silva et al. showed that the nisin:lipid II complex can only form pores when placed in membranes liposomes but not when solubilized in DMSO. Two types of membrane liposomes were investigated: reconstituted from model phospholipids and derived from bacterial cells. The 15–20 fold sensitivity reduction of the nisin:lipid II complex in cellular membranes compared to model phospholipids was overcome by two methods: conventional ssNMR ^1H-detection at 60 kHz MAS and MAS-DNP. The experiments confirmed that the structure of the complex in model phospholipid liposomes recapitulates the main features of the likely functional conformation of nisin in *Micrococcus flavus* cellular membranes (Figure 22). MAS-DNP spectra showed significant line broadening of S29 in both DOPC and cellular membranes at 100 K, indicating high levels of dynamics. The dynamics of S29 can be influenced by extremely flexible hinge residues nearby. Mutation of S29 and nearby hinge residues may potentially lead to nisin derivatives with enhanced antimicrobial activity for pharmaceutical development.[268]

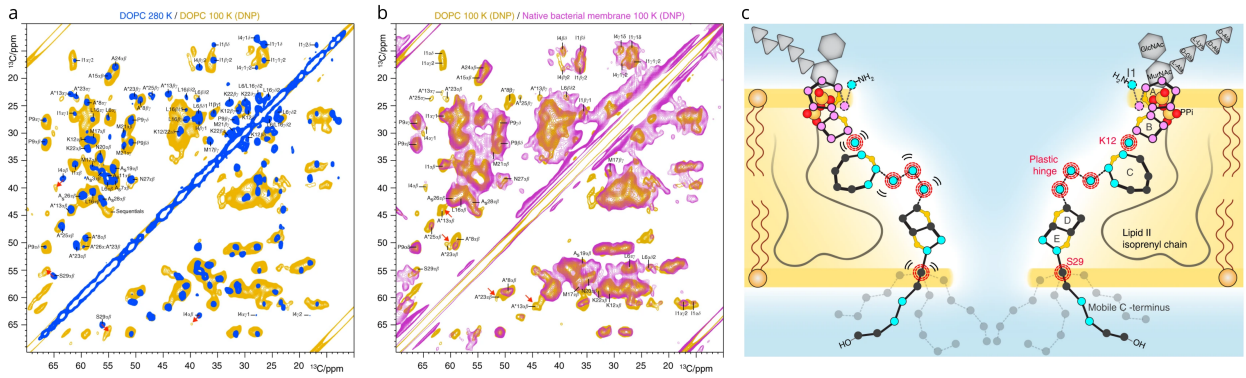

Figure 22: (a) 2D $^{13}C-^{13}C$ spin diffusion ssNMR spectra on the lipid II-bound state of nisin pores within membrane liposomes reconstituted from DOPC, a neutral phospholipid, at 280 K (blue) and at 100 K with DNP enhancement (orange). (b) Overlay of DNP-enhanced 2D $^{13}C-^{13}C$ spectra acquired in DOPC (orange) and in liposomes derived from the cellular membrane of *M. flavus* (magenta), a nisin-sensitive bacterium species. Red arrows highlight strong chemical shift perturbations. (c) Proposed structure of nisin:lipid II pores from ssNMR and MAS-DNP data. Dynamic residues identified in the current study are indicated with dashed rings. Adapted from ref. 268 under a Creative Commons (CC-BY 4.0) license.

Another antimicrobial peptide, teixobactin, has been investigated by MAS-DNP. It targets lipid II and lipid III in the bacterial cell membrane, with the putative binding mode involving the pyrophosphate functionality that is found specifically in these bacterial lipids. This feature is crucial for antimicrobial activity against a broad spectrum of bacteria, but with low toxicity to human cells. However, production of teixobactin is highly challenging as a natural product of an unculturable bacterium and development of analogues is hampered by the lack of information about its binding mode. As in the nisin study, MAS-DNP highlighted that the binding complex of teixobactin in model phospholipid liposomes is structurally similar to that found in cellular membranes extracted from *M. flavus*.[269]

3.5.2 Cell lysates

Considering the complexity of working with intact cells, cell lysates provide a useful middle ground where the heterogeneity in terms of types of biomolecules and variety of interactions is present, without the additional issue of compartmentalization by cellular membranes.

One of the key issue when working with low concentration of the targeted biomolecule

in a cellular environment is the removal of the signal arising from the cellular background, which may be partially isotopically labeled as well. Viennet et al. addressed this problem by a targeted DNP approach, and is one of the first to propose developments in this direction. The authors attached a TOTAPOL moiety to the ligand of the target protein Bcl-X_L, a 20 kDa apoptosis inhibitor, which was present in the crude lysate after overexpression at 50 µM, but not further purified or concentrated. When a fully deuterated buffer was used, the MAS-DNP enhancement provided by the modified ligand attached to the labeled protein was shown to be selective for the protein, reducing the influence of signals from the lysate background. The chemical shift range of the detected resonances were indicative of a high degree of α-helix structure, consistent with that of Bcl-X_L.[125]

In an elegant study, Frederick et al. used deuterated cell lysates with added ^{13}C,^{15}N-labeled yeast prion domain Sup35NM to study the mechanism by which Sup35NM mediates non-standard inheritance (see section 3.1.1 for further background). One of the key MAS-DNP experiment in this study was carried out at 16.4 T (^1H Larmor frequency of 700 MHz), which can improve resolution, but gave only a moderate enhancement of -8 to -10 with TOTAPOL (∼80% of maximum enhancement on standard proline on the same instrumental configuration). Interestingly, the 2D spectra showed that Sup35NM fibrils adopts less α-helical and more β-sheet conformations in lysates (Figure 23) compared to purified fibers at similar cryogenic temperature. In particular large chemical shift changes were observed for the lysine and proline residues of the M domain, which is unstructured in purified fibrils. This observation suggests that the M domain interacts with other cell components such as chaperones when in the cell lysate. In contrast, the core of the fibril does not seem to be affected by the cellular milieu. This study evidences that the cellular environment can significantly impact protein secondary structure. Incidentally, the study of Sup35NM fibrils in lysates required 1 week of signal averaging time even with DNP enhancement due to the very low amounts (10 µg) of labeled protein within the rotor.[127]

A recent study investigated polyphosphate (polyP) granules in *Xanthobacter autotrophi-*

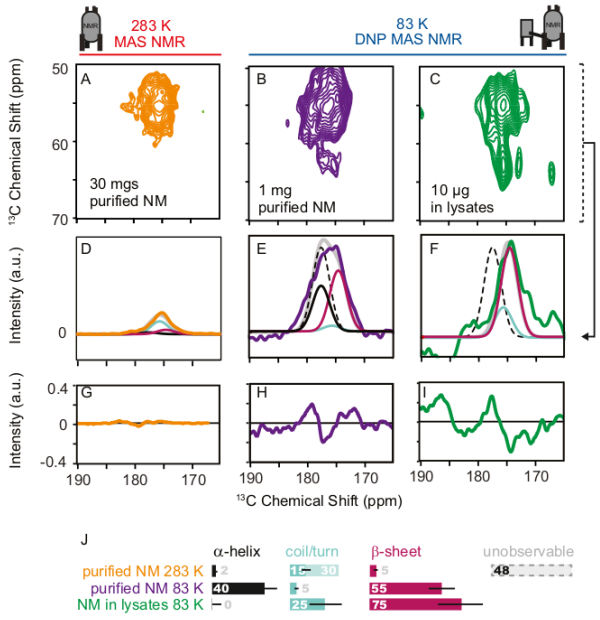

Figure 23: The secondary structure of Sup35NM (NM) fibers in cellular lysates differs from the secondary structure of in vitro-templated fibers. **(A–C)** Carbonyl carbon (C') region of $^{13}C-^{13}C$ correlation spectra at 700 MHz of (A) 30 mg of purified NM fibers in protonated buffer at 283 K acquired in 24 hr, (B) 1 mg of purified cryoprotected NM fibers at 83 K acquired in 6 hr and (C) cryoprotected NM fibers assembled in the presence of cellular lysates acquired in 1 week. (A) was acquired with ssNMR while (B–C) were acquired with MAS-DNP. **(D–F)** Line-fitting of (A–C) to find the distribution of secondary structures present in each sample, using three Gaussian distributions that describe the expected chemical shifts for the possible secondary structural motifs: α-helices (black), random coils and turns (light blue), and β-sheets (magenta). **(G–I)** Residuals of the fits in (D–F). **(J)** Relative secondary structure distributions (in percent) as determined by intensity of each Gaussian distribution for the protein backbone in each fiber sample, using the same color code as in (D–F). At room temperature, nearly half of the NM molecule is not observable by NMR (gray bar), while another third of the protein is undergoing unrestricted motions on the ps-ns timescale and is random coil in character (light blue bar). Comparison of spectra from frozen samples with the room temperature data is complicated by the interplay of experimental temperature and dynamic motions. Reprinted with permission from ref. 127. Copyright 2015 Elsevier.

cus, a bacterium involved in biotechnological applications and known to sequester phosphate from its growth medium. The polyP granules can modify proteins covalently and play a role in regulating protein folding. For their study, a cell-like environment with minimum extraction was preferred to avoid modification of the structure and distribution of native phosphate species. While conventional ssNMR and solution-state NMR were used for whole cell investigations, MAS-DNP was applied on the insoluble cell fraction that was enriched in polyP granules. The cryogenic temperatures of MAS-DNP were expected to immobilize all polyP granules present, and ^{31}P CSA measurements demonstrated that the predominant phosphate linkage present in the granules is cyclic Q_2 (Figure 24), in contradiction with previous assumptions that linear polyP chains would dominate.[270]

3.5.3 Whole cells

As discussed at the beginning of this section, the investigation of biomolecules within whole cells with MAS-DNP is challenging. There are a number of methodological issues to be addressed in relation with the compartmentalization and localization of the molecular species concerned. Many experimental choices have to be made regarding the protein/biomolecule, the cell type, the synthesis or delivery of proteins and polarizing agents into cells, and how the cellular background signals can be removed or reduced. The reducing intracellular environment can introduce additional challenges by quenching binitroxide-based polarizing agents. A specific sample preparation procedure for in-cell systems has to be developed for each cell type and biomolecule to be observed, and is especially important for achieving sufficient DNP enhancement of the intracellular species of interest.

After considering the methodological challenges specific to MAS-DNP, we must also consider the challenges from a biological perspective. All of the work described in this section have been carried out on bacterial cells or human-derived cell lines. It is important to consider the effect of various experimental features on the biological system, such as the centrifugal forces experienced by the sample during MAS, the low temperatures, and the

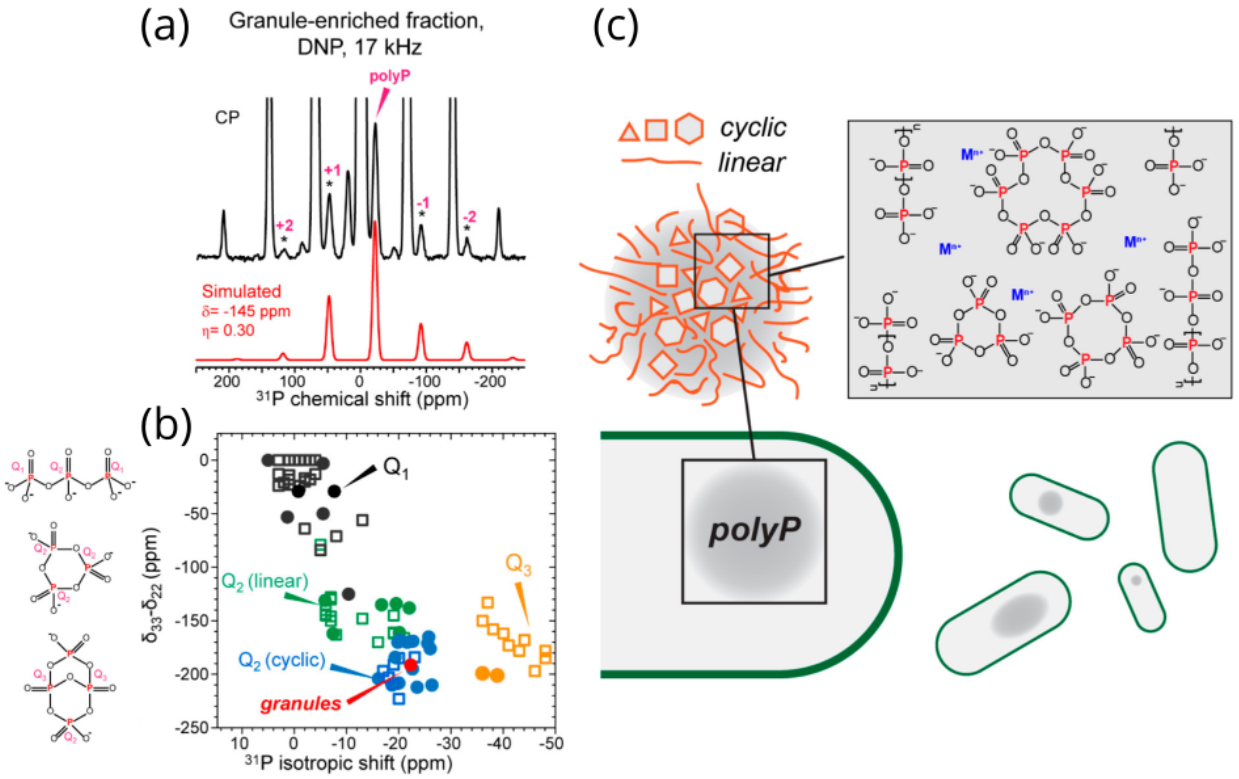

Figure 24: ^{31}P chemical shift anisotropy (CSA) of *X. autotrophicus* granules compared to model phosphate compounds. (a) ^{31}P DNP CP spectrum (black) of the granule-enriched fraction measured at 110 K under 17 kHz MAS on a 600 MHz spectrometer. CSA spinning sidebands are marked by an asterisk (*) and denoted as +2 to -2. Single-component best fit (red) gives a CSA that agrees well with the CSA of the dried sample. (b) Compilation of isotropic and anisotropic chemical shifts of phosphate model compounds (black, green, blue, orange) and *X. autotrophicus* granules (red). Data obtained in this study are shown as filled circles, while data reported previously are shown as open squares. Q_{1-3} illustrate different types of phosphate sites with some typical model compounds shown on the left of (b). (c) Schematic of the proposed polyP structures in *X. autotrophicus* granules. Linear and cyclic polyphosphates are packed together and chelated by metal cations (Mn^{+}) such as nickel and calcium. Similar size of linear phosphates and metaphosphates is only for illustration. Reprinted from ref. 270. Copyright 2020 American Chemical Society.

presence of polarizing agents and cryoprotectants.

Faced with the methodological challenges involved in preparing suitable samples, several teams have published detailed protocols for the purpose of enabling MAS-DNP in bacterial and human cell lines. For bacterial cells, Narasimhan et al. has published a detailed protocol for studying proteins in membrane extracts and delivering cytoplasmic-soluble proteins (e.g. ubiquitin) into whole cells.[263] For human cell lines, which can be more sensitive to the low temperatures used in MAS-DNP, Ghosh, Kragelj, Xiao et al. proposed a protocol, demonstrated with the HEK293 cell line, to transfer and load the cell sample in the NMR probehead at cryogenic conditions that preserve cell viability.[271] Another recent work by Ghosh et al. addresses further issues on maintaining viability of HEK293 cells during MAS-DNP and describes the delivery of AMUPol into cells by electroporation.[113] Furthermore, radical delivery to bacterial cell membranes may be improved by using spin-labeled antimicrobial peptides.[150,151] In this section, we will first review studies within bacterial cells, followed by investigations on human cell lines.

Bacterial cells A better understanding of biomolecules within bacterial cells can contribute to diverse applications, from the development of novel antibiotics to biocatalysis. Moreover, bacterial cells are relatively easy and economical to culture, a reason why first in-cell applications of MAS-DNP were attempted on bacterial cells. However, they also bring challenges such as a highly reductive cellular environment, as demonstrated by tracking the EPR signal of TOTAPOL in the presence of *E. coli* cells or cell lysates. While the EPR signal of TOTAPOL was completely lost within 10–15 minutes in the presence of cells, the radical quenching process was slowed down in certain conditions such as in lysates, at 4°C (38% remaining after 10 minutes), or by pre-treatment with N-ethylmaleimide to block cysteine thiol groups; radical reduction could as well be partly reversed by potassium ferricyanide.[272]

One of the earliest applications of MAS-DNP to investigate intact cells was carried out by Renault et al. The 150-residue integral membrane protein PagL was studied in three contexts:

E. coli whole cells, cell envelopes (cell surface membranes and peptidoglycan), and model proteoliposomes. For the whole cell samples, 15–40% glycerol was used for cryoprotection, balancing sample stability and viability. While no specific aspect of this study tracked the fate of biradicals in the presence of *E. coli* cells, sample were precooled to -20°C prior to MAS-DNP experiments. U-^{13}C, ^{15}N labeling and moderate enhancements ($\varepsilon_{on/off}$ = 10 for whole cells) enabled the acquisition of 2D NCA correlation spectra, which selectively detected signals from the protein-based components of the sample. Interestingly, apart from protein and other signals arising from components of the cell envelope, spectra on whole cell samples contained signals from RNA, which was likely to be present in the intracellular cytoplasmic space. As the cells were collected after 4 h of induction prior to the MAS-DNP experiment, RNA accounted for about 21 wt% of *E. coli* macromolecules. This finding suggests either a certain degree of cell lysis during sample preparation, or that the potential compartmentalizing effect of the cell membrane did not stop the entry of the radical into the cell, or that spin diffusion was highly efficient in delivering DNP hyperpolarization even to cytoplasmic components.[273] Similar RNA signals were also observed in a study on the bacterial cell wall of *B. subtilis*[143] (section 3.6.1).

Bacterial cells play an important role in many aspects of biotechnology, including the development of artificial metalloenzymes (ArMs) for the catalysis of unnatural chemical reactions. ArMs are designed protein scaffolds that can be expressed in a microbial host, and in which a catalytic transition metal complex can be incorporated through a self-assembly process. Chordia et al. demonstrated the catalytic ability of an ArM, which was both expressed and assembled in *E. coli* cells. The ArM complex was characterized by conventional and DNP-enhanced NMR. The bulk of the assignment was obtained under in vitro conditions with solution- and solid-state NMR. The intracellular self-assembly of the protein and the metal complex was then investigated by molecular biology techniques and MAS-DNP. Using deuteration to suppress background cellular signals, an excellent DNP enhancement of 100 was obtained. 3D ^{13}C DQ-SQ-SQ experiment (Figure 25) of ArM in the cell could be

carried out with sufficient resolution to allow unambiguous assignment of a selected number of residues. The very good agreement with the in vitro assignment is a strong indication of structural similarity and correct self-assembling of the ArM in the cell.[128]

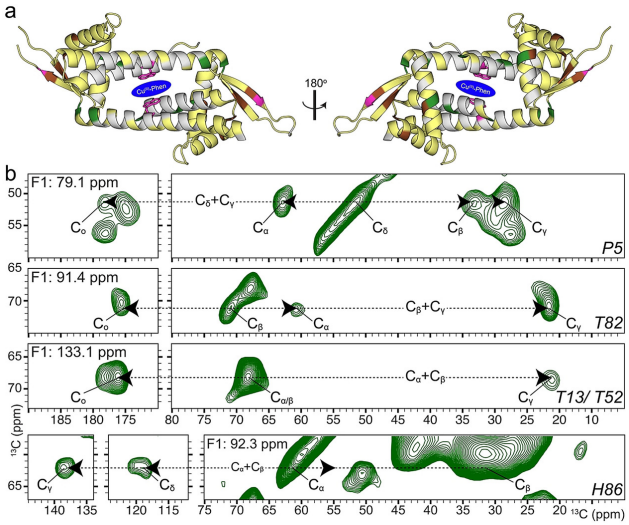

Figure 25: (a) Structure of the artificial metalloenzyme complex LmrR_A92E/Cu^{II}-Phen (PDB: 3F8F), with green residues assigned in *E. coli* cells using a (b) 3D ^{13}C DQ-SQ-SQ experiment carried out with MAS-DNP. Other colors indicate residues assigned via solution-state NMR and conventional ssNMR. Adapted with permission from ref. 128. Copyright 2021 John Wiley and Sons.

Human cell lines Compared to bacteria, the culture of mammalian cells is more demanding and labor-intensive. While studying biomolecules in native human cells may eventually be possible by MAS-DNP, the methodological developments required are currently proceeding with immortalized human cell lines such as HeLa, HEK293, Jukrat, which are often (but not always) derived from human cancers. Such cell lines are easier to grow and maintain indefinitely in culture than primary cell cultures derived from native tissues. As an established technology, it is often possible to transfect and express a desired protein within these cell lines in a reliable and reproducible manner.[274]

The first demonstration of MAS-DNP in human cells was reported by Albert et al. with HEK293F cells. In this work, a customized trimodal molecule (TotaFAM) was designed, which covalently linked both the polarizing agent TOTAPOL and the fluorophore 6-FAM

for cell localization to the intracellular targeting Tat peptide (47–57). This way, the uptake of TotaFAM by cells could be followed via confocal microscopy, making it possible to observe its intracellular localization. Fluorescence was observed across the whole cell but especially located at the nucleoli. The radical lifetime in the presence of cells was followed by EPR spectroscopy, which showed an approximately 40% drop of signal after 30 minutes. MAS-DNP was carried out at 6 K and 90 K. Reduction of the biradical was minimized by freeze-quenching the sample in under 3 minutes after addition of TotaFAM. At a concentration of 2.7 mM, TotaFAM outperformed AMUPol for obtaining a ^{13}C CP-MAS spectrum of HEK293F cells, presumably due to more effective targeting of the biradical into cells.[275]

In order to develop correlative studies using MAS-DNP as well as other biochemical and biophysical techniques, Narasimhan et al. developed a procedure for the delivery of ubiquitin protein into HeLa cells by electroporation. To track the diffusion of the polarizing agent through the cell membrane into the cytoplasm, the authors used a water-soluble bimodal molecule PyPol-TMR composed of PyPol, an AMUPol-like biradical, covalently bound to the fluorophore TMR/TAMRA. After 10–15 minutes of incubation and despite the fact that PyPol-TMR is not known to have intracellular targeting properties, fluorescence could be observed in both the nuclear and cytoplasmic cell compartments, thus demonstrating that AMUPol is likely capable of simply diffusing through the cell membrane. The authors obtained a DNP enhancement of 130 at 9.4 T (400 MHz ^{1}H-frequency) and 35 at 18.8 T (800 MHz) using a sample preparation protocol that involes: electroporation of ubiquitin, resuspension of cells in AMUPol-containing glycerol-based standard DNP matrix, mild centrifugation of cells into the rotor, and rapid freezing of the DNP rotor by liquid nitrogen. To improve spectral resolution, 3D DQ-SQ-SQ ^{13}C correlation spectra of ubiquitin were acquired, which confirmed that the protein remains similarly folded in-cell as in vitro.[276]

A study with relevance to antitumour drugs currently in clinical trials has been conducted by Schlagnitweit et al. in collaboration with AstraZeneca. They used HEK293T and HeLa cells to investigate danvatirsen, an antisense oligonucleotide (ASO) that downregu-

lates the transcription factor STAT3, which plays a key role in cell growth and apoptosis. It is especially attractive to characterize this 16-mer ASO in-cell by NMR, as other small fluorescent or biotin tags were shown to alter activity and localization, with tagged versions of ASO significantly less efficient than untagged ASO. However, the sensitivity challenge of clearly observing the unlabeled ASO in-cell had to be overcome with MAS-DNP and ^{31}P spectroscopy. ASO was delivered by electroporation into HEK293T cells, while AMUPol in DMSO, D_2O, H_2O was used as a buffer to provide the polarizing agent for MAS-DNP. $^{1}H-^{31}P$ 1D and 2D experiments were performed to detect the phosphorothioate backbone of ASO (Figure 26). This study demonstrates the potential of MAS-DNP in contributing to further development of this type towards the observation of pharmacological molecules in their interactive environment.[277]

Combining flow cytometry and MAS-DNP, Overall et al. used the Jukrat cell line derived from leukaemic human T-cells to develop methods for studying the reactivation of latent HIV infection, a bottleneck in the current antiretroviral therapy where HIV infection can only be controlled but not cured. The HIV genome is incorporated in the Jukrat T cell line variant JLat, which are able to produce near complete virions on reactivation and thus provide an adequate model system. The JLat cells were engineered to co-express HIV proteins and a reporter green fluorescent protein (GFP) to enable cytometry, in addition to a mutation that prevents the formation of infectious virions for biosafety reasons. The cells were cultured with ^{15}N-labeled medium, and the reactivation of HIV was followed both by cytometry and MAS-DNP, where the increase in ^{15}N cross polarization signal was quantified. The evolution of the ^{15}N signal intensity was found to qualitatively but not quantitatively reproduce the flow cytometry results. The correlation could be improved by flow cytometric sorting to reduce reactivation inhomogeneity in the population of cultured cells, thus remove the contribution of untransfected cells from the ^{15}N signal. It was noted that AMUPol is unusually stable in JLat cells, with EPR signal only reducing by 8% in 30 minutes,[278] which is much less than in previous work using HEK293 cells.[275] .

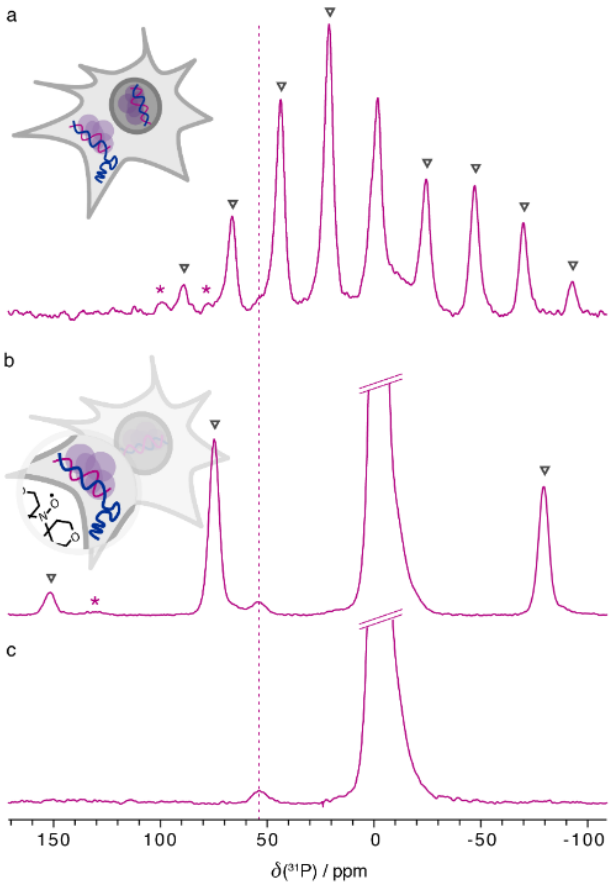

Figure 26: ^{31}P NMR spectra of frozen HEK293T cells containing ASO delivered by electroporation. The signal at 0 ppm is the cell background, the sidebands of which are indicated by triangles. The dotted line indicates the signal arising from the phosphorothioate backbone of ASO. (a) 1D CP obtained using conventional ssNMR at 240 K, MAS 5.5 kHz, 600 MHz spectrometer, signal averaged for 25 hours. (b) DNP-enhanced 1D CP obtained at 100 K, MAS 12.5 kHz, 400 MHz spectrometer, signal averaged for 1.5 hours. (c) Sum of 16 slices of a sheared DNP-enhanced 2D CP PASS spectrum to eliminate the spinning sidebands, signal averaged for 2.8 hours. Reprinted with permission from ref. 277. Copyright 2019 John Wiley and Sons.

While conventional mammalian cell cultures uses adherent cells that form a flat, 2D layer, there has been development of 3D cell culture techniques to provide an environment with mechanical properties and biological cues that are more similar to those found physiologically. In this context, Damman et al. have published a protocol for conducting ssNMR on spheroids of tumor cells, which can act as a model system for solid tumors. The spheroids formed were 600–700 µm in diameter, consisted of 70,000–100,000 cells, and remained intact up to an MAS spinning frequency of 5 kHz. The spheroids were formed from the epidermal carcinoma cell line A431, which expresses high levels of the membrane protein EGFR (introduced in section 3.5.1). A ^{13}C,^{15}N-labeled nanobody (single domain antibody) known to bind with high affinity to EGFR, was incorporated to the unlabeled spheroids. Despite the low amount of bound nanobody in the spheroid (only about 50% of the EGFR amount), DNP-enhanced 2D $^{13}C-^{13}C$ DQ-SQ correlation experiments were obtained showing specific resonances from the nanobody, illustrating the feasibility and potential of the approach.[279]

Most MAS-DNP studies carried out thus far did not thoroughly address the issue of biological viability of cells after undergoing the DNP procedure, aspects of which can be highly stressful: low temperatures, addition of polarizing agents, and shearing forces during MAS. This important aspect was investigated by Ghosh et al., who outlined the conditions that favor efficient DNP while maintaining HEK293 cell viability. The membrane integrity was tracked by Trypan dye exclusion to observe morphology and growth of the cells at multiple time points of the MAS-DNP sample preparation procedure and experiment (Figure 27). Conditions such as using 10% DMSO or 15% glycerol did not compromise viability, while a higher concentration of glycerol at 60% was found to disrupt membranes in over half the cells. The use of electroporation and slow freezing was found to give robust DNP-enhancement of above 40 for 10 mM of AMUPol, while maintaining cell viability at approximately 60%. The authors also demonstrated that good DNP enhancement can be achieved on all compartments and components of the cell, especially when aided by electroporation.[113]

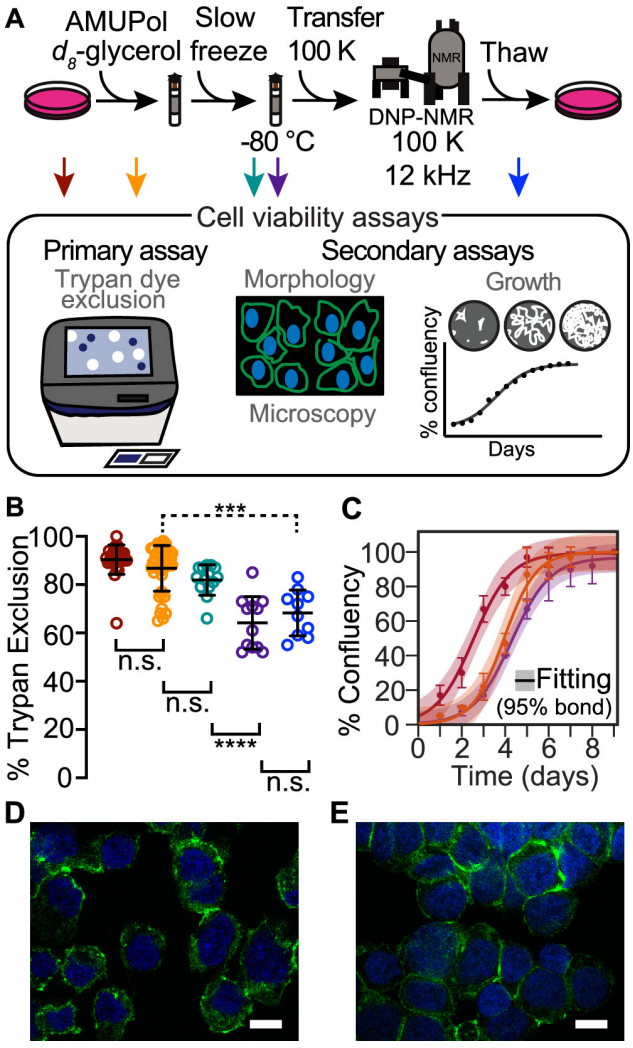

Figure 27: HEK293 cells are viable throughout the MAS-DNP process. (A) Experimental scheme of the MAS-DNP sample preparation procedure and cell viability assays. Colored arrows indicate points at which sample viability was assessed: after trypsinization and washing (dark red), after suspension in AMUPol and cryoprotectants (orange), after being frozen at 1 °C/min (green), after manipulation to remove the drive tip from the frozen rotor (purple), and after the entire MAS-DNP NMR experiment (blue). (B) Frozen cells best represent the state of the sample during MAS-DNP data collection. Percentage of cells with trypan-impermeable membranes at each sample assessment point, colored as in (A). Each point represents an independent sample. (C) Addition of glycerol affects growth kinetics, but further sample manipulations do not. Growth kinetics was assessed by confluency, colored as in (A). (D, E) Fluorescence microscopy of HEK293 cells immediately before (D) and immediately after freezing (E) by using phalloidin (green) and Hoechst 33342 (blue) to stain actin cytoskeleton and nucleus (scale bar: 10 µm), showing the preservation of cellular ultrastructure at the freezing rate used. Reprinted from ref. 113. Copyright 2021 American Chemical Society.

3.6 Cell walls

The cell wall of plants, fungi, and bacteria is a diverse and fascinating area of investigation, with applications in many fields including healthcare, agriculture, biotechnology, and new materials. The cell wall of these organisms possesses essential glycan-based components, which can exhibit incredible structural diversity in conformation and configuration, but also unfortunately show dense NMR spectral crowding in 1D and even 2D spectra. Certain essential components may be much less abundant and difficult to detect even with labeling of the sample. The heterogeneity of these biomaterials means that purification and extraction processes can be ineffective for some of their components. Some recent reviews of ssNMR investigations on plant and fungal cell walls, including the use of DNP enhancement, were carried out by the research teams of Stark[280] and Wang.[7,12,13]

3.6.1 Bacteria

The cell wall of bacteria is essential for its survival, growth, and division. A key component of the bacterial cell wall is the peptidoglycan (PG), a polymer of glycan chains with alternating *N*-acetylglucosamine-*N*-acetylmuramic acid (GlcNAc-MurNAc) crosslinked with short peptide bridges. The biochemical machinery for peptidoglycan biosynthesis does not have counterparts in humans or mammals; thus, it is a common target for antibiotics, many of which function by inhibiting peptidoglycan synthesis. Bacteria are relative easy to culture, with many well-characterized mutants presenting tuned cell wall characteristics; as such, they can be a good system for developing whole cell or in-cell DNP procedures. In the methodological context, Takahashi et al. have demonstrated that DNP enhancement can be obtained on entire *Bacillus subtilis* cells, and found that TOTAPOL has specific affinity for the peptidoglycan component of the cell wall.[143]

3.6.2 Fungi

The fungal cell wall is an important organelle that enables the fungi to adapt and survive environmental stresses. Unlike bacteria (gram positive/negative), there is not a simple classification of fungal cell wall architecture. While some components of the fungal cell wall are commonly found, the exact architecture can vary greatly. The fungal cell wall frequently consists of chitin (polymer of *N*-acetylglucosamine, GlcNAc) and glucans (polymers of glucose with varying linkages). While the chitin layer is relatively thin and close to the fungal membrane, the glucan layer is usually much thicker and further out from the fungal membrane. The glucan layer is frequently heavily modified with covalent linkage to many types of molecules, which vary depending on each fungal species and strain. Thus, the outer surface of the fungal cell wall can contain glycoproteins, other polysaccharides, and melanin. All these complex molecular species can mask the fungal cell from the native immune system.[281,282] Interestingly, unlike the case of bacteria, only a subset of antifungal agents targets the fungal cell wall, with traditional therapeutic modes aiming to perturb fungal membranes.[281,283] To gain insight on the fungal cell wall, Kang et al. used MAS-DNP to record 2D $^{13}C-^{15}N$ and $^{15}N-^{15}N$ correlation spectra, and identified three additional minor types of chitin on intact cells of *Aspergillus fumigatus*. The polymorphism identified by the authors in the cell wall of whole fungal cells partly explains the complexity of developing effective antifungal agents. To overcome the problem of spectral crowding, the authors performed spectral editing consisting of a $^{15}N-^{13}C$ dipolar filter to select the chitin amide, followed by polarization transfer to nearby glucans using a spin diffusion step. By taking then the difference of two spectra recorded with different spin diffusion times, the authors were able to obtain a well-resolved spectrum containing only intermolecular long-range cross peaks from the interaction partners of chitin[284] (Figure 28). Considering the limited amount of chitin in the cell wall and the requirement for a spectra difference, this informative spectral editing experiment was very insensitive and only made possible with the sensitivity enhancement brought by MAS-DNP.

Melanin is a polyaromatic dark pigment found in certain fungal cell walls and associated

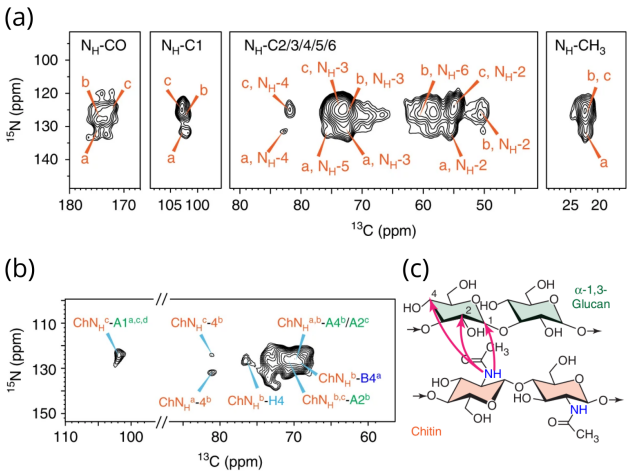

Figure 28: (a) DNP-enhanced ^{15}N−^{13}C correlation spectra measured using 3 mg of *A. fumigatus* fungal cells. Labels of signals with a, b, c indicate the three major types of chitin identified in this sample. (b) DNP-enhanced, chitin-edited ^{15}N−^{13}C correlation spectrum with unambiguously detected signals from chitin itself (orange labels) or glucans that are spatially proximal (light blue, green, and blue labels). The DNP experiments were conducted on a 600 MHz/395 GHz spectrometer. (c) Illustration of chitin–glucan packing interactions that were discovered by the chitin-edited spectrum in (b). (a, b) Reprinted in part from ref. 284 under a Creative Commons (CC-BY 4.0) license. (c) Reprinted in part with permission from ref. 13. Copyright 2020 John Wiley and Sons.

with virulence. Its structure is difficult to investigate due to being insoluble, heterogeneous, amorphous, and moreover, slightly paramagnetic. Using a cell-free method, Chatterjee et al. obtained labeled fungal melanin samples that were studied with MAS-DNP. Even with a modest enhancement, the authors were able to obtain 2D ^{13}C−^{15}N z-filtered transferred echo double resonance (TEDOR) spectra on these challenging samples, bringing insight on the precursor requirement and time course of the biosynthetic process of this protective fungal pigment.[285]

A chemoenzymatic investigation of melanin derived from tyrosinase of *Agaricus bisporus*, the most common species of edible mushrooms, was performed combining characterization with MAS-DNP, ssNMR, and scanning electron microscopy. Starting with ^{13}C, ^{15}N-labeled Tyr, the formation of melanin was found to not follow a strictly stepwise biosynthetic pathway, but has a wider scope of reactants including many monomeric intermediates. MAS-DNP was applied on labeled melanin obtained from the action of the fungal tyrosinase, and 2D

$^{13}C-^{13}C$ correlation spectra could be assigned to specific intermediates. Such a study can shed light on the diversity of structures present in melanin and develop structure–function correlations of this pigment.[286]

3.6.3 Plants

The main component of the plant cell wall is cellulose, which consists of β-1,4-linked glucose chains and is the most abundant glycan-based biomaterial on Earth. During growth, the plant cell produces primary cell wall which can accommodate cell expansion; after growth has ceased and expansion is complete, secondary cell wall is produced to provide greater rigidity and strength. Both types of cell wall contain cellulose and different types of hemicelluose. Secondary cell walls also contain lignin, an heterogeneous polyaromatic polymer.[287] The composition, the amount, and interactions between these different plant cell-wall polymers is species specific, and has implications for the chemicophysical material properties, as well as for the extraction and purification of cellulose, which is obviously of significant industrial importance.

Early MAS-DNP methodological work on cellulose was carried out using a matrix-free sample preparation method.[41] The sensitivity enhancement achieved via DNP enhancement enabled 2D DQ-SQ $^{13}C-^{13}C$ correlation spectra to be acquired on natural abundance cellulose, in 20 minutes at 9.4 T with TOTAPOL[41] and in 16 hours at 18.8 T with TEMTriPol-1.[50]

Meanwhile, in an early biological application of MAS-DNP, Wang et al. investigated expansin, a protein which loosen the assemblies of cellulose and other glycans in the cell wall during plant growth. DNP signal enhancement was required as the amount of expansin is only 0.1% by weight of the cell wall. In order to characterize the binding interaction of this protein, highly selective experiments were devised to detect signals of glycans that are in close proximity to the expansin protein.[288]

Subsequently, the Wang group has developed protocols for preparing fungal and plant materials for ssNMR analysis, both with and without DNP signal enhancement,[122] and often

without isotopic enrichment.[289] Using these methodologies, they investigated the impact of ball milling on the crystallinity of commercial cotton cellulose at natural abundance using MAS-DNP.[119] The crystalline to amorphous conversion upon that specific treatment was corroborated to observations made using over ten other techniques.[290]

In an interdisciplinary effort to understand the role of acetylation in the correct formation of native cell wall architecture, Zhang et al. obtained DNP-enhanced 2D $^{13}C-^{13}C$ correlation spectra on natural abundance samples of wild type and mutant rice to investigate their differences in the acetylation of arabinoxylan, the major hemicellulose species.[291]

Using a series of labeled samples from herbaceous plants, including maize, *Arabidopsis*, switchgrass, and rice, Kang et al. designed NMR experiments that specifically excite hemicellulose signals (mainly xylan) that are bound to the lignin aromatic groups (Figure 29). DNP signal enhancement was key for the acquisition of such lignin-edited spectra, since the signal selection is based on the combination of an aromatic-selective dipolar gating sequence[292] and a frequency filter, as well as a short recycle delay, all of which significantly reduces the sensitivity and increase the challenge of obtaining 2D spectra.[293] The excellent selectivity achieved in this study was partly enabled by customization of the gyrotron microwave source, which was equipped with a shutter to turn off the microwave after the initial CP excitation step, thus avoiding repolarization of the dominant bulk signals.[294]

There are also a number of MAS-DNP studies in the broad context of material science, aiming to observe the effect of various extraction processes and covalent modifications for industrial applications, such as the effect of lignin removal treatments on wood[295,296] or the characterization of chemically modified cellulose-based materials.[297,298] Such work is carried out in the great majority at natural abundance, where DNP signal enhancement is required for a detailed analysis based on 2D NMR spectroscopy.

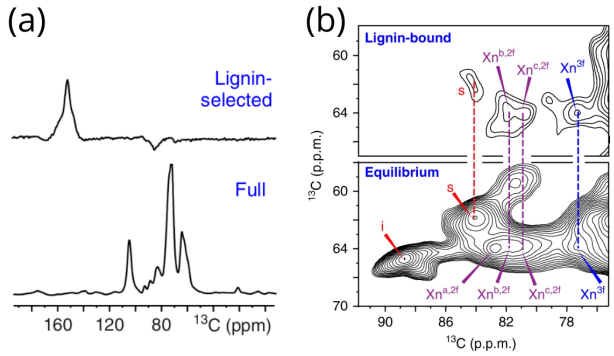

Figure 29: MAS-DNP reveals the conformational selectivity of xylan for lignin-binding using experiments on maize stem samples. (a) 1D lignin-selective (top) and non-selective (bottom) ^{13}C DNP-enhanced CP-MAS spectra. In the lignin-selective spectrum, the aromatic signal is clearly far more prominent than the carbohydrate signals. (b) Lignin-edited (top) and control (bottom) ^{13}C−^{13}C correlation spectra obtained with MAS-DNP. The lignin-edited spectrum only shows polysaccharides spatially proximal to lignin, including three-fold xylan (blue labels, Xn^{3f}), a subset of two-fold xylan (purple labels, Xn^{2f}, types b and c), and surface cellulose (s). The interior cellulose (i) signal was absent in the lignin-edited spectrum, as expected. Adapted with permission from ref. 13. Copyright 2020 John Wiley and Sons. Reprinted in part from ref. 293 under a Creative Commons (CC-BY 4.0) license.

3.7 Biomolecules in the extracellular context

Biological activity in all organisms, whether unicellular or multicellular, is not limited to within the cell. The extracellular space, or more correctly the extracellular matrix, can often demonstrate as much complexity as the in-cell environment. In bacteria and yeast, a biofilm is often secreted in many growth conditions, providing an external environment that can encourage robust adherence and colonization of the surface. For multicellular organisms, the extracellular matrix is much more than a passive scaffold, but a key player with signaling functions that can determine cell behavior and fate.[299]

The extracellular matrix can comprise of inorganic minerals and organic components. The inorganic phase can be crystalline or amorphous, depending on the biological state of the organism(s) involved. For the organic components, it is possible to find a full repertoire of biomolecule types as those found in-cell, including proteins, glycans, lipids, and nucleic acids, albeit at different proportions. Frequently, the extracellular matrix is composed of insoluble, heterogeneous, heavily modified, and cross-linked components, making it challenging

to characterize, quantify, and observe biomolecular interactions. Moreover, the components can be highly dynamic and undergo significant turnover. The species of interest may occur as a minor component, thus requiring DNP signal enhancement for detection and investigation. Here we outline some emerging applications of MAS-DNP on this type of systems.

3.7.1 Calcified biominerals

A review by Gervais, Bonhomme, and Laurencin highlights the possibilities by which state-of-the-art NMR techniques, including MAS-DNP, can be applied to the study of synthetic and natural calcium phosphates, the most well-known examples of which is found in bones and teeth.[20] Two DNP studies were reported on carbonated substituted hydroxyapatite (CHAp) phase of calcium phosphate, a synthetic model for the mineral phase of bone tissue. The first one reports the feasibility of efficiently detecting $^{1}H-^{43}Ca$ NMR correlation signals on natural abundance synthetic nanoparticles and mice teeth. While this type of experiment is highly useful for structural investigation of such materials, it would be impossible to access it without the sensitivity enhancement provided by DNP.[300] In the second study, MAS-DNP on ^{13}C-labeled CHAp enabled the detection of substitutions in the bulk of the material. The CHAp domains could be characterized according to the type of carbonate substitution by using $^{31}P-^{13}C$ and $^{13}C-^{13}C$ correlation experiments. Even with ^{13}C labeling, such experiments are challenging due to the relatively low amount of carbonate substitution present within the mineral.[121]

Using DNP signal enhancement, Sinha and co-workers carried out a number of proof-of-concept investigations on natural abundance collagen-containing tissues. Singh et al. demonstrated that correlations between imino acids and aromatic residues can be obtained via $^{1}H-^{13}C$ HETCOR experiments on natural abundance bone samples;[301] while imino acids are relatively abundant (>20%) in collagen type I in bone, aromatic residues are rare (2%), rendering interchain correlations between these two types of residues on a natural abundance sample highly challenging to detect. More recently, Tiwari et al. demonstrated 2D $^{13}C-^{13}C$

correlation spectra on natural abundance bone and cartilage samples.[302] Using the signal enhancement provided by DNP, the authors confirmed previously observed signals arising from citrate in bone[303,304] and from glycosaminoglycans in cartilage, and attempted to identify their interaction with collagen proteins. Although tryptophan was identified as one of the possible interaction partners, collagen type I and II, the predominant types of collagen found in these tissues, lack tryptophan. It is possible that this observation involves tryptophan residues from other proteins found in these native tissues.

Azaïs et al. have demonstrated the capability of DNP combined with CP to provide surface-specific enhancement (DNP SENS[140]) in biominerals, with two main examples on sheep bone tissue and European abalone shell nacre.[305] Both of these are calcified organic matrices; bone is predominately a collagen matrix that is mineralized with calcium phosphate (hydroxyapatite-like), and European abalone nacre is an organic matrix of glycans and proteins that is mineralized with calcium carbonate (aragonite). On the bone sample, DNP signal enhancement enabled a long series of ^{13}C $\{^{31}P\}$ REDOR spectra to be obtained, which confirmed the fraction of surface-bound citrate present in the mineral phase of bone in line with previously published studies.[304] For shell nacre, a 2D $^{1}H-^{13}C$ HETCOR experiment recorded in 16 minutes allowed the easy identification of many exposed carbonate sites as protonated bicarbonate ions, and provided insight into the disordered phase in this material.

3.7.2 Mammalian ECM

In studies on collagen-based extracellular matrices, a glycerol-containing DNP matrix is often not used, and does not appear to deliver additional DNP enhancement.[120] Reasonable enhancement factors ($\varepsilon_{on/off} \approx 15$–$60$) were obtained by a D_2O/H_2O mixture or simply using D_2O and relying on the protonated sample to provide the necessary ^{1}H spin diffusion to spread hyperpolarization.[306]

Duer and coworkers designed MAS-DNP studies to investigate low level species in the extracellular matrix (ECM), using mammalian primary cell cultures supplemented with

isotopically-labeled precursors. The use of cells that are extracted from a tissue of interest and underwent a limited number of subcultures, rather than immortalized cell lines which are usually easier to culture, is important for obtaining ECM that is faithful to a physiological rather than a pathological state. This approach was successful for probing hydroxylysines in two types of samples: mouse skin tissue, and ECM obtained from bovine vascular muscle cell culture. Hydroxylysine is a post-translational modification that is specific to collagen and occur at less than 2% of the collagen sequence. These residues are essential sites for crosslinking and glycosylation, which modify the mechanical and surface properties of collagen fibrils; their loss can lead to certain forms of osteogenesis imperfecta. MAS-DNP enabled the detection of hydroxylysines in these native and native-like samples, and was able to detect subpopulations of different types of covalent modifications at these sites.[120]

The molecular mechanisms linking intracellular DNA-damage response to extracellular matrix calcification has been investigated by Müller et al. in a highly interdisciplinary study. The authors cultivated cell culture models of vascular ECM with labeled glucose, which was converted by vascular cells into poly-(ADP ribose) (PAR); thereafter, the cells were lysed and the sugar species detected. DNP signal enhancement was required to unambiguously assign PAR that remained associated with the vascular ECM after cell lysis, and to confirm that any DNA released during the lysis procedure was removed and no longer associated with the ECM.[307]

By labeling the ECM of fetal sheep osteoblasts with specific amino acids such as histidine and lysine, Goldberga et al. discovered by MAS-DNP the presence of low levels of nucleic acid within the ECM. The presence of these nucleic acid at this non-canonical location is suggested to be due to matrix vesicles that are involved in biomineralization and cell signaling in the extracellular space.[308]

One of the potential applications of MAS-DNP is the study of natural abundance autopsy samples obtained from humans. In this direction, Chow et al. investigated changes

in cartilage structure of patients suffering from alkaptonuria and osteoarthritis using MAS-DNP. Alkaptonuria (AKU) is a rare disease where patients often suffer from osteoarthritis that progresses rapidly at an early age. The joint degeneration is strongly linked to dark pigmentation that accumulates in weight-bearing joints, though the mechanism of disease progression has not yet been conclusively demonstrated. A series of 2D $^{1}H-^{13}C$ HETCOR experiments were carried out with DNP enhancement on natural abundance samples of human cartilage tissue obtained as surgical waste (Figure 30). Using MAS-DNP and EPR, the authors conclusively linked the chemical structure of the pigment to the metabolite (homogentisic acid) that is elevated in these patients, gained insight into the disease mechanism, and proposed a novel degeneration pathway for collagen proteins in cartilage that may be common to patients of both AKU and osteoarthritis.[309]

3.7.3 Silk

Although spiders can be fed a diet with isotopically-enriched amino acids, the exposure to relatively high concentrations of specific amino acids is known to affect the spiders and their silk, which makes this biomaterial difficult to enrich. A fascinating study was carried out by Craig et al., who used MAS-DNP to obtain 2D $^{1}H-^{13}C$ HETCOR spectra on natural abundance spider silk in only 10 minutes rather than 8 hours as per conventional NMR. With this experiment, the authors probed the hydrogen bonding in the silk from three different spider species, which was found to correlate with the stiffness (Figure 31). Moreover, hydroxyproline residues were detected for the first time by NMR in one of these spider silks, and different conformations of arginine were observed in the silks from the different species.[310]

3.7.4 Biosilica

MAS-DNP has been used in several investigations on diatoms. Diatoms are single-cell algae whose cell wall is mineralized with silica. The intact biosilica is a hybrid organic-inorganic material, which has been characterized by solid-state NMR.[311] The organic phase is complex,

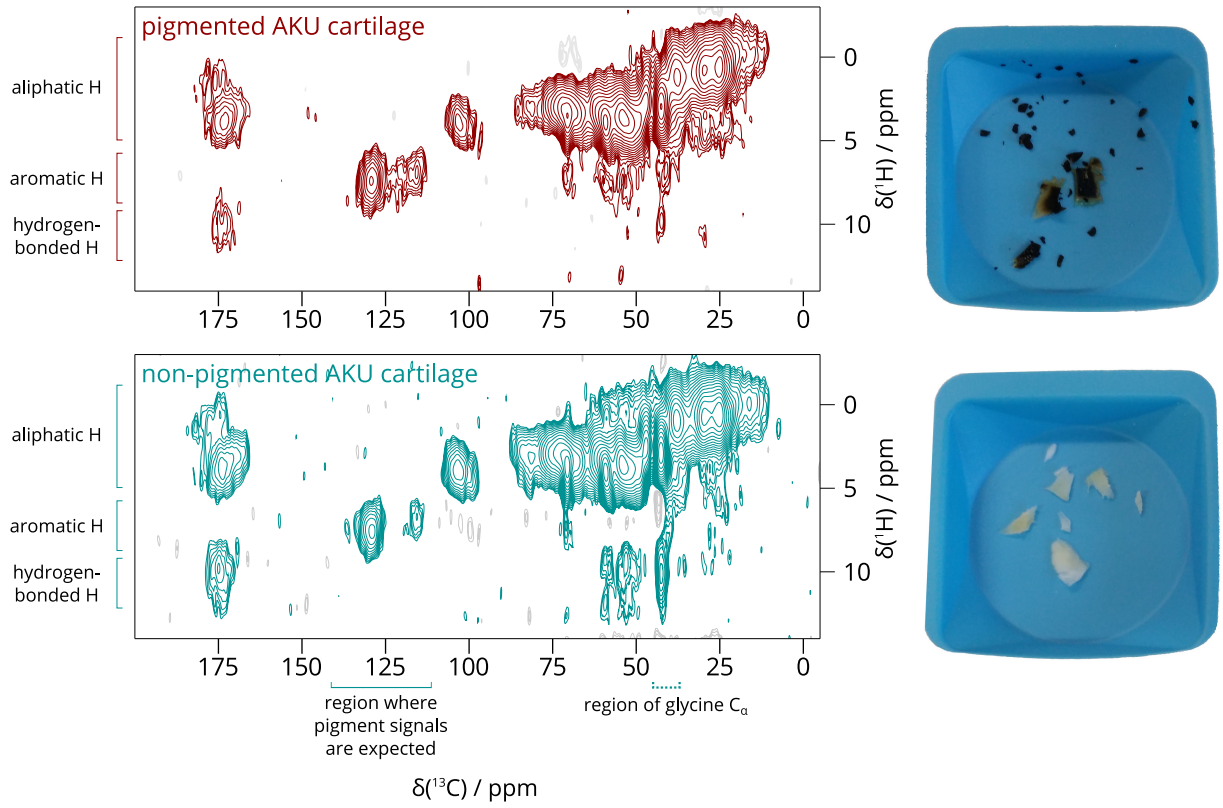

Figure 30: Left: 2D DNP-enhanced $^{1}H-^{13}C$ HETCOR spectra obtained from pigmented (red) and non-pigmented (green) human AKU cartilage at 50 µs contact time. Spectral differences in the aromatic region indicated pigmentation species; in the glycine C_α region, differences suggested collagen degradation in the pigmented cartilage. Right: Human cartilage samples used in the DNP experiment, showing the dark pigmentation due to AKU. Adapted from ref. 309 under a Creative Commons (CC-BY 4.0) license.

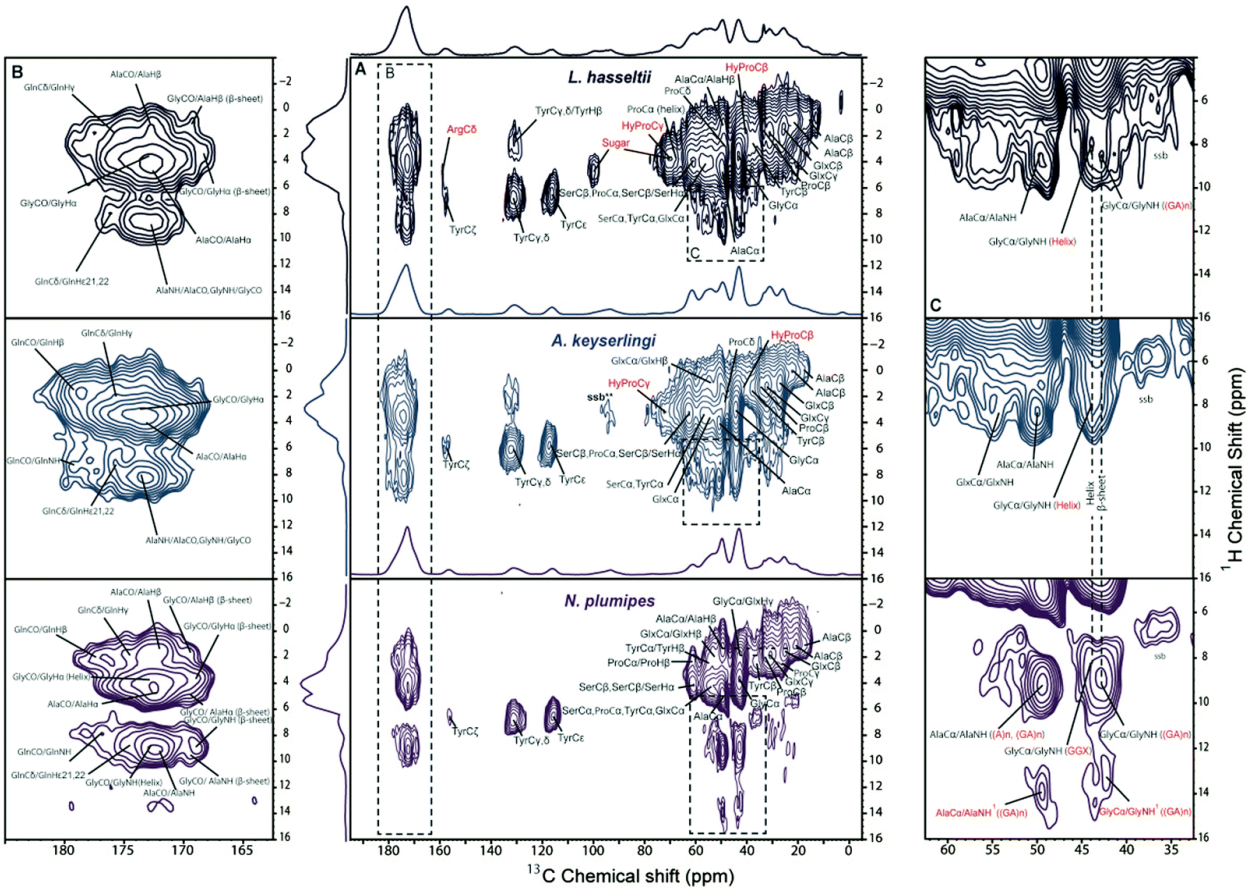

Figure 31: 2D ^{1}H−^{13}C HETCOR MAS-DNP experiments on natural abundance spider silks with a contact time of 150 µs. The silks are taken from *L. hasselti* (top), *A. keyserlingi* (middle), and *N. plumipes* (bottom). Full spectrum (A), with expanded carbonyl (B) and glycine C_α (C) sections. Reproduced from ref. 310 with permission from the Royal Society of Chemistry.

containing mineral-associated proteins, long chain polyamines, and carbohydrates. Combining ^{13}C, ^{15}N, and ^{29}Si labeling with DNP enhancement, Jantschke et al. were able to identify all components of the organic phase of the diatom *Stephanopyxis turris*, even for the low abundance polyamine and lysine components. For the protein fraction, mainly β-strand and random-coil conformations were observed, in agreement with molecular dynamics results. A model was proposed, which consists of a 3 nm surface organic layer covering the 40–80 nm thick silica phase substituted with the polyamines.[312] Two further species of diatoms, *Cyclotella cryptica* and *Thalassiosira pseudonana* were analyzed with MAS-DNP in a more recent publication. These diatoms are producing chitin fibrils, both external to the cell wall as well as attached to the silica mineral phase. By comparing the DNP signal enhancement of the various organic components, including chitin, in different species of labeled diatoms, the authors suggest different arrangements and thickness of the chitin layer relative to the silica phase, which is low in ^{1}H and shows reduced spin diffusion.[104]

It is known that specific long chain polyamines and proteins assist in the biomineralization of diatoms, which is much faster than abiotic silica formation. One such protein is silaffin, with lysine-rich repeat segments. To accelerate the synthesis of biomimetic silica for biotechnological applications, a 12-mer peptide derived from silaffin and containing 5 lysines was proposed. The peptide as well as the resultant silica were analyzed by a range of techniques, including MAS-DNP. The experimental time required to detect the silica-embedded peptide in 1D ^{13}C CPMAS spectra was reduced from 17 hours with conventional ssNMR to only 16 scans (64 seconds) with MAS-DNP. This enhancement in sensitivity enabled additional 2D experiments to probe the peptide backbone conformation.[313] Biomimetic silica can be used to immobilize enzymes in the context of a wider range of technological applications. While various proteins can be successfully embedded in silica and analyzed by ssNMR, such samples suffer from low sensitivity. A preliminary study of several silica-entrapped enzymes by Ravera, Michaelis et al. demonstrated promising DNP enhancements ($\varepsilon_{on/off}$ of 20 and 55) on this type of systems at 5 T, and still reasonable enhancements ($\varepsilon_{on/off}$ of 16 and 15)

at 16.4 T, though the authors note that the spectral resolution was fairly low.[314]

4 Outlook

MAS-DNP is a versatile technique that has recently been applied on various biological problems found in all domains of life. While the first DNP report on a biological system was nearly 25 years ago, the technique became more widely available commercially over the last decade. The enhancement in sensitivity provided by MAS-DNP undoubtedly expanded the scope of solid-state NMR spectroscopy and many methodologies currently in development will certainly maintain and even accelerate this momentum. These on-going developments include ultra-low temperature DNP with sustainable helium spinning for even higher sensitivities and MAS spinning frequencies,[49,52–55] high temperature DNP that will perhaps rely predominantly on the Overhauser DNP mechanism,[48,315] sterically-shielded radicals with enhanced stability against reduction for in-cell applications,[81,275] pulsed excitation of electron spins,[316,317] electron decoupling,[318] improved targeting strategies to focus on specific molecules or regions of the biological system,[8] and so on.

A key challenge yet to be fully overcome is the resolution of spectra at cryogenic temperature, which must be addressed in order to further broaden the biological application scope of MAS-DNP. Nevertheless, insightful information could already be obtained on well-defined questions, mainly using specific labeling, as evidenced by the number and variety of work published so far. It is clear that MAS-DNP and even solid-state NMR are only one part of the solution towards understanding the complex function and mechanism of biomolecular systems and assemblies. Often, it is best to consider an integrative approach, using all available structural and biophysical tools, including MAS-DNP.

While new biological applications will always be enabled by developments in methodology, it is also interesting to consider new applications on specific types of samples. For example, MAS-DNP using a stable and naturally-occurring radical in a protein was demonstrated

nearly ten years ago.[319] With the recent interest in using endogenous radicals in material investigations,[320,321] this approach can perhaps be revisited for investigating these types of systems via MAS-DNP in addition to photo-CIDNP. Another potentially important trend is the demonstrated feasibility of obtaining useful 2D spectra with natural abundance samples. While some of this line of work has been mentioned above and was already reviewed by Smith et al.,[322] the ability to robustly carry out 2D spectra on natural abundance biological samples will open up many areas for investigation.

The diversity of biology is such that MAS-DNP has most certainly not yet exhausted all fruitful routes of investigation. Many imaginative and bold applications await us still, both with current technology and new methodologies being developed. Almost all current MAS-DNP facilities worldwide are hosted in publicly-funded and national institutions. The significant cost of investing in the instrumentation, consumables, and maintenance required for MAS-DNP, often borne by citizens, should motivate us to continually seek out fresh insights that can justify the privilege of being able to access this technology.

5 Biographies

5.1 Wing Ying Chow

Wing Ying Chow is a postdoctoral researcher funded by the French National Center for Scientific Research (CNRS) and working since 2020 at the Interdisciplinary Research Institute of Grenoble (IRIG). She obtained her Ph.D. from the University of Cambridge, UK, under the supervision of Prof. M. J. Duer. She developed an approach to investigate collagen proteins in the mammalian extracellular matrix by solid-state NMR during her doctoral research, for which she was awarded an Engineering and Physical Sciences Research Council Doctoral Prize. In 2014, she moved to the Forschungsinstitut für Molekulare Pharmakologie in Berlin, Germany to work with Prof. H. Oschkinat as a Leibniz-DAAD Research Fellow. She is interested in using solid-state NMR to gain insight on challenging biological systems,

especially those with relevance to human health and disease.

5.2 Gaël De Paëpe

Gaël De Paëpe leads the Magnetic Resonance team of the Modeling and Exploration of Materials (MEM) laboratory at IRIG. He obtained his Ph.D. from the Ecole Normale Supérieure de Lyon, France, under the supervision of Prof. L. Emsley. In 2004, he moved to MIT to carry out postdoctoral research with Prof. R. G. Griffin. He returned to France in 2008 with a National Research Agency (ANR)-funded "Chaire d'Excellence" to set up high-field MAS-DNP at the Alternative Energies and Atomic Energy Commission (CEA). He received the Vold Memorial Prize (2013) and an European Research Council Consolidator Grant (2015). His group focuses on MAS-DNP method and technology development for applications in materials science, chemistry, and biology.

5.3 Sabine Hediger

Sabine Hediger holds a CNRS research position at MEM/IRIG. She obtained her Ph.D. from the Swiss Federal Institute of Technology in Zurich (ETHZ), under the supervision of Profs. R. R. Ernst and B. H. Meier. She was then employed as a research scientist in charge of solid-state NMR at the Nestlé Research Center in Lausanne, Switzerland. In 1999, she obtained a CNRS research position at ENS Lyon, then moved to CEA Grenoble where she develops her research interests in solid-state NMR and DNP methodology, specifically towards biomolecular applications.

Acknowledgement

This work was supported by the French National Research Agency (Labex ARCANE ANR-11-LABX-0003-01, CBH-EUR-GS Grant ANR-17-EURE-0003, Glyco@Alps ANR-15-IDEX-02, and ANR-16-CE11-0030-03).

Abbreviations

α-LP	α-lytic protease
αS	α-synuclein
A431	a human epidermoid carcinoma cell line
ABC transporter	ATP-binding cassette transporter (membrane protein)
ADP	adenosine 5'-diphosphate
AIDS	acquired immunodeficiency syndrome
AKU	alkaptonuria, a rare human disease
AMP	adenosine monophosphate
AMP-PNP	adenylyl-imidodiphosphate
AP205	bacteriophage that infects Acinetobacter bacteria
ASO	antisense oligonucleotide
ASR	absolute sensitivity ratio
ATP	adenosine 5'-triphosphate
ApoF	apoferritin
ArM	artificial metalloenzyme
B_1R, B_2R	subtypes of bradykinin receptors which are also GCPRs
Bam	β-barrel assembly machinery, a pentameric complex (A–E)
Bcl-X_L	B-cell lymphoma-extra large protein
BMRB	biological magnetic resonance bank
bR	bacteriorhodopsin
CIDNP	chemically induced dynamic nuclear polarization
CORD	combined $R2_n^\nu$-Driven
CP	cross polarization
cryoEM	cryogenic electron microscopy
CSA	chemical shift anisotropy
CSP	chemical shift perturbation

CW	continuous wave
CA	capsid domain of the Gag protein of HIV-1
CaM	calmodulin
ChR	channelrhodopsin
CsgA	curli, a bacterial amylogenic protein
CypA	cyclophilin A
DARR	dipolar assisted rotational resonance
DFT	density functional theory
DGK	diacylglycerol kinase
DLPC	1,2-dilauroyl-sn-glycero-3-phosphocholine
DMPA	1,2-dimyristoyl-sn-glycero-3-phosphate (sodium salt)
DMPC	1,2-dimyristoyl-sn-glycero-3-phosphocholine
DMPE	1,2-dimyristoyl-sn-glycero-3-phosphoethanolamine
DMSO	dimethyl sulfoxide
DNA	deoxyribonucleic acid
DNP	dynamic nuclear polarization
DOPC	1,2-dioleoyl-sn-glycero-3-phosphocholine
DOTA	dodecane tetraacetic acid
DP	direct polarization
DQ, DQF	double quantum, double quantum filtered
DRAWS	dipolar recoupling with a windowless sequence
DSPC	1,2-distearoyl-sn-glycero-3-phosphocholine
DnaB	bacterial helicase
$\boldsymbol{\varepsilon_B}$	Boltzmann polarization
$\boldsymbol{\varepsilon_{on/off}}$	enhancement value
ECM	extracellular matrix
EGFR	epidermal growth factor receptor

EmrE	efflux-multidrug resistance E
EPR	electron paramagnetic (spin) resonance spectroscopy
FAM	fluorescein fluorophore
GBC	γB-crystallin
GFP	green fluorescent protein
GPCR	G-protein-coupled receptor
GPR	green proteorhodopsin
GlcNAc	N-acetylglucosamine
HADDOCK	'high ambiguity driven biomolecular docking' software
HEK293	human embryonic kidney cell line
HETCOR	heteronuclear correlation
HIV	human immunodeficiency virus
HP35	villin headpiece subdomain,
HPLC	high-performance liquid chromatography
HSQC	heteronuclear single quantum coherence experiment
HeLa	a human cervical cancer cell line
HttEx1	first exon of mutant huntingtin protein
IAPP	islet amyloid polypeptide, also known as amylin
IDP	intrinsically disordered protein
IF1	prokaryotic translation initiation factor
INEPT	insensitive nuclei enhancement by polarization transfer experiment
ITC	isothermal titration calorimetry
KL_4	peptide that mimics lung surfactant protein
KcsA	K^+ channel of streptomyces A
LAH	influenza virus hemagglutinin stalk long α-helix
LPS	lipopolysaccharides
LamB	signal peptide in *E. coli*

LecA a galactose-binding lectin from *Pseudomonas aeruginosa.*

M2 proton channel of influenza virus

MAS magic-angle spinning

MD molecular dynamics

MF matrix-free

MTS diamagnetic version of MTSSL

MTSSL 1-oxyl-2,2,5,5-tetramethyl methanethiosulfonate spin label

MsbA ABC exporter from *E. coli* that translocates lipopolysaccharides to the outer membrane of gram-negative bacteria

MurNAc N-acetylmuramic acid

NBD nucleotide binding domain

NMR nuclear magnetic resonance

NOE nuclear Overhauser effect

NOVEL nuclear orientation via electron spin locking

PA polarizing agent

PagL lipid A deacylase of *E. coli*

PAR (NMR) proton assisted recoupling experiment

PAR (biopolymer) poly-(ADP ribose)

PASS phase-adjusted spinning sidebands experiment

PCB phycocyanobilin

PDB protein data bank

PDSD proton-driven spin diffusion

PG peptidoglycan of the bacterial cell wall

PG-1 antimicrobial peptide protegrin-1

PI3 phosphatidylinositol 3-kinase

POPC 1-palmitoyl-2-oleoyl-glycero-3-phosphocholine

POPG 1-palmitoyl-2-oleoyl-sn-glycero-3-phospho-(1'-rac-glycerol) (sodium salt)

pR	proteorhodopsin
PRE	paramagnetic relaxation enhancement
pSB	retinal-bound protonated Schiff base
QM/MM	quantum mechanics/molecular mechanics molecular simulations
rAK	reverse adenylate kinase site of MsbA
REAPDOR	rotational echo adiabatic passage double resonance experiment
REDOR	rotational echo double resonance experiment
RF	radiofrequency
RFDR	radiofrequency driven recoupling experiment
RNA	ribonucleic acid
RNC	ribosome–nascent chain complex
RT	room temperature
SCREAM	specific cross relaxation enhancement by active motions under DNP
SENS	surface enhanced NMR spectroscopy
SH3	α-spectrin Src-homology 3 domain
SIMPLE	selective detection of internuclear contacts by methyl poLarization enhancement
SP1	spacer peptide 1 of the Gag protein of HIV-1
SPECIFIC CP	spectrally induced filtering in combination with cross polarization
SQ	single quantum
STAT3	signal transducer and activator of transcription 3
SecM	secretion monitor protein that can stall protein translation on the ribosome
SecYEG	channel protein responsible for secretion/translocation of proteins across the cytosolic membrane
***Sel*DNP**	selective DNP
ssNMR	solid-state NMR

TAMRA	carboxytetramethylrhodamine
TAP	ABC transporter associated with antigen processing
T_B	hyperpolarization buildup time constant
TEDOR	transferred echo double resonance experiment
TMD	transmembrane (domain)
TMR	tetramethylrhodamine
TOAC	2,2,6,6-tetramethyl-piperidine-1-oxyl-4-amino-4-carboxylic acid
TPP	tetraphenylphosphonium
TTR	transthyretin
VLP	virus-like particle
VM/VMS	virus-mimetic membrane
WT	wild-type
Y2R	neuropeptide Y2 receptor, a GPCR

References

(1) Su, Y.; Andreas, L.; Griffin, R. G. Magic Angle Spinning NMR of Proteins: High-Frequency Dynamic Nuclear Polarization and 1H Detection. *Annu. Rev. Biochem.* **2015**, *84*, 465–497.

(2) Akbey, Ü.; Oschkinat, H. Structural Biology Applications of Solid State MAS DNP NMR. *J. Magn. Reson.* **2016**, *269*, 213–224.

(3) Smith, A. N.; Long, J. R. Dynamic Nuclear Polarization as an Enabling Technology for Solid State Nuclear Magnetic Resonance Spectroscopy. *Anal. Chem.* **2016**, *88*, 122–132.

(4) Lilly Thankamony, A. S.; Wittmann, J. J.; Kaushik, M.; Corzilius, B. Dynamic Nuclear Polarization for Sensitivity Enhancement in Modern Solid-State NMR. *Prog. Nucl. Magn. Reson. Spectrosc.* **2017**, *102-103*, 120–195.

(5) Jaudzems, K.; Polenova, T.; Pintacuda, G.; Oschkinat, H.; Lesage, A. DNP NMR of Biomolecular Assemblies. *J. Struct. Biol.* **2019**, *206*, 90–98.

(6) Mandala, V. S.; Hong, M. High-Sensitivity Protein Solid-State NMR Spectroscopy. *Curr. Opin. Struct. Biol.* **2019**, *58*, 183–190.

(7) Chakraborty, A.; Deligey, F.; Quach, J.; Mentink-Vigier, F.; Wang, P.; Wang, T. Biomolecular Complex Viewed by Dynamic Nuclear Polarization Solid-State NMR Spectroscopy. *Biochem. Soc. Trans.* **2020**, *48*, 1089–1099.

(8) Gauto, D.; Dakhlaoui, O.; Marin-Montesinos, I.; Hediger, S.; De Paëpe, G. Targeted DNP for Biomolecular Solid-State NMR. *Chem. Sci.* **2021**, *12*, 6223–6237.

(9) König, A.; Schölzel, D.; Uluca, B.; Viennet, T.; Akbey, Ü.; Heise, H. Hyperpolarized MAS NMR of Unfolded and Misfolded Proteins. *Solid State Nucl. Magn. Reson.* **2019**, *98*, 1–11.

(10) Tycko, R. NMR at Low and Ultralow Temperatures. *Acc. Chem. Res.* **2013**, *46*, 1923–1932.

(11) Becker-Baldus, J.; Glaubitz, C. Cryo-Trapped Intermediates of Retinal Proteins Studied by DNP-Enhanced MAS NMR Spectroscopy. In *eMagRes*; Wiley, 2018; Vol. 7; pp 79–92.

(12) Zhao, W.; Fernando, L. D.; Kirui, A.; Deligey, F.; Wang, T. Solid-State NMR of Plant and Fungal Cell Walls: A Critical Review. *Solid State Nucl. Magn. Reson.* **2020**, *107*, 101660.

(13) Fernando, L. D.; Zhao, W.; Dickwella Widanage, M. C.; Mentink-Vigier, F.; Wang, T. Solid-State NMR and DNP Investigations of Carbohydrates and Cell-Wall Biomaterials. In *eMagRes*; Wiley, 2020; Vol. 9; pp 251–258.

(14) Porat-Dahlerbruch, G.; Goldbourt, A.; Polenova, T. Virus Structures and Dynamics by Magic-Angle Spinning NMR. *Annu. Rev. Virol.* **2021**, *8*, 219–237.

(15) Elkins, M. R.; Hong, M. Elucidating Ligand-Bound Structures of Membrane Proteins using Solid-State NMR Spectroscopy. *Curr. Opin. Struct. Biol.* **2019**, *57*, 103–109.

(16) Ladizhansky, V. Applications of Solid-State NMR to Membrane Proteins. *Biochim. Biophys. Acta - Proteins Proteomics* **2017**, *1865*, 1577–1586.

(17) Narasimhan, S.; Folkers, G. E.; Baldus, M. When Small Becomes Too Big: Expanding the Use of In-Cell Solid-State NMR Spectroscopy. *ChemPlusChem* **2020**, *85*, 760–768.

(18) Paioni, A. L.; Renault, M. A.; Baldus, M. DNP and Cellular Solid-State NMR. In *eMagRes*; Wiley, 2018; Vol. 7; pp 51–62.

(19) Warnet, X. L.; Arnold, A. A.; Marcotte, I.; Warschawski, D. E. In-Cell Solid-State NMR: An Emerging Technique for the Study of Biological Membranes. *Biophys. J.* **2015**, *109*, 2461–2466.

(20) Gervais, C.; Bonhomme, C.; Laurencin, D. Recent Directions in the Solid-State NMR Study of Synthetic and Natural Calcium Phosphates. *Solid State Nucl. Magn. Reson.* **2020**, *107*, 101663.

(21) Ardenkjaer-Larsen, J. H.; Boebinger, G. S.; Comment, A.; Duckett, S.; Edison, A. S.; Engelke, F.; Griesinger, C.; Griffin, R. G.; Hilty, C.; Maeda, H. et al. Facing and Overcoming Sensitivity Challenges in Biomolecular NMR Spectroscopy. *Angew. Chem. Int. Ed.* **2015**, *54*, 9162–9185.

(22) Biedenbänder, T.; Aladin, V.; Saeidpour, S.; Corzilius, B. Dynamic Nuclear Polarization for Sensitivity Enhancement in Biomolecular Solid-State NMR. *Chem. Rev.* **2022**, Article ASAP. DOI: 10.1021/acs.chemrev.1c00776 (accessed 2022–03–14).

(23) Corzilius, B. High-Field Dynamic Nuclear Polarization. *Annu. Rev. Phys. Chem.* **2020**, *71*, 143–170.

(24) Bode, B. E.; Thamarath, S. S.; Gupta, K. B. S. S.; Alia, A.; Jeschke, G.; Matysik, J. The Solid-State Photo-CIDNP Effect and Its Analytical Application. In *Hyperpolarization Methods in NMR Spectroscopy*; Topics in Current Chemistry Series; Springer, 2012; Vol. 310; pp 105–121.

(25) Matysik, J.; Ding, Y.; Kim, Y.; Kurle, P.; Yurkovskaya, A.; Ivanov, K.; Alia, A. Photo-CIDNP in Solid State. *Appl. Magn. Reson.* **2021**, 1–17. DOI: 10.1007/s00723–021–01322–5.

(26) Hall, D. A.; Maus, D. C.; Gerfen, G. J.; Inati, S. J.; Becerra, L. R.; Dahlquist, F. W.; Griffin, R. G. Polarization-Enhanced NMR Spectroscopy of Biomolecules in Frozen Solution. *Science* **1997**, *276*, 930–932.

(27) Potapov, A.; Thurber, K. R.; Yau, W.-M.; Tycko, R. Dynamic Nuclear Polarization-enhanced 1H-13C Double Resonance NMR in Static Samples Below 20K. *J. Magn. Reson.* **2012**, *221*, 32–40.

(28) Thurber, K.; Tycko, R. Low-Temperature Dynamic Nuclear Polarization with Helium-Cooled Samples and Nitrogen-Driven Magic-Angle Spinning. *J. Magn. Reson.* **2016**, *264*, 99–106.

(29) Sesti, E. L.; Saliba, E. P.; Alaniva, N.; Barnes, A. B. Electron Decoupling with Cross Polarization and Dynamic Nuclear Polarization Below 6 K. *J. Magn. Reson.* **2018**, *295*, 1–5.

(30) Jakdetchai, O.; Denysenkov, V.; Becker-Baldus, J.; Dutagaci, B.; Prisner, T. F.; Glaubitz, C. Dynamic Nuclear Polarization-Enhanced NMR on Aligned Lipid Bilayers at Ambient Temperature. *J. Am. Chem. Soc.* **2014**, *136*, 15533–15536.

(31) Salnikov, E. S.; Sarrouj, H.; Reiter, C.; Aisenbrey, C.; Purea, A.; Aussenac, F.; Ouari, O.; Tordo, P.; Fedotenko, I.; Engelke, F. et al. Solid-State NMR/Dynamic Nuclear Polarization of Polypeptides in Planar Supported Lipid Bilayers. *J. Phys. Chem. B* **2015**, *119*, 14574–14583.

(32) Rosay, M.; Blank, M.; Engelke, F. Instrumentation for Solid-State Dynamic Nuclear Polarization with Magic Angle Spinning NMR. *J. Magn. Reson.* **2016**, *264*, 88–98.

(33) Maly, T.; Debelouchina, G. T.; Bajaj, V. S.; Hu, K.-N.; Joo, C.-G.; Mak-Jurkauskas, M. L.; Sirigiri, J. R.; van der Wel, P. C. a.; Herzfeld, J.; Temkin, R. J. et al. Dynamic Nuclear Polarization at High Magnetic Fields. *J. Chem. Phys.* **2008**, *128*, 052211.

(34) Barnes, A. B.; De Paëpe, G.; van der Wel, P. C.; Hu, K.-N.; Joo, C. G.; Bajaj, V. S.; Mak-Jurkauskas, M. L.; Sirigiri, J. R.; Herzfeld, J.; Temkin, R. J. et al. High-Field Dynamic Nuclear Polarization for Solid and Solution Biological NMR. *Appl. Magn. Reson.* **2008**, *34*, 237–263.

(35) Ni, Q. Z.; Daviso, E.; Can, T. V.; Markhasin, E.; Jawla, S. K.; Swager, T. M.; Temkin, R. J.; Herzfeld, J.; Griffin, R. G. High Frequency Dynamic Nuclear Polarization. *Acc. Chem. Res.* **2013**, *46*, 1933–1941.

(36) Mak-Jurkauskas, M. L.; Griffin, R. G. High-Frequency Dynamic Nuclear Polarization. *Encycl. Magn. Reson.* **2010**, 1–12.

(37) Lee, D.; Hediger, S.; De Paëpe, G. Is Solid-State NMR Enhanced by Dynamic Nuclear Polarization? *Solid State Nucl. Magn. Reson.* **2015**, *66–67*, 6–20.

(38) Thurber, K. R.; Tycko, R. Perturbation of Nuclear Spin Polarizations in Solid State NMR of Nitroxide-Doped Samples by Magic-Angle Spinning without Microwaves. *J. Chem. Phys.* **2014**, *140*, 184201.

(39) Mentink-Vigier, F.; Paul, S.; Lee, D.; Feintuch, A.; Hediger, S.; Vega, S.; De Paëpe, G. Nuclear Depolarization and Absolute Sensitivity in Magic-Angle Spinning Cross Effect Dynamic Nuclear Polarization. *Phys. Chem. Chem. Phys.* **2015**, *17*, 21824–21836.

(40) Hediger, S.; Lee, D.; Mentink-Vigier, F.; De Paëpe, G. MAS-DNP Enhancements: Hyperpolarization, Depolarization, and Absolute Sensitivity. In *eMagRes*; Wiley, 2018; Vol. 7; pp 105–116.

(41) Takahashi, H.; Lee, D.; Dubois, L.; Bardet, M.; Hediger, S.; De Paëpe, G. Rapid Natural-Abundance 2D 13C-13C Correlation Spectroscopy using Dynamic Nuclear Polarization Enhanced Solid-State NMR and Matrix-Free Sample Preparation. *Angew. Chem. Int. Ed.* **2012**, *51*, 11766–11769.

(42) Takahashi, H.; Fernández-De-Alba, C.; Lee, D.; Maurel, V.; Gambarelli, S.; Bardet, M.; Hediger, S.; Barra, A. L.; De Paëpe, G. Optimization of an Absolute Sensitivity in a Glassy Matrix During DNP-Enhanced Multidimensional Solid-State NMR Experiments. *J. Magn. Reson.* **2014**, *239*, 91–99.

(43) Lopez Del Amo, J. M.; Schneider, D.; Loquet, A.; Lange, A.; Reif, B. Cryogenic Solid State NMR Studies of Fibrils of the Alzheimer's Disease Amyloid-β Peptide: Perspectives for DNP. *J. Biomol. NMR* **2013**, *56*, 359–363.

(44) Bahri, S.; Silvers, R.; Michael, B.; Jaudzems, K.; Lalli, D.; Casano, G.; Ouari, O.; Lesage, A.; Pintacuda, G.; Linse, S. et al. 1H Detection and Dynamic Nuclear Polarization–enhanced NMR of Aβ1-42 Fibrils. *Proc. Natl. Acad. Sci. U. S. A.* **2022**, *119*, e2114413119.

(45) Fricke, P.; Mance, D.; Chevelkov, V.; Giller, K.; Becker, S.; Baldus, M.; Lange, A. High Resolution Observed in 800 MHz DNP Spectra of Extremely Rigid Type III Secretion Needles. *J. Biomol. NMR* **2016**, *65*, 121–126.

(46) Jaudzems, K.; Bertarello, A.; Chaudhari, S. R.; Pica, A.; Cala-De Paepe, D.; Barbet-Massin, E.; Pell, A. J.; Akopjana, I.; Kotelovica, S.; Gajan, D. et al. Dynamic Nuclear Polarization-Enhanced Biomolecular NMR Spectroscopy at High Magnetic Field with Fast Magic-Angle Spinning. *Angew. Chem. Int. Ed.* **2018**, *57*, 7458–7462.

(47) Chaudhari, S. R.; Wisser, D.; Pinon, A. C.; Berruyer, P.; Gajan, D.; Tordo, P.; Ouari, O.; Reiter, C.; Engelke, F.; Copéret, C. et al. Dynamic Nuclear Polarization Efficiency Increased by Very Fast Magic Angle Spinning. *J. Am. Chem. Soc.* **2017**, *139*, 10609–10612.

(48) Berruyer, P.; Björgvinsdóttir, S.; Bertarello, A.; Stevanato, G.; Rao, Y.; Karthikeyan, G.; Casano, G.; Ouari, O.; Lelli, M.; Reiter, C. et al. Dynamic Nuclear Polarization Enhancement of 200 at 21.15 T Enabled by 65 KHz Magic Angle Spinning. *J. Phys. Chem. Lett.* **2020**, *11*, 8386–8391.

(49) Bouleau, E.; Saint-Bonnet, P.; Mentink-Vigier, F.; Takahashi, H.; Jacquot, J.-F.; Bardet, M.; Aussenac, F.; Purea, A.; Engelke, F.; Hediger, S. et al. Pushing NMR Sensitivity Limits using Dynamic Nuclear Polarization with Closed-Loop Cryogenic Helium Sample Spinning. *Chem. Sci.* **2015**, *6*, 6806–6812.

(50) Mentink-Vigier, F.; Mathies, G.; Liu, Y.; Barra, A.-L.; Caporini, M. A.; Lee, D.; Hediger, S.; G. Griffin, R.; De Paëpe, G. Efficient Cross-Effect Dynamic Nuclear Polarization without Depolarization in High-Resolution MAS NMR. *Chem. Sci.* **2017**, *8*, 8150–8163.

(51) Lund, A.; Casano, G.; Menzildjian, G.; Kaushik, M.; Stevanato, G.; Yulikov, M.; Jabbour, R.; Wisser, D.; Renom-Carrasco, M.; Thieuleux, C. et al. TinyPols: A Family of Water-Soluble Binitroxides Tailored for Dynamic Nuclear Polarization Enhanced NMR Spectroscopy at 18.8 and 21.1 T. *Chem. Sci.* **2020**, *11*, 2810–2818.

(52) Lee, D.; Bouleau, E.; Saint-Bonnet, P.; Hediger, S.; De Paëpe, G. Ultra-Low Temperature MAS-DNP. *J. Magn. Reson.* **2016**, *264*, 116–124.

(53) Matsuki, Y.; Nakamura, S.; Fukui, S.; Suematsu, H.; Fujiwara, T. Closed-Cycle Cold Helium Magic-Angle Spinning for Sensitivity-Enhanced Multi-Dimensional Solid-State NMR. *J. Magn. Reson.* **2015**, *259*, 76–81.

(54) Matsuki, Y.; Idehara, T.; Fukazawa, J.; Fujiwara, T. Advanced Instrumentation for DNP-Enhanced MAS NMR for Higher Magnetic Fields and Lower Temperatures. *J. Magn. Reson.* **2016**, *264*, 107–115.

(55) Matsuki, Y.; Fujiwara, T. Cryogenic Platforms and Optimized DNP Sensitivity. In *eMagRes*; Wiley, 2018; Vol. 7; pp 9–24.

(56) Ni, Q. Z.; Markhasin, E.; Can, T. V.; Corzilius, B.; Tan, K. O.; Barnes, A. B.; Daviso, E.; Su, Y.; Herzfeld, J.; Griffin, R. G. Peptide and Protein Dynamics and Low-Temperature/DNP Magic Angle Spinning NMR. *J. Phys. Chem. B* **2017**, *121*, 4997–5006.

(57) Fricke, P.; Demers, J. P.; Becker, S.; Lange, A. Studies on the MxiH Protein in T3SS Needles using DNP-Enhanced SsNMR Spectroscopy. *ChemPhysChem* **2014**, *15*, 57–60.

(58) Linden, A. H.; Franks, W. T.; Akbey, Ü.; Lange, S.; Van Rossum, B. J.; Oschkinat, H. Cryogenic Temperature Effects and Resolution Upon Slow Cooling of Protein Preparations in Solid State NMR. *J. Biomol. NMR* **2011**, *51*, 283–292.

(59) Bauer, T.; Dotta, C.; Balacescu, L.; Gath, J.; Hunkeler, A.; Böckmann, A.; Meier, B. H. Line-Broadening in Low-Temperature Solid-State NMR Spectra of Fibrils. *J. Biomol. NMR* **2017**, *67*, 51–61.

(60) Bajaj, V. S.; van der Wel, P. C.; Griffin, R. G. Observation of a Low-Temperature, Dynamically Driven Structural Transition in a Polypeptide by Solid-State NMR Spectroscopy. *J. Am. Chem. Soc.* **2009**, *131*, 118–128.

(61) Hu, K.-N.; Yau, W. M.; Tycko, R. Detection of a Transient Intermediate in a Rapid Protein Folding Process by Solid-State Nuclear Magnetic Resonance. *J. Am. Chem. Soc.* **2010**, *132*, 24–25.

(62) Akbey, Ü.; Linden, A. H.; Oschkinat, H. High-Temperature Dynamic Nuclear Polarization Enhanced Magic-Angle-Spinning NMR. *Appl. Magn. Reson.* **2012**, *43*, 81–90.

(63) Geiger, M.-A.; Orwick-Rydmark, M.; Märker, K.; Franks, W. T.; Akhmetzyanov, D.; Stöppler, D.; Zinke, M.; Specker, E.; Nazaré, M.; Diehl, A. et al. Temperature Dependence of Cross-Effect Dynamic Nuclear Polarization in Rotating Solids: Advantages of Elevated Temperatures. *Phys. Chem. Chem. Phys.* **2016**, *18*, 30696–30704.

(64) Ghosh, R.; Madrid, C. L.; Frederick, K. K. Segmental Labeling: Applications to Protein NMR and DNP. In *eMagRes*; Wiley, 2020; Vol. 9; pp 71–80.

(65) Frederick, K. K.; Michaelis, V. K.; Caporini, M. A.; Andreas, L. B.; Debelouchina, G. T.; Griffin, R. G.; Lindquist, S. Combining DNP NMR with Segmental and Specific Labeling to Study a Yeast Prion Protein Strain That Is Not Parallel In-Register. *Proc. Natl. Acad. Sci. U. S. A.* **2017**, *114*, 3642–3647.

(66) Mehler, M.; Eckert, C. E.; Busche, A.; Kulhei, J.; Michaelis, J.; Becker-Baldus, J.; Wachtveitl, J.; Dötsch, V.; Glaubitz, C. Assembling a Correctly Folded and Functional Heptahelical Membrane Protein by Protein Trans-Splicing. *J. Biol. Chem.* **2015**, *290*, 27712–27722.

(67) Lu, M.; Wang, M.; Sergeyev, I. V.; Quinn, C. M.; Struppe, J.; Rosay, M.; Maas, W.; Gronenborn, A. M.; Polenova, T. 19F Dynamic Nuclear Polarization at Fast Magic

Angle Spinning for NMR of HIV-1 Capsid Protein Assemblies. *J. Am. Chem. Soc.* **2019**, *141*, 5681–5691.

(68) Hu, K.-N.; Yu, H. H.; Swager, T. M.; Griffin, R. G. Dynamic Nuclear Polarization with Biradicals. *J. Am. Chem. Soc.* **2004**, *126*, 10844–10845.

(69) Song, C.; Hu, K.-N.; Joo, C. G.; Swager, T. M.; Griffin, R. G. TOTAPOL: A Biradical Polarizing Agent for Dynamic Nuclear Polarization Experiments in Aqueous Media. *J. Am. Chem. Soc.* **2006**, *128*, 11385–11390.

(70) Sauvée, C.; Rosay, M.; Casano, G.; Aussenac, F.; Weber, R. T.; Ouari, O.; Tordo, P. Highly Efficient, Water-Soluble Polarizing Agents for Dynamic Nuclear Polarization at High Frequency. *Angew. Chem. Int. Ed.* **2013**, *52*, 10858–10861.

(71) Mathies, G.; Caporini, M. A.; Michaelis, V. K.; Liu, Y.; Hu, K.-N.; Mance, D.; Zweier, J. L.; Rosay, M.; Baldus, M.; Griffin, R. G. Efficient Dynamic Nuclear Polarization at 800 MHz/527 GHz with Trityl-Nitroxide Biradicals. *Angew. Chem. Int. Ed.* **2015**, *54*, 11770–11774.

(72) Mentink-Vigier, F.; Marin-Montesinos, I.; Jagtap, A. P.; Halbritter, T.; van Tol, J.; Hediger, S.; Lee, D.; Sigurdsson, S. T.; De Paëpe, G. Computationally Assisted Design of Polarizing Agents for Dynamic Nuclear Polarization Enhanced NMR: The AsymPol Family. *J. Am. Chem. Soc.* **2018**, *140*, 11013–11019.

(73) Cai, X.; Lucini Paioni, A.; Adler, A.; Yao, R.; Zhang, W.; Beriashvili, D.; Safeer, A.; Gurinov, A.; Rockenbauer, A.; Song, Y. et al. Highly Efficient Trityl-Nitroxide Biradicals for Biomolecular High-Field Dynamic Nuclear Polarization. *Chem. - A Eur. J.* **2021**, *27*, 12758–12762.

(74) Sauvée, C.; Casano, G.; Abel, S.; Rockenbauer, A.; Akhmetzyanov, D.; Karoui, H.; Siri, D.; Aussenac, F.; Maas, W.; Weber, R. T. et al. Tailoring of Polarizing Agents in

the BTurea Series for Cross-Effect Dynamic Nuclear Polarization in Aqueous Media. *Chem. - A Eur. J.* **2016**, *22*, 5598–5606.

(75) Stevanato, G.; Casano, G.; Kubicki, D. J.; Rao, Y.; Hofer, L. E.; Menzildjian, G.; Karoui, H.; Siri, D.; Cordova, M.; Yulikov, M. et al. Open and Closed Radicals: Local Geometry Around Unpaired Electrons Governs Magic-Angle Spinning Dynamic Nuclear Polarization Performance. *J. Am. Chem. Soc.* **2020**, *142*, 16587–16599.

(76) Zhai, W.; Lucini Paioni, A.; Cai, X.; Narasimhan, S.; Medeiros-Silva, J.; Zhang, W.; Rockenbauer, A.; Weingarth, M.; Song, Y.; Baldus, M. et al. Postmodification Via Thiol-Click Chemistry Yields Hydrophilic Trityl-Nitroxide Biradicals for Biomolecular High-Field Dynamic Nuclear Polarization. *J. Phys. Chem. B* **2020**, *124*, 9047–9060.

(77) Jagtap, A. P.; Geiger, M.-A.; Stöppler, D.; Orwick-Rydmark, M.; Oschkinat, H.; Sigurdsson, S. T. BcTol: a Highly Water-Soluble Biradical for Efficient Dynamic Nuclear Polarization of Biomolecules. *Chem. Commun.* **2016**, *52*, 7020–7023.

(78) Geiger, M. A.; Jagtap, A. P.; Kaushik, M.; Sun, H.; Stöppler, D.; Sigurdsson, S. T.; Corzilius, B.; Oschkinat, H. Efficiency of Water-Soluble Nitroxide Biradicals for Dynamic Nuclear Polarization in Rotating Solids at 9.4 T: BcTol-M and Cyolyl-TOTAPOL as New Polarizing Agents. *Chem. - A Eur. J.* **2018**, *24*, 13485–13494.

(79) Mandal, S.; Sigurdsson, S. T. Water-Soluble BDPA Radicals with Improved Persistence. *Chem. Commun.* **2020**, *56*, 13121–13124.

(80) Mentink-Vigier, F.; Dubroca, T.; Van Tol, J.; Sigurdsson, S. T. The Distance Between G-Tensors of Nitroxide Biradicals Governs MAS-DNP Performance: The Case of the BTurea Family. *J. Magn. Reson.* **2021**, *329*, 107026.

(81) Bonucci, A.; Ouari, O.; Guigliarelli, B.; Belle, V.; Mileo, E. In-Cell EPR: Progress Towards Structural Studies Inside Cells. *Chembiochem* **2020**, *21*, 451–460.

(82) Haugland, M. M.; Lovett, J. E.; Anderson, E. A. Advances in the Synthesis of Nitroxide Radicals for Use in Biomolecule Spin Labelling. *Chem. Soc. Rev.* **2018**, *47*, 668–680.

(83) Brodrecht, M.; Herr, K.; Bothe, S.; de Oliveira, M.; Gutmann, T.; Buntkowsky, G. Efficient Building Blocks for Solid-Phase Peptide Synthesis of Spin Labeled Peptides for Electron Paramagnetic Resonance and Dynamic Nuclear Polarization Applications. *ChemPhysChem* **2019**, *20*, 1475–1487.

(84) Mentink-Vigier, F.; Vega, S.; De Paëpe, G. Fast and Accurate MAS-DNP Simulations of Large Spin Ensembles. *Phys. Chem. Chem. Phys.* **2017**, *19*, 3506–3522.

(85) Harrabi, R.; Halbritter, T.; Aussenac, F.; Dakhlaoui, O.; van Tol, J.; Damodaran, K. K.; Lee, D.; Paul, S.; Hediger, S.; Mentink-Vigier, F. et al. Highly Efficient Polarizing Agents for MAS-DNP of Proton-Dense Molecular Solids. *Angew. Chem. Int. Ed.* **2022**, *61*, e202114103.

(86) Yau, W. M.; Thurber, K. R.; Tycko, R. Synthesis and Evaluation of Nitroxide-Based Oligoradicals for Low-Temperature Dynamic Nuclear Polarization in Solid State NMR. *J. Magn. Reson.* **2014**, *244*, 98–106.

(87) Yau, W. M.; Jeon, J.; Tycko, R. Succinyl-DOTOPA: An Effective Triradical Dopant for Low-Temperature Dynamic Nuclear Polarization with High Solubility in Aqueous Solvent Mixtures at Neutral pH. *J. Magn. Reson.* **2020**, *311*, 106672.

(88) Wang, X.; Caulkins, B. G.; Riviere, G.; Mueller, L. J.; Mentink-Vigier, F.; Long, J. R. Direct Dynamic Nuclear Polarization of 15 N and 13 C Spins at 14.1 T using a Trityl Radical and Magic Angle Spinning. *Solid State Nucl. Magn. Reson.* **2019**, *100*, 85–91.

(89) Corzilius, B. Paramagnetic Metal Ions for Dynamic Nuclear Polarization. In *eMagRes*; Wiley, 2018; Vol. 7; pp 179–194.

(90) Heiliger, J.; Matzel, T.; Çetiner, E. C.; Schwalbe, H.; Kuenze, G.; Corzilius, B. Site-Specific Dynamic Nuclear Polarization in a Gd(III)-Labeled Protein. *Phys. Chem. Chem. Phys.* **2020**, *22*, 25455–25466.

(91) Kaushik, M.; Qi, M.; Godt, A.; Corzilius, B. Bis-Gadolinium Complexes for Solid Effect and Cross Effect Dynamic Nuclear Polarization. *Angew. Chem. Int. Ed.* **2017**, *56*, 4295–4299.

(92) Corzilius, B. Theory of Solid Effect and Cross Effect Dynamic Nuclear Polarization with Half-Integer High-Spin Metal Polarizing Agents in Rotating Solids. *Phys. Chem. Chem. Phys.* **2016**, *18*, 27190–27204.

(93) Corzilius, B.; Smith, A. A.; Barnes, A. B.; Luchinat, C.; Bertini, I.; Griffin, R. G. High-Field Dynamic Nuclear Polarization with High-Spin Transition Metal Ions. *J. Am. Chem. Soc.* **2011**, *133*, 5648–5651.

(94) Daube, D.; Vogel, M.; Suess, B.; Corzilius, B. Dynamic Nuclear Polarization on a Hybridized Hammerhead Ribozyme: An Explorative Study of RNA Folding and Direct DNP with a Paramagnetic Metal Ion Cofactor. *Solid State Nucl. Magn. Reson.* **2019**, *101*, 21–30.

(95) Itin, B.; Sergeyev, I. V. Strategies for Efficient Sample Preparation for Dynamic Nuclear Polarization Solid-State NMR of Biological Macromolecules. *Methods Mol. Biol.* **2018**, *1688*, 133–154.

(96) Barnes, A. B.; Corzilius, B.; Mak-Jurkauskas, M. L.; Andreas, L. B.; Bajaj, V. S.; Matsuki, Y.; Belenky, M. L.; Lugtenburg, J.; Sirigiri, J. R.; Temkin, R. J. et al. Resolution and Polarization Distribution in Cryogenic DNP/MAS Experiments. *Phys. Chem. Chem. Phys.* **2010**, *12*, 5861–5867.

(97) Rosay, M.; Zeri, A. C.; Astrof, N. S.; Opella, S. J.; Herzfeld, J.; Griffin, R. G. Sensitivity-Enhanced NMR of Biological Solids: Dynamic Nuclear Polarization of

Y21M Fd Bacteriophage and Purple Membrane. *J. Am. Chem. Soc.* **2001**, *123*, 1010–1011.

(98) Daube, D.; Aladin, V.; Heiliger, J.; Wittmann, J. J.; Barthelmes, D.; Bengs, C.; Schwalbe, H.; Corzilius, B. Heteronuclear Cross-Relaxation Under Solid-State Dynamic Nuclear Polarization. *J. Am. Chem. Soc.* **2016**, *138*, 16572–16575.

(99) Aladin, V.; Corzilius, B. Methyl Dynamics in Amino Acids Modulate Heteronuclear Cross Relaxation in the Solid State Under MAS DNP. *Solid State Nucl. Magn. Reson.* **2019**, *99*, 27–35.

(100) Park, H.; Uluca-Yazgi, B.; Heumann, S.; Schlögl, R.; Granwehr, J.; Heise, H.; Schleker, P. P. M. Heteronuclear Cross-Relaxation Effect Modulated by the Dynamics of N-Functional Groups in the Solid State Under 15N DP-MAS DNP. *J. Magn. Reson.* **2020**, *312*, 106688.

(101) Hoffmann, M. M.; Bothe, S.; Gutmann, T.; Buntkowsky, G. Unusual Local Molecular Motions in the Solid State Detected by Dynamic Nuclear Polarization Enhanced NMR Spectroscopy. *J. Phys. Chem. C* **2017**, *121*, 22948–22957.

(102) Sergeyev, I. V.; Quinn, C. M.; Struppe, J.; Gronenborn, A. M.; Polenova, T. Competing Transfer Pathways in Direct and Indirect Dynamic Nuclear Polarization Magic Angle Spinning Nuclear Magnetic Resonance Experiments on HIV-1 Capsid Assemblies: Implications for Sensitivity and Resolution. *Magn. Reson.* **2021**, *2*, 239–249.

(103) van Der Wel, P. C. A.; Hu, K.-N.; Lewandowski, J. R.; Griffin, R. G. Dynamic Nuclear Polarization of Amyloidogenic Peptide Nanocrystals: GNNQQNY, a Core Segment of the Yeast Prion Protein Sup35p. *J. Am. Chem. Soc.* **2006**, *128*, 10840–10846.

(104) Ehren, H. L.; Kolbe, F.; Lucini Paioni, A.; Brunner, E.; Baldus, M. DNP-Supported Solid-State NMR Studies of 13C,15N,29Si-Enriched Biosilica of Cyclotella Cryptica and Thalassiosira Pseudonana. *Discov. Mater.* **2021**, *1*, 9.

(105) Mazur, P. The Role of Intracellular Freezing in the Death of Cells Cooled at Supraoptimal Rates. *Cryobiology* **1977**, *14*, 251–272.

(106) Wiebe, J. P.; Dinsdale, C. J. Inhibition of Cell Proliferation by Glycerol. *Life Sci.* **1991**, *48*, 1511–1517.

(107) Baust, J. G.; Gao, D.; Baust, J. M. Cryopreservation: An Emerging Paradigm Change. *Organogenesis* **2009**, *5*, 90–96.

(108) Farrant, J.; Walter, C. A.; Lee, H.; Morris, G. J.; Clarke, K. J. Structural and Functional Aspects of Biological Freezing Techniques. *J. Microsc.* **1977**, *111*, 17–34.

(109) Pflugrath, J. W. Practical Macromolecular Cryocrystallography. *Acta Crystallogr. Sect. F, Structural Biol. Commun.* **2015**, *71*, 622–642.

(110) Fahy, G. M.; Levy, D. I.; Ali, S. E. Some Emerging Principles Underlying the Physical Properties, Biological Actions, and Utility of Vitrification Solutions. *Cryobiology* **1987**, *24*, 196–213.

(111) Gupta, R.; Lu, M.; Hou, G.; Caporini, M. A.; Rosay, M.; Maas, W.; Struppe, J.; Suiter, C.; Ahn, J.; Byeon, I.-J. L. et al. Dynamic Nuclear Polarization Enhanced MAS NMR Spectroscopy for Structural Analysis of HIV-1 Protein Assemblies. *J. Phys. Chem. B* **2016**, *120*, 329–339.

(112) Tran, N. T.; Mentink-Vigier, F.; Long, J. R. Dynamic Nuclear Polarization of Biomembrane Assemblies. *Biomolecules* **2020**, *10*, 1246.

(113) Ghosh, R.; Xiao, Y.; Kragelj, J.; Frederick, K. K. In-Cell Sensitivity-Enhanced NMR of Intact Viable Mammalian Cells. *J. Am. Chem. Soc.* **2021**, *143*, 18454–18466.

(114) Fernández-de Alba, C.; Takahashi, H.; Richard, A.; Chenavier, Y.; Dubois, L.; Maurel, V.; Lee, D.; Hediger, S.; De Paëpe, G. Matrix-Free DNP-Enhanced NMR Spec-

troscopy of Liposomes Using a Lipid-Anchored Biradical. *Chem. - A Eur. J.* **2015**, *21*, 4512–4517.

(115) Ravera, E.; Corzilius, B.; Michaelis, V. K.; Luchinat, C.; Griffin, R. G.; Bertini, I. DNP-Enhanced MAS NMR of Bovine Serum Albumin Sediments and Solutions. *J. Phys. Chem. B* **2014**, *118*, 2957–2965.

(116) Wiegand, T.; Liao, W. C.; Ong, T. C.; Däpp, A.; Cadalbert, R.; Copéret, C.; Böckmann, A.; Meier, B. H. Protein-Nucleotide Contacts in Motor Proteins Detected by DNP-Enhanced Solid-State NMR. *J. Biomol. NMR* **2017**, *69*, 157–164.

(117) Smith, A. N.; Caporini, M. A.; Fanucci, G. E.; Long, J. R. A Method for Dynamic Nuclear Polarization Enhancement of Membrane Proteins. *Angew. Chem. Int. Ed.* **2015**, *54*, 1542–1546.

(118) Salnikov, E. S.; Abel, S.; Karthikeyan, G.; Karoui, H.; Aussenac, F.; Tordo, P.; Bechinger, B.; Ouari, O. Dynamic Nuclear Polarization/Solid-State NMR Spectroscopy of Membrane Polypeptides: Free-Radical Optimization for Matrix-Free Lipid Bilayer Samples. *ChemPhysChem* **2017**, *18*, 2103–2113.

(119) Kirui, A.; Ling, Z.; Kang, X.; Dickwella Widanage, M. C.; Mentink-Vigier, F.; French, A. D.; Wang, T. Atomic Resolution of Cotton Cellulose Structure Enabled by Dynamic Nuclear Polarization Solid-State NMR. *Cellulose* **2019**, *26*, 329–339.

(120) Chow, W. Y.; Li, R.; Goldberga, I.; Reid, D. G.; Rajan, R.; Clark, J.; Oschkinat, H.; Duer, M. J.; Hayward, R.; Shanahan, C. M. Essential but Sparse Collagen Hydroxylysyl Post-Translational Modifications Detected by DNP NMR. *Chem. Commun.* **2018**, *54*, 12570–12573.

(121) Leroy, C.; Aussenac, F.; Bonhomme-Coury, L.; Osaka, A.; Hayakawa, S.; Babonneau, F.; Coelho-Diogo, C.; Bonhomme, C. Hydroxyapatites: Key Structural Ques-

tions and Answers from Dynamic Nuclear Polarization. *Anal. Chem.* **2017**, *89*, 10201–10207.

(122) Kirui, A.; Dickwella Widanage, M. C.; Mentink-Vigier, F.; Wang, P.; Kang, X.; Wang, T. Preparation of Fungal and Plant Materials for Structural Elucidation Using Dynamic Nuclear Polarization Solid-State NMR. *J. Vis. Exp.* **2019**, *144*, e59152.

(123) Rosay, M. M. Sensitivity-Enhanced Nuclear Magnetic Resonance of Biological Solids. PhD, Massachusetts Institute of Technology, 2001.

(124) Voinov, M. A.; Good, D. B.; Ward, M. E.; Milikisiyants, S.; Marek, A.; Caporini, M. A.; Rosay, M.; Munro, R. A.; Ljumovic, M.; Brown, L. S. et al. Cysteine-Specific Labeling of Proteins with a Nitroxide Biradical for Dynamic Nuclear Polarization NMR. *J. Phys. Chem. B* **2015**, *119*, 10180–10190.

(125) Viennet, T.; Viegas, A.; Kuepper, A.; Arens, S.; Gelev, V.; Petrov, O.; Grossmann, T. N.; Heise, H.; Etzkorn, M. Selective Protein Hyperpolarization in Cell Lysates Using Targeted Dynamic Nuclear Polarization. *Angew. Chem. Int. Ed.* **2016**, *55*, 10746–10750.

(126) Rogawski, R.; Sergeyev, I. V.; Li, Y.; Ottaviani, M. F.; Cornish, V.; McDermott, A. E. Dynamic Nuclear Polarization Signal Enhancement with High-Affinity Biradical Tags. *J. Phys. Chem. B* **2017**, *121*, 1169–1175.

(127) Frederick, K. K.; Michaelis, V. K.; Corzilius, B.; Ong, T. C.; Jacavone, A. C.; Griffin, R. G.; Lindquist, S. Sensitivity-Enhanced NMR Reveals Alterations in Protein Structure by Cellular Milieus. *Cell* **2015**, *163*, 620–628.

(128) Chordia, S.; Narasimhan, S.; Lucini Paioni, A.; Baldus, M.; Roelfes, G. In Vivo Assembly of Artificial Metalloenzymes and Application in Whole-Cell Biocatalysis. *Angew. Chem. Int. Ed.* **2021**, *60*, 5913–5920.

(129) Kaushik, M.; Bahrenberg, T.; Can, T. V.; Caporini, M. A.; Silvers, R.; Heiliger, J.; Smith, A. A.; Schwalbe, H.; Griffin, R. G.; Corzilius, B. Gd(III) and Mn(II) Complexes for Dynamic Nuclear Polarization: Small Molecular Chelate Polarizing Agents and Applications with Site-Directed Spin Labeling of Proteins. *Phys. Chem. Chem. Phys.* **2016**, *18*, 27205–27218.

(130) Perras, F. A.; Reinig, R. R.; Slowing, I. I.; Sadow, A. D.; Pruski, M. Effects of Biradical Deuteration on the Performance of DNP: Towards Better Performing Polarizing Agents. *Phys. Chem. Chem. Phys.* **2016**, *18*, 65–69.

(131) Kubicki, D. J.; Casano, G.; Schwarzwälder, M.; Abel, S.; Sauvée, C.; Ganesan, K.; Yulikov, M.; Rossini, A. J.; Jeschke, G.; Copéret, C. et al. Rational Design of Dinitroxide Biradicals for Efficient Cross-Effect Dynamic Nuclear Polarization. *Chem. Sci.* **2016**, *7*, 550–558.

(132) Akbey, Ü.; Franks, W. T.; Linden, A.; Lange, S.; Griffin, R. G.; Van Rossum, B. J.; Oschkinat, H. Dynamic Nuclear Polarization of Deuterated Proteins. *Angew. Chem. Int. Ed.* **2010**, *49*, 7803–7806.

(133) Potapov, A.; Yau, W. M.; Ghirlando, R.; Thurber, K. R.; Tycko, R. Successive Stages of Amyloid-β Self-Assembly Characterized by Solid-State Nuclear Magnetic Resonance with Dynamic Nuclear Polarization. *J. Am. Chem. Soc.* **2015**, *137*, 8294–8307.

(134) Liao, S. Y.; Lee, M.; Wang, T.; Sergeyev, I. V.; Hong, M. Efficient DNP NMR of Membrane Proteins: Sample Preparation Protocols, Sensitivity, and Radical Location. *J. Biomol. NMR* **2016**, *64*, 223–237.

(135) Reif, B. Proton-Detection in Biological MAS Solid-State NMR Spectroscopy. In *Mod. Magn. Reson.*; Springer, 2017; pp 1–33.

(136) Schanda, P.; Ernst, M. Studying Dynamics by Magic-Angle Spinning Solid-State NMR

Spectroscopy: Principles and Applications to Biomolecules. *Prog. Nucl. Magn. Reson. Spectrosc.* **2016**, *96*, 1–46.

(137) Reif, B. Ultra-High Resolution in MAS Solid-State NMR of Perdeuterated Proteins: Implications for Structure and Dynamics. *J. Magn. Reson.* **2012**, *216*, 1–12.

(138) Ravera, E.; Corzilius, B.; Michaelis, V. K.; Rosa, C.; Griffin, R. G.; Luchinat, C.; Bertini, I. Dynamic Nuclear Polarization of Sedimented Solutes. *J. Am. Chem. Soc.* **2013**, *135*, 1641–1644.

(139) Lesage, A.; Lelli, M.; Gajan, D.; Caporini, M. A.; Vitzthum, V.; Miéville, P.; Alauzun, J.; Roussey, A.; Thieuleux, C.; Mehdi, A. et al. Surface Enhanced NMR Spectroscopy by Dynamic Nuclear Polarization. *J. Am. Chem. Soc.* **2010**, *132*, 15459–15461.

(140) Rossini, A. J.; Zagdoun, A.; Lelli, M.; Lesage, A.; Copéret, C.; Emsley, L. Dynamic Nuclear Polarization Surface Enhanced NMR Spectroscopy. *Acc. Chem. Res.* **2013**, *46*, 1942–1951.

(141) Lehnert, E.; Mao, J.; Mehdipour, A. R.; Hummer, G.; Abele, R.; Glaubitz, C.; Tampé, R. Antigenic Peptide Recognition on the Human ABC Transporter TAP Resolved by DNP-Enhanced Solid-State NMR Spectroscopy. *J. Am. Chem. Soc.* **2016**, *138*, 13967–13974.

(142) Takahashi, H.; Hediger, S.; De Paëpe, G. Matrix-Free Dynamic Nuclear Polarization Enables Solid-State NMR 13C-13C Correlation Spectroscopy of Proteins at Natural Isotopic Abundance. *Chem. Commun.* **2013**, *49*, 9479–9481.

(143) Takahashi, H.; Ayala, I.; Bardet, M.; De Paëpe, G.; Simorre, J. P.; Hediger, S. Solid-State NMR on Bacterial Cells: Selective Cell Wall Signal Enhancement and Resolution Improvement using Dynamic Nuclear Polarization. *J. Am. Chem. Soc.* **2013**, *135*, 5105–5110.

(144) Nagaraj, M.; Franks, T. W.; Saeidpour, S.; Schubeis, T.; Oschkinat, H.; Ritter, C.; van Rossum, B.-J. Surface Binding of TOTAPOL Assists Structural Investigations of Amyloid Fibrils by Dynamic Nuclear Polarization NMR Spectroscopy. *ChemBioChem* **2016**, *17*, 1308–1311.

(145) Vitzthum, V.; Borcard, F.; Jannin, S.; Morin, M.; Miéville, P.; Caporini, M. A.; Sienkiewicz, A.; Gerber-Lemaire, S.; Bodenhausen, G. Fractional Spin-Labeling of Polymers for Enhancing NMR Sensitivity by Solvent-Free Dynamic Nuclear Polarization. *ChemPhysChem* **2011**, *12*, 2929–2932.

(146) Wylie, B. J.; Dzikovski, B. G.; Pawsey, S.; Caporini, M.; Rosay, M.; Freed, J. H.; McDermott, A. E. Dynamic Nuclear Polarization of Membrane Proteins: Covalently Bound Spin-Labels at Protein-Protein Interfaces. *J. Biomol. NMR* **2015**, *61*, 361–367.

(147) van der Cruijsen, E. A.; Koers, E. J.; Sauvée, C.; Hulse, R. E.; Weingarth, M.; Ouari, O.; Perozo, E.; Tordo, P.; Baldus, M. Biomolecular DNP-Supported NMR Spectroscopy using Site-Directed Spin Labeling. *Chem. - A Eur. J.* **2015**, *21*, 12971–12977.

(148) Smith, A. N.; Twahir, U. T.; Dubroca, T.; Fanucci, G. E.; Long, J. R. Molecular Rationale for Improved Dynamic Nuclear Polarization of Biomembranes. *J. Phys. Chem. B* **2016**, *120*, 7880–7888.

(149) Good, D. B.; Voinov, M. A.; Bolton, D.; Ward, M. E.; Sergeyev, I. V.; Caporini, M.; Scheffer, P.; Lo, A.; Rosay, M.; Marek, A. et al. A Biradical-Tagged Phospholipid as a Polarizing Agent for Solid-State MAS Dynamic Nuclear Polarization NMR of Membrane Proteins. *Solid State Nucl. Magn. Reson.* **2019**, *100*, 92–101.

(150) Sani, M. A.; Zhu, S.; Hofferek, V.; Separovic, F. Nitroxide Spin-Labeled Peptides for DNP-NMR In-Cell Studies. *FASEB J.* **2019**, *33*, 11021–11027.

(151) Zhu, S.; Kachooei, E.; Harmer, J.; Brown, L.; Separovic, F.; Sani, M.-A. TOAC Spin-Labelled Peptides Tailored for DNP-NMR Studies in Lipid Membrane Environments. *Biophys. J.* **2021**, *120*, 4501–4511.

(152) Rogawski, R.; McDermott, A. E. New NMR Tools for Protein Structure and Function: Spin Tags for Dynamic Nuclear Polarization Solid State NMR. *Arch. Biochem. Biophys.* **2017**, *628*, 102–113.

(153) Rogawski, R.; Sergeyev, I. V.; Zhang, Y.; Tran, T. H.; Li, Y.; Tong, L.; McDermott, A. E. NMR Signal Quenching from Bound Biradical Affinity Reagents in DNP Samples. *J. Phys. Chem. B* **2017**, *121*, 10770–10781.

(154) Marin-Montesinos, I.; Goyard, D.; Gillon, E.; Renaudet, O.; Imberty, A.; Hediger, S.; De Paëpe, G. Selective High-Resolution DNP-Enhanced NMR of Biomolecular Binding Sites. *Chem. Sci.* **2019**, *10*, 3366–3374.

(155) Lim, B. J.; Ackermann, B. E.; Debelouchina, G. T. Targetable Tetrazine-Based Dynamic Nuclear Polarization Agents for Biological Systems. *ChemBioChem* **2020**, *21*, 1315–1319.

(156) Herr, K.; Fleckenstein, M.; Brodrecht, M.; Höfler, M. V.; Heise, H.; Aussenac, F.; Gutmann, T.; Reggelin, M.; Buntkowsky, G. A Novel Strategy for Site Selective Spin-Labeling to Investigate Bioactive Entities by DNP and EPR Spectroscopy. *Sci. Rep.* **2021**, *11*, 13714.

(157) Mao, J.; Aladin, V.; Jin, X.; Leeder, A. J.; Brown, L. J.; Brown, R. C.; He, X.; Corzilius, B.; Glaubitz, C. Exploring Protein Structures by DNP-Enhanced Methyl Solid-State NMR Spectroscopy. *J. Am. Chem. Soc.* **2019**, *141*, 19888–19901.

(158) Salnikov, E. S.; Ouari, O.; Koers, E.; Sarrouj, H.; Franks, T.; Rosay, M.; Pawsey, S.; Reiter, C.; Bandara, P.; Oschkinat, H. et al. Developing DNP/Solid-State NMR Spectroscopy of Oriented Membranes. *Appl. Magn. Reson.* **2012**, *43*, 91–106.

(159) Bechinger, B. DNP Solid-State NMR of Biological Membranes. In *eMagRes*; Wiley, 2018; Vol. 7; pp 25–34.

(160) Salnikov, E.; Rosay, M.; Pawsey, S.; Ouari, O.; Tordo, P.; Bechinger, B. Solid-State NMR Spectroscopy of Oriented Membrane Polypeptides at 100 K with Signal Enhancement by Dynamic Nuclear Polarization. *J. Am. Chem. Soc.* **2010**, *132*, 5940–5941.

(161) Salnikov, E. S.; Aussenac, F.; Abel, S.; Purea, A.; Tordo, P.; Ouari, O.; Bechinger, B. Dynamic Nuclear Polarization / Solid-State NMR of Membranes. Thermal Effects and Sample Geometry. *Solid State Nucl. Magn. Reson.* **2019**, *100*, 70–76.

(162) Salnikov, E. S.; Aisenbrey, C.; Aussenac, F.; Ouari, O.; Sarrouj, H.; Reiter, C.; Tordo, P.; Engelke, F.; Bechinger, B. Membrane Topologies of the PGLa Antimicrobial Peptide and a Transmembrane Anchor Sequence by Dynamic Nuclear Polarization/solid-State NMR Spectroscopy. *Sci. Rep.* **2016**, *6*, 4–10.

(163) Berman, H. M.; Westbrook, J.; Feng, Z.; Gilliland, G.; Bhat, T. N.; Weissig, H.; Shindyalov, I. N.; Bourne, P. E. The Protein Data Bank. *Nucleic Acids Res.* **2000**, *28*, 235–242.

(164) Jumper, J.; Evans, R.; Pritzel, A.; Green, T.; Figurnov, M.; Ronneberger, O.; Tunyasuvunakool, K.; Bates, R.; Žídek, A.; Potapenko, A. et al. Highly Accurate Protein Structure Prediction with AlphaFold. *Nature* **2021**, *596*, 583–589.

(165) Crick, F. H. C. On Protein Synthesis. *Symp. Soc. Exp. Biol.* **1958**, *12*, 138–163.

(166) Anfinsen, C. B. Principles That Govern Protein Folding. *Science* **1973**, *181*, 223–230.

(167) Kulkarni, P.; Solomon, T. L.; He, Y.; Chen, Y.; Bryan, P. N.; Orban, J. Structural Metamorphism and Polymorphism in Proteins on the Brink of Thermodynamic Stability. *Protein Sci.* **2018**, *27*, 1557–1567.

(168) Porter, L. L.; Looger, L. L. Extant Fold-Switching Proteins Are Widespread. *Proc. Natl. Acad. Sci. U. S. A.* **2018**, *115*, 5968–5973.

(169) Wright, P. E.; Dyson, H. J. Intrinsically Disordered Proteins in Cellular Signalling and Regulation. *Nat. Rev. Mol. Cell Biol.* **2015**, *16*, 18–29.

(170) Castellani, F.; van Rossum, B.; Diehl, A.; Schubert, M.; Rehbein, K.; Oschkinat, H. Structure of a Protein Determined by Solid-State Magic-Angle-Spinning NMR Spectroscopy. *Nature* **2002**, *420*, 98–102.

(171) Rienstra, C. M.; Tucker-Kellogg, L.; Jaroniec, C. P.; Hohwy, M.; Reif, B.; McMahon, M. T.; Tidor, B.; Lozano-Perez, T.; Griffin, R. G. De Novo Determination of Peptide Structure with Solid-State Magic-Angle Spinning NMR Spectroscopy. *Proc. Natl. Acad. Sci. U. S. A.* **2002**, *99*, 10260–10265.

(172) Rosay, M.; Weis, V.; Kreischer, K. E.; Temkin, R. J.; Griffin, R. G. Two-Dimensional 13C-13C Correlation Spectroscopy with Magic Angle Spinning and Dynamic Nuclear Polarization. *J. Am. Chem. Soc.* **2002**, *124*, 3214–3215.

(173) Rosay, M.; Lansing, J. C.; Haddad, K. C.; Bachovchin, W. W.; Herzfeld, J.; Temkin, R. J.; Griffin, R. G. High-Frequency Dynamic Nuclear Polarization in MAS Spectra of Membrane and Soluble Proteins. *J. Am. Chem. Soc.* **2003**, *125*, 13626–13627.

(174) Chiti, F.; Dobson, C. M. Protein Misfolding, Amyloid Formation, and Human Disease: A Summary of Progress Over the Last Decade. *Annu. Rev. Biochem.* **2017**, *86*, 27–68.

(175) Fowler, D. M.; Koulov, A. V.; Alory-Jost, C.; Marks, M. S.; Balch, W. E.; Kelly, J. W. Functional Amyloid Formation Within Mammalian Tissue. *PLoS Biol.* **2006**, *4*, 0100–0107.

(176) Maji, S. K.; Perrin, M. H.; Sawaya, M. R.; Jessberger, S.; Vadodaria, K.; Rissman, R. A.; Singru, P. S.; Nilsson, K. P. R.; Simon, R.; Schubert, D. et al. Functional Amyloids as Natural Storage of Peptide Hormones in Pituitary Secretory Granules. *Science* **2009**, *325*, 328–332.

(177) Otzen, D.; Riek, R. Functional Amyloids. *Cold Spring Harb. Perspect. Biol.* **2019**, *11*, a033860.

(178) Balistreri, A.; Goetzler, E.; Chapman, M. Functional Amyloids Are the Rule Rather Than the Exception in Cellular Biology. *Microorganisms* **2020**, *8*, 1951.

(179) Pham, C. L.; Kwan, A. H.; Sunde, M. Functional Amyloid: Widespread in Nature, Diverse in Purpose. *Essays Biochem.* **2014**, *56*, 207–219.

(180) Loquet, A.; El Mammeri, N.; Stanek, J.; Berbon, M.; Bardiaux, B.; Pintacuda, G.; Habenstein, B. 3D Structure Determination of Amyloid Fibrils using Solid-State NMR Spectroscopy. *Methods* **2018**, *138-139*, 26–38.

(181) Fitzpatrick, A. W.; Saibil, H. R. Cryo-EM of Amyloid Fibrils and Cellular Aggregates. *Curr. Opin. Struct. Biol.* **2019**, *58*, 34–42.

(182) Tycko, R. Amyloid Polymorphism: Structural Basis and Neurobiological Relevance. *Neuron* **2015**, *86*, 632–645.

(183) Willbold, D.; Strodel, B.; Schröder, G. F.; Hoyer, W.; Heise, H. Amyloid-Type Protein Aggregation and Prion-Like Properties of Amyloids. *Chem. Rev.* **2021**, *121*, 8285–8307.

(184) Debelouchina, G. T.; Bayro, M. J.; van der Wel, P. C. A.; Caporini, M. A.; Barnes, A. B.; Rosay, M.; Maas, W. E.; Griffin, R. G. Dynamic Nuclear Polarization-Enhanced Solid-State NMR Spectroscopy of GNNQQNY Nanocrystals and Amyloid Fibrils. *Phys. Chem. Chem. Phys.* **2010**, *12*, 5911–5919.

(185) Bayro, M. J.; Debelouchina, G. T.; Eddy, M. T.; Birkett, N. R.; MacPhee, C. E.; Rosay, M.; Maas, W. E.; Dobson, C. M.; Griffin, R. G. Intermolecular Structure Determination of Amyloid Fibrils with Magic-Angle Spinning and Dynamic Nuclear Polarization NMR. *J. Am. Chem. Soc.* **2011**, *133*, 13967–13974.

(186) Debelouchina, G. T.; Bayro, M. J.; Fitzpatrick, A. W.; Ladizhansky, V.; Colvin, M. T.; Caporini, M. A.; Jaroniec, C. P.; Bajaj, V. S.; Rosay, M.; MacPhee, C. E. et al. Higher Order Amyloid Fibril Structure by MAS NMR and DNP Spectroscopy. *J. Am. Chem. Soc.* **2013**, *135*, 19237–19247.

(187) Patino, M. M.; Liu, J.-J.; Glover, J. R.; Lindquist, S. Support for the Prion Hypothesis for Inheritance of a Phenotypic Trait in Yeast. *Science* **1996**, *273*, 622–626.

(188) Iñaki Guijarro, J.; Sunde, M.; Jones, J. A.; Campbelli, I. D.; Dobson, C. M. Amyloid Fibril Formation by an SH3 Domain. *Proc. Natl. Acad. Sci. U. S. A.* **1998**, *95*, 4224–4228.

(189) Yee, A. W.; Aldeghi, M.; Blakeley, M. P.; Ostermann, A.; Mas, P. J.; Moulin, M.; de Sanctis, D.; Bowler, M. W.; Mueller-Dieckmann, C.; Mitchell, E. P. et al. A Molecular Mechanism for Transthyretin Amyloidogenesis. *Nat. Commun.* **2019**, *10*, 925.

(190) Weirich, F.; Gremer, L.; Mirecka, E. A.; Schiefer, S.; Hoyer, W.; Heise, H. Structural Characterization of Fibrils from Recombinant Human Islet Amyloid Polypeptide by Solid-State NMR: The Central FGAILS Segment Is Part of the β-Sheet Core. *PLoS One* **2016**, *11*, e0161243.

(191) Uluca, B.; Viennet, T.; Petrović, D.; Shaykhalishahi, H.; Weirich, F.; Gönülalan, A.; Strodel, B.; Etzkorn, M.; Hoyer, W.; Heise, H. DNP-Enhanced MAS NMR: A Tool to Snapshot Conformational Ensembles of α-Synuclein in Different States. *Biophys. J.* **2018**, *114*, 1614–1623.

(192) Viennet, T.; Wördehoff, M. M.; Uluca, B.; Poojari, C.; Shaykhalishahi, H.; Willbold, D.; Strodel, B.; Heise, H.; Buell, A. K.; Hoyer, W. et al. Structural Insights from Lipid-Bilayer Nanodiscs Link α-Synuclein Membrane-Binding Modes to Amyloid Fibril Formation. *Commun. Biol.* **2018**, *1*, 44.

(193) Zhang, W.; Falcon, B.; Murzin, A. G.; Fan, J.; Crowther, R. A.; Goedert, M.; Scheres, S. H. Heparin-Induced Tau Filaments Are Polymorphic and Differ from Those in Alzheimer's and Pick's Diseases. *Elife* **2019**, *8*, e43584.

(194) Chakraborty, P.; Rivière, G.; Liu, S.; de Opakua, A. I.; Dervişoğlu, R.; Hebestreit, A.; Andreas, L. B.; Vorberg, I. M.; Zweckstetter, M. Co-Factor-Free Aggregation of Tau into Seeding-Competent RNA-Sequestering Amyloid Fibrils. *Nat. Commun.* **2021**, *12*, 4231.

(195) Bayro, M. J.; Huber, M.; Ramachandran, R.; Davenport, T. C.; Meier, B. H.; Ernst, M.; Griffin, R. G. Dipolar Truncation in Magic-Angle Spinning NMR Recoupling Experiments. *J. Chem. Phys.* **2009**, *130*, 114506.

(196) Smith, A. N.; Märker, K.; Piretra, T.; Boatz, J. C.; Matlahov, I.; Kodali, R.; Hediger, S.; van der Wel, P. C. A.; De Paëpe, G. Structural Fingerprinting of Protein Aggregates by Dynamic Nuclear Polarization-Enhanced Solid-State NMR at Natural Isotopic Abundance. *J. Am. Chem. Soc.* **2018**, *140*, 14576–14580.

(197) Thurber, K. R.; Potapov, A.; Yau, W. M.; Tycko, R. Solid State Nuclear Magnetic Resonance with Magic-Angle Spinning and Dynamic Nuclear Polarization Below 25 K. *J. Magn. Reson.* **2013**, *226*, 100–106.

(198) Jeon, J.; Thurber, K. R.; Ghirlando, R.; Yau, W. M.; Tycko, R. Application of Millisecond Time-Resolved Solid State NMR to the Kinetics and Mechanism of Melittin Self-Assembly. *Proc. Natl. Acad. Sci. U. S. A.* **2019**, *116*, 16717–16722.

(199) Jeon, J.; Yau, W. M.; Tycko, R. Millisecond Time-Resolved Solid-State NMR Reveals a Two-Stage Molecular Mechanism for Formation of Complexes Between Calmodulin and a Target Peptide from Myosin Light Chain Kinase. *J. Am. Chem. Soc.* **2020**, *142*, 21220–21232.

(200) Schmidt, T.; Jeon, J.; Yau, W.-M.; Schwieters, C. D.; Tycko, R.; Clore, G. M. Time-Resolved DEER EPR and Solid-State NMR Afford Kinetic and Structural Elucidation of Substrate Binding to Ca2+-Ligated Calmodulin. *Proc. Natl. Acad. Sci. U. S. A.* **2022**, *119*, e2122308119.

(201) Waudby, C. A.; Dobson, C. M.; Christodoulou, J. Nature and Regulation of Protein Folding on the Ribosome. *Trends Biochem. Sci.* **2019**, *44*, 914–926.

(202) Gelis, I.; Vitzthum, V.; Dhimole, N.; Caporini, M. A.; Schedlbauer, A.; Carnevale, D.; Connell, S. R.; Fucini, P.; Bodenhausen, G. Solid-State NMR Enhanced by Dynamic Nuclear Polarization as a Novel Tool for Ribosome Structural Biology. *J. Biomol. NMR* **2013**, *56*, 85–93.

(203) Lange, S.; Franks, W. T.; Rajagopalan, N.; Döring, K.; Geiger, M. A.; Linden, A.; Van Rossum, B. J.; Kramer, G.; Bukau, B.; Oschkinat, H. Structural Analysis of a Signal Peptide Inside the Ribosome Tunnel by DNP MAS NMR. *Sci. Adv.* **2016**, *2*, e1600379.

(204) Schulte, L.; Mao, J.; Reitz, J.; Sreeramulu, S.; Kudlinzki, D.; Hodirnau, V. V.; Meier-Credo, J.; Saxena, K.; Buhr, F.; Langer, J. D. et al. Cysteine Oxidation and Disulfide Formation in the Ribosomal Exit Tunnel. *Nat. Commun.* **2020**, *11*, 5569.

(205) Siemons, L.; Uluca-Yazgi, B.; Pritchard, R. B.; McCarthy, S.; Heise, H.; Hansen, D. F. Determining Isoleucine Side-Chain Rotamer-Sampling in Proteins from 13C Chemical Shift. *Chem. Commun.* **2019**, *55*, 14107–14110.

(206) Holmes, J. B.; Liu, V.; Caulkins, B. G.; Hilario, E.; Ghosh, R. K.; Drago, V. N.; Young, R. P.; Romero, J. A.; Gill, A. D.; Bogie, P. M. et al. Imaging Active Site Chemistry and Protonation States: NMR Crystallography of the Tryptophan Synthase α-Aminoacrylate Intermediate. *Proc. Natl. Acad. Sci. U. S. A.* **2022**, *119*, e2109235119.

(207) Koers, E. J.; Lõpez-Deber, M. P.; Weingarth, M.; Nand, D.; Hickman, D. T.; Mlaki Ndao, D.; Reis, P.; Granet, A.; Pfeifer, A.; Muhs, A. et al. Dynamic Nuclear Polarization NMR Spectroscopy: Revealing Multiple Conformations in Lipid-Anchored Peptide Vaccines. *Angew. Chem. Int. Ed.* **2013**, *52*, 10905–10908.

(208) Viger-Gravel, J.; Paruzzo, F. M.; Cazaux, C.; Jabbour, R.; Leleu, A.; Canini, F.; Florian, P.; Ronzon, F.; Gajan, D.; Lesage, A. Atomic-Scale Description of Interfaces Between Antigen and Aluminum-Based Adjuvants Used in Vaccines by Dynamic Nuclear Polarization (DNP) Enhanced NMR Spectroscopy. *Chem. - A Eur. J.* **2020**, *26*, 8976–8982.

(209) Jaudzems, K.; Kirsteina, A.; Schubeis, T.; Casano, G.; Ouari, O.; Bogans, J.; Kazaks, A.; Tars, K.; Lesage, A.; Pintacuda, G. Structural Analysis of an Antigen Chemically Coupled on Virus-Like Particles in Vaccine Formulation. *Angew. Chem. Int. Ed.* **2021**, *60*, 12847–12851.

(210) Aladin, V.; Vogel, M.; Binder, R.; Burghardt, I.; Suess, B.; Corzilius, B. Complex Formation of the Tetracycline-Binding Aptamer Investigated by Specific Cross-Relaxation Under DNP. *Angew. Chem. Int. Ed.* **2019**, *58*, 4863–4868.

(211) Wenk, P.; Kaushik, M.; Richter, D.; Vogel, M.; Suess, B.; Corzilius, B. Dynamic Nuclear Polarization of Nucleic Acid with Endogenously Bound Manganese. *J. Biomol. NMR* **2015**, *63*, 97–109.

(212) Gupta, R.; Zhang, H.; Lu, M.; Hou, G.; Caporini, M.; Rosay, M.; Maas, W.; Struppe, J.; Ahn, J.; Byeon, I. J. L. et al. Dynamic Nuclear Polarization Magic-Angle

Spinning Nuclear Magnetic Resonance Combined with Molecular Dynamics Simulations Permits Detection of Order and Disorder in Viral Assemblies. *J. Phys. Chem. B* **2019**, *123*, 5048–5058.

(213) Ulrich, E. L.; Akutsu, H.; Doreleijers, J. F.; Harano, Y.; Ioannidis, Y. E.; Lin, J.; Livny, M.; Mading, S.; Maziuk, D.; Miller, Z. et al. BioMagResBank. *Nucleic Acids Res.* **2008**, *36*, 402–408.

(214) Sergeyev, I. V.; Day, L. A.; Goldbourt, A.; McDermott, A. E. Chemical Shifts for the Unusual DNA Structure in Pf1 Bacteriophage from Dynamic-Nuclear-Polarization-Enhanced Solid-State NMR Spectroscopy. *J. Am. Chem. Soc.* **2011**, *133*, 20208–20217.

(215) Sergeyev, I. V.; Itin, B.; Rogawski, R.; Day, L. A.; McDermott, A. E. Efficient Assignment and NMR Analysis of an Intact Virus using Sequential Side-Chain Correlations and DNP Sensitization. *Proc. Natl. Acad. Sci. U. S. A.* **2017**, *114*, 5171–5176.

(216) Alphonse, S.; Itin, B.; Khayat, R.; Ghose, R. Sequential Protein Expression and Capsid Assembly in Cell: Toward the Study of Multiprotein Viral Capsids Using Solid-State Nuclear Magnetic Resonance Techniques. *Biochemistry* **2018**, *57*, 1568–1571.

(217) Cheng, C.-Y.; Han, S. Dynamic Nuclear Polarization Methods in Solids and Solutions to Explore Membrane Proteins and Membrane Systems. *Annu. Rev. Phys. Chem.* **2013**, *64*, 507–532.

(218) Ullrich, S. J.; Glaubitz, C. Perspectives in Enzymology of Membrane Proteins by Solid-State NMR. *Acc. Chem. Res.* **2013**, *46*, 2164–2171.

(219) Kaiser, A.; Coin, I. Capturing Peptide-GPCR Interactions and Their Dynamics. *Molecules* **2020**, *25*, 4724.

(220) Lee, M.; Hong, M. Cryoprotection of Lipid Membranes for High-Resolution Solid-State NMR Studies of Membrane Peptides and Proteins at Low Temperature. *J. Biomol. NMR* **2014**, *59*, 263–277.

(221) Möbius, K.; Kazemi, S.; Güntert, P.; Jakob, A.; Heckel, A.; Becker-Baldus, J.; Glaubitz, C. Global Response of Diacylglycerol Kinase Towards Substrate Binding Observed by 2D and 3D MAS NMR. *Sci. Rep.* **2019**, *9*, 3995.

(222) Yamamoto, K.; Dürr, U. H.; Xu, J.; Im, S. C.; Waskell, L.; Ramamoorthy, A. Dynamic Interaction Between Membrane-Bound Full-Length Cytochrome P450 and Cytochrome B5 Observed by Solid-State NMR Spectroscopy. *Sci. Rep.* **2013**, *3*, 2538.

(223) Yamamoto, K.; Caporini, M. A.; Im, S. C.; Waskell, L.; Ramamoorthy, A. Transmembrane Interactions of Full-Length Mammalian Bitopic Cytochrome-P450-Cytochrome-B 5 Complex in Lipid Bilayers Revealed by Sensitivity-Enhanced Dynamic Nuclear Polarization Solid-State NMR Spectroscopy. *Sci. Rep.* **2017**, *7*, 4116.

(224) Ong, Y. S.; Lakatos, A.; Becker-Baldus, J.; Pos, K. M.; Glaubitz, C. Detecting Substrates Bound to the Secondary Multidrug Efflux Pump EmrE by DNP-Enhanced Solid-State NMR. *J. Am. Chem. Soc.* **2013**, *135*, 15754–15762.

(225) Koers, E. J.; van der Cruijsen, E. A. W.; Rosay, M.; Weingarth, M.; Prokofyev, A.; Sauvée, C.; Ouari, O.; van der Zwan, J.; Pongs, O.; Tordo, P. et al. NMR-Based Structural Biology Enhanced by Dynamic Nuclear Polarization at High Magnetic Field. *J. Biomol. NMR* **2014**, *60*, 157–168.

(226) Visscher, K. M.; Medeiros-Silva, J.; Mance, D.; Rodrigues, J. P. G. L. M.; Daniëls, M.; Bonvin, A. M. J. J.; Baldus, M.; Weingarth, M. Supramolecular Organization and Functional Implications of K + Channel Clusters in Membranes. *Angew. Chem. Int. Ed.* **2017**, *56*, 13222–13227.

(227) Andreas, L. B.; Barnes, A. B.; Corzilius, B.; Chou, J. J.; Miller, E. A.; Caporini, M.; Rosay, M.; Griffin, R. G. Dynamic Nuclear Polarization Study of Inhibitor Binding to the M2 18-60 Proton Transporter from Influenza A. *Biochemistry* **2013**, *52*, 2774–2782.

(228) Elkins, M. R.; Williams, J. K.; Gelenter, M. D.; Dai, P.; Kwon, B.; Sergeyev, I. V.; Pentelute, B. L.; Hong, M. Cholesterol-Binding Site of the Influenza M2 Protein in Lipid Bilayers from Solid-State NMR. *Proc. Natl. Acad. Sci.* **2017**, *114*, 12946–12951.

(229) Elkins, M. R.; Sergeyev, I. V.; Hong, M. Determining Cholesterol Binding to Membrane Proteins by Cholesterol 13C Labeling in Yeast and Dynamic Nuclear Polarization NMR. *J. Am. Chem. Soc.* **2018**, *140*, 15437–15449.

(230) Movellan, K. T.; Derviş̧oğlu, R.; Becker, S.; Andreas, L. B. Pore-Bound Water at the Key Residue Histidine 37 in Influenza A M2. *Angew. Chem. Int. Ed.* **2021**, *60*, 24075–24079.

(231) Kaur, H.; Lakatos-Karoly, A.; Vogel, R.; Nöll, A.; Tampé, R.; Glaubitz, C. Coupled ATPase-Adenylate Kinase Activity in ABC Transporters. *Nat. Commun.* **2016**, *7*, 13864.

(232) Kaur, H.; Abreu, B.; Akhmetzyanov, D.; Lakatos-Karoly, A.; Soares, C. M.; Prisner, T.; Glaubitz, C. Unexplored Nucleotide Binding Modes for the ABC Exporter MsbA. *J. Am. Chem. Soc.* **2018**, 14112–14125.

(233) Spadaccini, R.; Kaur, H.; Becker-Baldus, J.; Glaubitz, C. The Effect of Drug Binding on Specific Sites in Transmembrane Helices 4 and 6 of the ABC Exporter MsbA Studied by DNP-Enhanced Solid-State NMR. *Biochim. Biophys. Acta - Biomembr.* **2018**, *1860*, 833–840.

(234) Pinto, C.; Mance, D.; Sinnige, T.; Daniëls, M.; Weingarth, M.; Baldus, M. Formation

of the β-Barrel Assembly Machinery Complex in Lipid Bilayers as Seen by Solid-State NMR. *Nat. Commun.* **2018**, *9*, 4135.

(235) Lopez, J. J.; Shukla, A. K.; Reinhart, C.; Schwalbe, H.; Michel, H.; Glaubitz, C. The Structure of the Neuropeptide Bradykinin Bound to the Human G-Protein Coupled Receptor Bradykinin B2 as Determined by Solid-State NMR Spectroscopy. *Angew. Chem. Int. Ed.* **2008**, *47*, 1668–1671.

(236) Joedicke, L.; Mao, J.; Kuenze, G.; Reinhart, C.; Kalavacherla, T.; Jonker, H. R.; Richter, C.; Schwalbe, H.; Meiler, J.; Preu, J. et al. The Molecular Basis of Subtype Selectivity of Human Kinin G-Protein-Coupled Receptors. *Nat. Chem. Biol.* **2018**, *14*, 284–290.

(237) Krug, U.; Gloge, A.; Schmidt, P.; Becker-Baldus, J.; Bernhard, F.; Kaiser, A.; Montag, C.; Gauglitz, M.; Vishnivetskiy, S. A.; Gurevich, V. V. et al. The Conformational Equilibrium of the Neuropeptide Y2 Receptor in Bilayer Membranes. *Angew. Chem. Int. Ed.* **2020**, *59*, 23854–23861.

(238) Ernst, O. P.; Lodowski, D. T.; Elstner, M.; Hegemann, P.; Brown, L. S.; Kandori, H. Microbial and Animal Rhodopsins: Structures, Functions, and Molecular Mechanisms. *Chem. Rev.* **2014**, *114*, 126–163.

(239) Leeder, A. J.; Brown, L. J.; Becker-Baldus, J.; Mehler, M.; Glaubitz, C.; Brown, R. C. Synthesis of Isotopically Labeled All-Trans Retinals for DNP-Enhanced Solid-State NMR Studies of Retinylidene Proteins. *J. Label. Compd. Radiopharm.* **2018**, *61*, 922–933.

(240) Bajaj, V. S.; Hornstein, M. K.; Kreischer, K. E.; Sirigiri, J. R.; Woskov, P. P.; Mak-Jurkauskas, M. L.; Herzfeld, J.; Temkin, R. J.; Griffin, R. G. 250 GHz CW Gyrotron Oscillator for Dynamic Nuclear Polarization in Biological Solid State NMR. *J. Magn. Reson.* **2007**, *189*, 251–279.

(241) Mak-Jurkauskas, M. L.; Bajaj, V. S.; Hornstein, M. K.; Belenky, M.; Griffin, R. G.; Herzfeld, J. Energy Transformations Early in the Bacteriorhodopsin Photocycle Revealed by DNP-Enhanced Solid-State NMR. *Proc. Natl. Acad. Sci. U. S. A.* **2008**, *105*, 883–888.

(242) Bajaj, V. S.; Mak-Jurkauskas, M. L.; Belenky, M.; Herzfeld, J.; Griffin, R. G. Functional and Shunt States of Bacteriorhodopsin Resolved by 250 GHz Dynamic Nuclear Polarization-Enhanced Solid-State NMR. *Proc. Natl. Acad. Sci. U. S. A.* **2009**, *106*, 9244–9249.

(243) Ni, Q. Z.; Can, T. V.; Daviso, E.; Belenky, M.; Griffin, R. G.; Herzfeld, J. Primary Transfer Step in the Light-Driven Ion Pump Bacteriorhodopsin: An Irreversible U-Turn Revealed by Dynamic Nuclear Polarization-Enhanced Magic Angle Spinning NMR. *J. Am. Chem. Soc.* **2018**, *140*, 4085–4091.

(244) Bamann, C.; Bamberg, E.; Wachtveitl, J.; Glaubitz, C. Proteorhodopsin. *Biochim. Biophys. Acta - Bioenerg.* **2014**, *1837*, 614–625.

(245) Mehler, M.; Scholz, F.; Ullrich, S. J.; Mao, J.; Braun, M.; Brown, L. J.; Brown, R. C.; Fiedler, S. A.; Becker-Baldus, J.; Wachtveitl, J. et al. The EF Loop in Green Proteorhodopsin Affects Conformation and Photocycle Dynamics. *Biophys. J.* **2013**, *105*, 385–397.

(246) Mao, J.; Do, N. N.; Scholz, F.; Reggie, L.; Mehler, M.; Lakatos, A.; Ong, Y. S.; Ullrich, S. J.; Brown, L. J.; Brown, R. C. et al. Structural Basis of the Green-Blue Color Switching in Proteorhodopsin as Determined by NMR Spectroscopy. *J. Am. Chem. Soc.* **2014**, *136*, 17578–17590.

(247) Mehler, M.; Eckert, C. E.; Leeder, A. J.; Kaur, J.; Fischer, T.; Kubatova, N.; Brown, L. J.; Brown, R. C.; Becker-Baldus, J.; Wachtveitl, J. et al. Chromophore

Distortions in Photointermediates of Proteorhodopsin Visualized by Dynamic Nuclear Polarization-Enhanced Solid-State NMR. *J. Am. Chem. Soc.* **2017**, *139*, 16143–16153.

(248) Maciejko, J.; Mehler, M.; Kaur, J.; Lieblein, T.; Morgner, N.; Ouari, O.; Tordo, P.; Becker-Baldus, J.; Glaubitz, C. Visualizing Specific Cross-Protomer Interactions in the Homo-Oligomeric Membrane Protein Proteorhodopsin by DNP-Enhanced Solid-State NMR. *J. Am. Chem. Soc.* **2015**, *137*, 9032–9043.

(249) Maciejko, J.; Kaur, J.; Becker-Baldus, J.; Glaubitz, C. Photocycle-Dependent Conformational Changes in the Proteorhodopsin Cross-Protomer Asp-His-Trp Triad Revealed by DNP-Enhanced MAS-NMR. *Proc. Natl. Acad. Sci. U. S. A.* **2019**, *116*, 8342–8349.

(250) Watanabe, H. C.; Welke, K.; Schneider, F.; Tsunoda, S.; Zhang, F.; Deisseroth, K.; Hegemann, P.; Elstner, M. Structural Model of Channelrhodopsin. *J. Biol. Chem.* **2012**, *287*, 7456–7466.

(251) Kato, H. E.; Zhang, F.; Yizhar, O.; Ramakrishnan, C.; Nishizawa, T.; Hirata, K.; Ito, J.; Aita, Y.; Tsukazaki, T.; Hayashi, S. et al. Crystal Structure of the Channelrhodopsin Light-Gated Cation Channel. *Nature* **2012**, *482*, 369–374.

(252) Bruun, S.; Stoeppler, D.; Keidel, A.; Kuhlmann, U.; Luck, M.; Diehl, A.; Geiger, M. A.; Woodmansee, D.; Trauner, D.; Hegemann, P. et al. Light-Dark Adaptation of Channelrhodopsin Involves Photoconversion Between the All-Trans and 13-Cis Retinal Isomers. *Biochemistry* **2015**, *54*, 5389–5400.

(253) Becker-Baldus, J.; Bamann, C.; Saxena, K.; Gustmann, H.; Brown, L. J.; Brown, R. C.; Reiter, C.; Bamberg, E.; Wachtveitl, J.; Schwalbe, H. et al. Enlightening the Photoactive Site of Channelrhodopsin-2 by DNP-Enhanced Solid-State NMR Spectroscopy. *Proc. Natl. Acad. Sci. U. S. A.* **2015**, *112*, 9896–9901.

(254) Becker-Baldus, J.; Leeder, A.; Brown, L. J.; Brown, R. C. D.; Bamann, C.; Glaubitz, C. The Desensitized Channelrhodopsin-2 Photointermediate Contains 13-Cis , 15-Syn Retinal Schiff Base. *Angew. Chem. Int. Ed.* **2021**, *60*, 16442–16447.

(255) Kubatova, N.; Mao, J.; Eckert, C. E.; Saxena, K.; Gande, S. L.; Wachtveitl, J.; Glaubitz, C.; Schwalbe, H. Light Dynamics of the Retinal-Disease-Relevant G90D Bovine Rhodopsin Mutant. *Angew. Chem. Int. Ed.* **2020**, *132*, 15786–15794.

(256) Stöppler, D.; Song, C.; van Rossum, B. J.; Geiger, M. A.; Lang, C.; Mroginski, M. A.; Jagtap, A. P.; Sigurdsson, S. T.; Matysik, J.; Hughes, J. et al. Dynamic Nuclear Polarization Provides New Insights into Chromophore Structure in Phytochrome Photoreceptors. *Angew. Chem. Int. Ed.* **2016**, *55*, 16017–16020.

(257) Luchinat, E.; Banci, L. In-Cell NMR: a Topical Review. *IUCrJ* **2017**, *4*, 108–118.

(258) Plitzko, J. M.; Schuler, B.; Selenko, P. Structural Biology Outside the Box—inside the Cell. *Curr. Opin. Struct. Biol.* **2017**, *46*, 110–121.

(259) Freedberg, D. I.; Selenko, P. Live Cell NMR. *Annu. Rev. Biophys.* **2014**, *43*, 171–192.

(260) Linden, A. H.; Lange, S.; Franks, W. T.; Akbey, Ü.; Specker, E.; Van Rossum, B. J.; Oschkinat, H. Neurotoxin II Bound to Acetylcholine Receptors in Native Membranes Studied by Dynamic Nuclear Polarization NMR. *J. Am. Chem. Soc.* **2011**, *133*, 19266–19269.

(261) Kaplan, M.; Narasimhan, S.; de Heus, C.; Mance, D.; van Doorn, S.; Houben, K.; Popov-Čeleketić, D.; Damman, R.; Katrukha, E. A.; Jain, P. et al. EGFR Dynamics Change During Activation in Native Membranes as Revealed by NMR. *Cell* **2016**, *167*, 1241–1251.

(262) Beriashvili, D.; Schellevis, R. D.; Napoli, F.; Weingarth, M.; Baldus, M. High-

Resolution Studies of Proteins in Natural Membranes by Solid-State NMR. *J. Vis. Exp.* **2021**, e62197.

(263) Narasimhan, S.; Pinto, C.; Lucini Paioni, A.; van der Zwan, J.; Folkers, G. E.; Baldus, M. Characterizing Proteins in a Native Bacterial Environment using Solid-State NMR Spectroscopy. *Nat. Protoc.* **2021**, *16*, 893–918.

(264) Reggie, L.; Lopez, J. J.; Collinson, I.; Glaubitz, C.; Lorch, M. Dynamic Nuclear Polarization-Enhanced Solid-State NMR of a 13C-Labeled Signal Peptide Bound to Lipid-Reconstituted Sec Translocon. *J. Am. Chem. Soc.* **2011**, *133*, 19084–19086.

(265) Yamamoto, K.; Caporini, M. A.; Im, S.-C.; Waskell, L.; Ramamoorthy, A. Cellular Solid-State NMR Investigation of a Membrane Protein using Dynamic Nuclear Polarization. *Biochim. Biophys. Acta - Biomembr.* **2015**, *1848*, 342–349.

(266) Jacso, T.; Franks, W. T.; Rose, H.; Fink, U.; Broecker, J.; Keller, S.; Oschkinat, H.; Reif, B. Characterization of Membrane Proteins in Isolated Native Cellular Membranes by Dynamic Nuclear Polarization Solid-State NMR Spectroscopy without Purification and Reconstitution. *Angew. Chem. Int. Ed.* **2012**, *51*, 432–435.

(267) Kaplan, M.; Cukkemane, A.; van Zundert, G. C. P.; Narasimhan, S.; Daniëls, M.; Mance, D.; Waksman, G.; Bonvin, A. M. J. J.; Fronzes, R.; Folkers, G. E. et al. Probing a Cell-Embedded Megadalton Protein Complex by DNP-Supported Solid-State NMR. *Nat. Methods* **2015**, *12*, 5–9.

(268) Medeiros-Silva, J.; Jekhmane, S.; Paioni, A. L.; Gawarecka, K.; Baldus, M.; Swiezewska, E.; Breukink, E.; Weingarth, M. High-Resolution NMR Studies of Antibiotics in Cellular Membranes. *Nat. Commun.* **2018**, *9*, 3963.

(269) Shukla, R.; Medeiros-Silva, J.; Parmar, A.; Vermeulen, B. J.; Das, S.; Paioni, A. L.; Jekhmane, S.; Lorent, J.; Bonvin, A. M.; Baldus, M. et al. Mode of Action of Teixobactins in Cellular Membranes. *Nat. Commun.* **2020**, *11*, 2848.

(270) Mandala, V. S.; Loh, D. M.; Shepard, S. M.; Geeson, M. B.; Sergeyev, I. V.; Nocera, D. G.; Cummins, C. C.; Hong, M. Bacterial Phosphate Granules Contain Cyclic Polyphosphates: Evidence from 31P Solid-State NMR. *J. Am. Chem. Soc.* **2020**, *142*, 18407–18421.

(271) Ghosh, R.; Kragelj, J.; Xiao, Y.; Frederick, K. K. Cryogenic Sample Loading into a Magic Angle Spinning Nuclear Magnetic Resonance Spectrometer That Preserves Cellular Viability. *J. Vis. Exp.* **2020**, *2020*, e61733.

(272) McCoy, K. M.; Rogawski, R.; Stovicek, O.; McDermott, A. E. Stability of Nitroxide Biradical TOTAPOL in Biological Samples. *J. Magn. Reson.* **2019**, *303*, 115–120.

(273) Renault, M.; Pawsey, S.; Bos, M. P.; Koers, E. J.; Nand, D.; Tommassen-Van Boxtel, R.; Rosay, M.; Tommassen, J.; Maas, W. E.; Baldus, M. Solid-State NMR Spectroscopy on Cellular Preparations Enhanced by Dynamic Nuclear Polarization. *Angew. Chem. Int. Ed.* **2012**, *51*, 2998–3001.

(274) Stacey, G. Primary Cell Cultures and Immortal Cell Lines. *eLS* **2006**,

(275) Albert, B. J.; Gao, C.; Sesti, E. L.; Saliba, E. P.; Alaniva, N.; Scott, F. J.; Sigurdsson, S. T.; Barnes, A. B. Dynamic Nuclear Polarization Nuclear Magnetic Resonance in Human Cells Using Fluorescent Polarizing Agents. *Biochemistry* **2018**, *57*, 4741–4746.

(276) Narasimhan, S.; Scherpe, S.; Lucini Paioni, A.; van der Zwan, J.; Folkers, G. E.; Ovaa, H.; Baldus, M. DNP-Supported Solid-State NMR Spectroscopy of Proteins Inside Mammalian Cells. *Angew. Chem. Int. Ed.* **2019**, *58*, 12969–12973.

(277) Schlagnitweit, J.; Friebe Sandoz, S.; Jaworski, A.; Guzzetti, I.; Aussenac, F.; Carbajo, R. J.; Chiarparin, E.; Pell, A. J.; Petzold, K. Observing an Antisense Drug Complex in Intact Human Cells by In-Cell NMR Spectroscopy. *ChemBioChem* **2019**, *20*, 2474–2478.

(278) Overall, S. A.; Price, L. E.; Albert, B. J.; Gao, C.; Alaniva, N.; Judge, P. T.; Sesti, E. L.; Wender, P. A.; Kyei, G. B.; Barnes, A. B. In Situ Detection of Endogenous HIV Activation by Dynamic Nuclear Polarization NMR and Flow Cytometry. *Int. J. Mol. Sci.* **2020**, *21*, 4649.

(279) Damman, R.; Lucini Paioni, A.; Xenaki, K. T.; Beltrán Hernández, I.; van Bergen en Henegouwen, P. M.; Baldus, M. Development of in Vitro-Grown Spheroids as a 3D Tumor Model System for Solid-State NMR Spectroscopy. *J. Biomol. NMR* **2020**, *74*, 401–412.

(280) Kelly, J. E.; Chrissian, C.; Stark, R. E. Tailoring NMR Experiments for Structural Characterization of Amorphous Biological Solids: A Practical Guide. *Solid State Nucl. Magn. Reson.* **2020**, *109*, 101686.

(281) Garcia-Rubio, R.; de Oliveira, H. C.; Rivera, J.; Trevijano-Contador, N. The Fungal Cell Wall: *Candida*, *Cryptococcus*, and *Aspergillus* Species. *Front. Microbiol.* **2020**, *10*, 2993.

(282) Erwig, L. P.; Gow, N. A. Interactions of Fungal Pathogens with Phagocytes. *Nat. Rev. Microbiol.* **2016**, *14*, 163–176.

(283) Odds, F. C.; Brown, A. J.; Gow, N. A. Antifungal Agents: Mechanisms of Action. *Trends Microbiol.* **2003**, *11*, 272–279.

(284) Kang, X.; Kirui, A.; Muszyński, A.; Widanage, M. C. D.; Chen, A.; Azadi, P.; Wang, P.; Mentink-Vigier, F.; Wang, T. Molecular Architecture of Fungal Cell Walls Revealed by Solid-State NMR. *Nat. Commun.* **2018**, *9*, 2747.

(285) Chatterjee, S.; Prados-Rosales, R.; Tan, S.; Phan, V. C.; Chrissian, C.; Itin, B.; Wang, H.; Khajo, A.; Magliozzo, R. S.; Casadevall, A. et al. The Melanization Road More Traveled By: Precursor Substrate Effects on Melanin Synthesis in Cell-Free and Fungal Cell Systems. *J. Biol. Chem.* **2018**, *293*, 20157–20168.

(286) Ni, Q. Z.; Sierra, B. N.; La Clair, J. J.; Burkart, M. D. Chemoenzymatic Elaboration of the Raper-Mason Pathway Unravels the Structural Diversity Within Eumelanin Pigments. *Chem. Sci.* **2020**, *11*, 7836–7841.

(287) Cosgrove, D. J.; Jarvis, M. C. Comparative Structure and Biomechanics of Plant Primary and Secondary Cell Walls. *Front. Plant Sci.* **2012**, *3*, 14.

(288) Wang, T.; Park, Y. B.; Caporini, M. A.; Rosay, M.; Zhong, L.; Cosgrove, D. J.; Hong, M. Sensitivity-Enhanced Solid-State NMR Detection of Expansin's Target in Plant Cell Walls. *Proc. Natl. Acad. Sci. U. S. A.* **2013**, *110*, 16444–16449.

(289) Zhao, W.; Kirui, A.; Deligey, F.; Mentink-Vigier, F.; Zhou, Y.; Zhang, B.; Wang, T. Solid-State NMR of Unlabeled Plant Cell Walls: High-Resolution Structural Analysis without Isotopic Enrichment. *Biotechnol. Biofuels* **2021**, *14*, 14.

(290) Ling, Z.; Wang, T.; Makarem, M.; Santiago Cintrón, M.; Cheng, H. N.; Kang, X.; Bacher, M.; Potthast, A.; Rosenau, T.; King, H. et al. Effects of Ball Milling on the Structure of Cotton Cellulose. *Cellulose* **2019**, *26*, 305–328.

(291) Zhang, L.; Gao, C.; Mentink-Vigier, F.; Tang, L.; Zhang, D.; Wang, S.; Cao, S.; Xu, Z.; Liu, X.; Wang, T. et al. Arabinosyl Deacetylase Modulates the Arabinoxylan Acetylation Profile and Secondary Wall Formation. *Plant Cell* **2019**, *31*, 1113–1126.

(292) Williams, J. K.; Schmidt-Rohr, K.; Hong, M. Aromatic Spectral Editing Techniques for Magic-Angle-Spinning Solid-State NMR Spectroscopy of Uniformly 13C-Labeled Proteins. *Solid State Nucl. Magn. Reson.* **2015**, *72*, 118–126.

(293) Kang, X.; Kirui, A.; Dickwella Widanage, M. C.; Mentink-Vigier, F.; Cosgrove, D. J.; Wang, T. Lignin-Polysaccharide Interactions in Plant Secondary Cell Walls Revealed by Solid-State NMR. *Nat. Commun.* **2019**, *10*, 347.

(294) Dubroca, T.; Smith, A. N.; Pike, K. J.; Froud, S.; Wylde, R.; Trociewitz, B.; McKay, J.; Mentink-Vigier, F.; van Tol, J.; Wi, S. et al. A Quasi-Optical and Corrugated Waveguide Microwave Transmission System for Simultaneous Dynamic Nuclear Polarization NMR on Two Separate 14.1 T Spectrometers. *J. Magn. Reson.* **2018**, *289*, 35–44.

(295) Viger-Gravel, J.; Lan, W.; Pinon, A. C.; Berruyer, P.; Emsley, L.; Bardet, M.; Luterbacher, J. Topology of Pretreated Wood Fibers Using Dynamic Nuclear Polarization. *J. Phys. Chem. C* **2019**, *123*, 30407–30415.

(296) Perras, F. A.; Luo, H.; Zhang, X.; Mosier, N. S.; Pruski, M.; Abu-Omar, M. M. Atomic-Level Structure Characterization of Biomass Pre- and Post-Lignin Treatment by Dynamic Nuclear Polarization-Enhanced Solid-State NMR. *J. Phys. Chem. A* **2017**, *121*, 623–630.

(297) Kumar, A.; Durand, H.; Zeno, E.; Balsollier, C.; Watbled, B.; Sillard, C.; Fort, S.; Baussanne, I.; Belgacem, N.; Lee, D. et al. The Surface Chemistry of a Nanocellulose Drug Carrier Unravelled by MAS-DNP. *Chem. Sci.* **2020**, *11*, 3868–3877.

(298) Berruyer, P.; Gericke, M.; Moutzouri, P.; Jakobi, D.; Bardet, M.; Karlson, L.; Schantz, S.; Heinze, T.; Emsley, L. Advanced Characterization of Regioselectively Substituted Methylcellulose Model Compounds by DNP Enhanced Solid-State NMR Spectroscopy. *Carbohydr. Polym.* **2021**, *262*, 117944.

(299) Frantz, C.; Stewart, K. M.; Weaver, V. M. The Extracellular Matrix at a Glance. *J. Cell Sci.* **2010**, *123*, 4195–4200.

(300) Lee, D.; Leroy, C.; Crevant, C.; Bonhomme-Coury, L.; Babonneau, F.; Laurencin, D.; Bonhomme, C.; De Paëpe, G. Interfacial Ca2+ Environments in Nanocrystalline Apatites Revealed by Dynamic Nuclear Polarization Enhanced 43Ca NMR Spectroscopy. *Nat. Commun.* **2017**, *8*, 14104.

(301) Singh, C.; Rai, R. K.; Aussenac, F.; Sinha, N. Direct Evidence of Imino Acid-Aromatic Interactions in Native Collagen Protein by DNP-Enhanced Solid-State NMR Spectroscopy. *J. Phys. Chem. Lett.* **2014**, *5*, 4044–4048.

(302) Tiwari, N.; Wi, S.; Mentink-Vigier, F.; Sinha, N. Mechanistic Insights into the Structural Stability of Collagen-Containing Biomaterials Such as Bones and Cartilage. *J. Phys. Chem. B* **2021**, *125*, 4757–4766.

(303) Hu, Y. Y.; Rawal, A.; Schmidt-Rohr, K. Strongly Bound Citrate Stabilizes the Apatite Nanocrystals in Bone. *Proc. Natl. Acad. Sci. U. S. A.* **2010**, *107*, 22425–22429.

(304) Davies, E.; Müller, K. H.; Wong, W. C.; Pickard, C. J.; Reid, D. G.; Skepper, J. N.; Duer, M. J. Citrate Bridges Between Mineral Platelets in Bone. *Proc. Natl. Acad. Sci. U. S. A.* **2014**, *111*, E1354–E13563.

(305) Azaïs, T.; Von Euw, S.; Ajili, W.; Auzoux-Bordenave, S.; Bertani, P.; Gajan, D.; Emsley, L.; Nassif, N.; Lesage, A. Structural Description of Surfaces and Interfaces in Biominerals by DNP SENS. *Solid State Nucl. Magn. Reson.* **2019**, *102*, 2–11.

(306) Chow, W. Y. Investigation of Triple-Helix Collagen Hydroxylation by Solid-State NMR Spectroscopy. *Methods Mol. Biol.* **2019**, *1944*, 57–77.

(307) Müller, K. H.; Hayward, R.; Rajan, R.; Whitehead, M.; Cobb, A. M.; Ahmad, S.; Sun, M.; Goldberga, I.; Li, R.; Bashtanova, U. et al. Poly(ADP-Ribose) Links the DNA Damage Response and Biomineralization. *Cell Rep.* **2019**, *27*, 3124–3138.

(308) Goldberga, I.; Li, R.; Chow, W. Y.; Reid, D. G.; Bashtanova, U.; Rajan, R.; Puszkarska, A.; Oschkinat, H.; Duer, M. J. Detection of Nucleic Acids and Other Low Abundance Components in Native Bone and Osteosarcoma Extracellular Matrix by Isotope Enrichment and DNP-Enhanced NMR. *RSC Adv.* **2019**, *9*, 26686–26690.

(309) Chow, W. Y.; Norman, B. P.; Roberts, N. B.; Ranganath, L. R.; Teutloff, C.; Bittl, R.; Duer, M. J.; Gallagher, J. A.; Oschkinat, H. Pigmentation Chemistry and Radical-Based Collagen Degradation in Alkaptonuria and Osteoarthritic Cartilage. *Angew. Chem. Int. Ed.* **2020**, *59*, 11937–11942.

(310) Craig, H. C.; Blamires, S. J.; Sani, M.-A.; Kasumovic, M. M.; Rawal, A.; Hook, J. M. DNP NMR Spectroscopy Reveals New Structures, Residues and Interactions in Wild Spider Silks. *Chem. Commun.* **2019**, *55*, 10–13.

(311) Hildebrand, M.; Lerch, S. J.; Shrestha, R. P. Understanding Diatom Cell Wall Silicification-Moving Forward. *Front. Mar. Sci.* **2018**, *5*, 125.

(312) Jantschke, A.; Koers, E.; Mance, D.; Weingarth, M.; Brunner, E.; Baldus, M. Insight into the Supramolecular Architecture of Intact Diatom Biosilica from DNP-Supported Solid-State NMR Spectroscopy. *Angew. Chem. Int. Ed.* **2015**, *54*, 15069–15073.

(313) Geiger, Y.; Gottlieb, H. E.; Akbey, Ü.; Oschkinat, H.; Goobes, G. Studying the Conformation of a Silaffin-Derived Pentalysine Peptide Embedded in Bioinspired Silica using Solution and Dynamic Nuclear Polarization Magic-Angle Spinning NMR. *J. Am. Chem. Soc.* **2016**, *138*, 5561–5567.

(314) Ravera, E.; Michaelis, V. K.; Ong, T.-C.; Keeler, E. G.; Martelli, T.; Fragai, M.; Griffin, R. G.; Luchinat, C. Biosilica-Entrapped Enzymes Studied by Using Dynamic Nuclear-Polarization-Enhanced High-Field NMR Spectroscopy. *ChemPhysChem* **2015**, *16*, 2751–2754.

(315) Lelli, M.; Chaudhari, S. R.; Gajan, D.; Casano, G.; Rossini, A. J.; Ouari, O.; Tordo, P.; Lesage, A.; Emsley, L. Solid-State Dynamic Nuclear Polarization at 9.4 and 18.8 T from 100 K to Room Temperature. *J. Am. Chem. Soc.* **2015**, *137*, 14558–14561.

(316) Can, T. V.; Ni, Q. Z.; Griffin, R. G. Mechanisms of Dynamic Nuclear Polarization in Insulating Solids. *J. Magn. Reson.* **2015**, *253*, 23–35.

(317) Scott, F. J.; Saliba, E. P.; Albert, B. J.; Alaniva, N.; Sesti, E. L.; Gao, C.; Golota, N. C.; Choi, E. J.; Jagtap, A. P.; Wittmann, J. J. et al. Frequency-Agile Gyrotron for Electron Decoupling and Pulsed Dynamic Nuclear Polarization. *J. Magn. Reson.* **2018**, *289*, 45–54.

(318) Judge, P. T.; Sesti, E. L.; Price, L. E.; Albert, B. J.; Alaniva, N.; Saliba, E. P.; Halbritter, T.; Sigurdsson, S. T.; Kyei, G. B.; Barnes, A. B. Dynamic Nuclear Polarization with Electron Decoupling in Intact Human Cells and Cell Lysates. *J. Phys. Chem. B* **2020**, *124*, 2323–2330.

(319) Maly, T.; Cui, D.; Griffin, R. G.; Miller, A. F. 1H Dynamic Nuclear Polarization Based on an Endogenous Radical. *J. Phys. Chem. B* **2012**, *116*, 7055–7065.

(320) Harchol, A.; Reuveni, G.; Ri, V.; Thomas, B.; Carmieli, R.; Herber, R. H.; Kim, C.; Leskes, M. Endogenous Dynamic Nuclear Polarization for Sensitivity Enhancement in Solid-State NMR of Electrode Materials. *J. Phys. Chem. C* **2020**, *124*, 7082–7090.

(321) Wolf, T.; Kumar, S.; Singh, H.; Chakrabarty, T.; Aussenac, F.; Frenkel, A. I.; Major, D. T.; Leskes, M. Endogenous Dynamic Nuclear Polarization for Natural Abundance 17 O and Lithium NMR in the Bulk of Inorganic Solids. *J. Am. Chem. Soc.* **2019**, *141*, 451–462.

(322) Smith, A. N.; Märker, K.; Hediger, S.; De Paëpe, G. Natural Isotopic Abundance 13C and 15N Multidimensional Solid-State NMR Enabled by Dynamic Nuclear Polarization. *J. Phys. Chem. Lett.* **2019**, *10*, 4652–4662.

TOC Graphic


plant cell wall
membrane proteins
in-cell
tissues
virus
protein folding
fungi
DNP